HIGH RESOLUTION PATTERNING OF POLYMER THIN FILMS FOR NANOTECHNOLOGY APPLICATIONS

A Dissertation

Presented to the Faculty of the Graduate School

of Cornell University

In Partial Fulfillment of the Requirements for the Degree of

Doctor of Philosophy

by

Abhinav Rastogi

August 2009

HIGH RESOLUTION PATTERNING OF POLYMER THIN FILMS FOR NANOTECHNOLOGY APPLICATIONS

Abhinav Rastogi, Ph. D.

Cornell University 2009

The ability to pattern functional polymers at different length scales is important for the advancement of modern science and technology. This dissertation mainly describes the work done on the high resolution patterning of polymer thin films that have a variety of potential uses.

The nanoscale patterning of spun-coated polar polymers was demonstrated using environmentally benign supercritical carbon dioxide ($scCO_2$) as a processing solvent. The use of $scCO_2$ as a processing solvent has several technical advantages that help resolve some of the key problems faced in lithography. In addition, it helps reduce the energy and resource usage that can negatively affect the environment. $scCO_2$ is generally a poor solvent for high molecular weight polymers that are used as standard photoresists. Chapter 2 describes a series of fluorinated quaternary ammonium salts that were synthesized and used as CO_2 compatible additives to aid the dissolution of polar polymer photoresists in $scCO_2$. Using these dissolution aids, patterns as small as 100 nm lines were obtained with $scCO_2$ development.

Chapters 3 and 4 focus on the patterning of high-tech thin polymer films referred to as polymer brushes. In these films the polymer chains are covalently attached to a surface. A direct method of patterning polymer brushes in a single step using electron beam lithography has been described. Polymer brushes of different structures such as poly(methyl methacrylate) (PMMA) brushes , poly(2-hydroxyethyl

methacrylate) (PHEMA) brushes, poly(isobutyl methacrylate) (PIBMA) brushes, poly(neopentyl methacrylate) (PNPMA) brushes and poly(2,2,2-trifluoroethyl methacrylate) (PTFEMA) brushes were grown via atom transfer radical polymerization. These brushes were directly patterned using e-beam and their sensitivity to e-beam patterning has been compared and explained. This direct patterning approach produced polymer brush patterns down to 50 nm lines.

Due to the number of advantages of using $scCO_2$ as a processing solvent, the dry development of a directly patterned low surface energy coating composed of PTFEMA brushes in $scCO_2$ has been demonstrated in Chapter 4. Using $scCO_2$ as a developer, patterned PTFEMA brushes with 150 nm lines were obtained.

Polymer brushes have been used to prepare biocompatible surfaces with reduced non-specific adsorption. Chapter 5 describes the synthesis of a new oligo(ethylene glycol) containing ATRP intiator to prevent non-specific adsorption of biomolecules on polymer brush coated gold electrodes. The adsorption of non-specific antibodies on modified gold electrodes was studied using cyclic voltammetry. Poly(acrylic acid) brushes grown using this new ATRP initiator showed reduced non-specific binding of the gold electrodes.

There has been a continuing need for developing new medical countermeasures for emerging infectious diseases. Chapter 6 describes the role of functionalized poly(acrylic acid) brushes in the development of a biosensor based on sensitive electrochemical detection of the intrinsic catalytic activity of antibodies. Poly(acrylic acid) brushes have been functionalized with 2,4-dinitrophenyl groups (model antigen) and Ni-NTA to immobilize specific antibodies on the sensor surface. The modification of gold surfaces with polymer brushes provides a bio- and electronically compatible substrate with high density of specific haptens with reduced non-specific adsorption.

BIOGRAPHICAL SKETCH

Abhinav Rastogi is the son of Prof. Ashok K. Rastogi and Anju Rastogi. He was born on 16th April 1979 in the holy land of Banaras, India. Fortunately, he moved to Mumbai (Bombay) at a very early age, where he grew up in a beautiful and scientific environment at the Indian Institute of Technology (I.I.T) campus. As an undergraduate student as Ramnarain Ruia College in Mumbai, he always dreamt of becoming a professional singer and got trained in Indian classical music for a couple of years. However, fate took its toll and he got interested in science and ended up earning a bachelor's degree in chemistry at Ramnarain Ruia College affiliated to the University of Mumbai.

Abhinav migrated to the United States in Fall 2002 to join the master's program in the department of chemistry at University of North Carolina at Charlotte. At UNCC he worked with Prof. Craig A. Ogle and Dr. Steven Bertz in the area of asymmetric induction. This work earned him his first publication and made him realize that he has the potential to think as a researcher and do exciting, cutting-edge research. After earning his M.S in organic chemistry, he moved to Cornell University in Fall 2004 in quest of deeper knowledge.

Abhinav loved the multidisciplinary atmosphere at Cornell and joined Prof. Christopher K. Ober's research group, a group that has been involved in several application oriented and industry-related projects. In Ober's group, Abhinav worked on the synthesis and high resolution patterning of polymer thin films. He got the opportunity to present his research work at various national and international conferences and also learnt the art of writing manuscripts, annual funding reviews and grant proposals. All these skills helped him earn his doctorate degree.

In his final year as a graduate student at Cornell, Abhinav met an amazing lady, Kruti Pandya in the beautiful city of Boston, MA. Abhinav and Kruti were married on December 20th, 2008. Recently, Abhinav accepted a job offer at Intel Corporation's Logic Technology Development group in Hillsboro, Oregon. Upon leaving Cornell, Abhinav plans to work on new technologies for the production of "next generation" microprocessors and is excited about moving to the west coast.

Dedicated to

My awesome parents, Dr. Ashok K. Rastogi and Anju Rastogi, who have always loved me and motivated me to work hard and do my best in every aspect of life;

My caring sister, Ashita, who has always respected me and has been a source of motivation for me;

My adoring wife, Kruti, who has been extremely patient and supportive during the course of my doctoral studies;

All my teachers who have passed on their knowledge to educate me;

All my relatives & friends for their love and words of encouragement;

Finally, this thesis is dedicated to all those who believe in the richness of learning.

ACKNOWLEDGMENTS

First and foremost, I would like to thank my Ph.D. advisor, Prof. Christopher K. Ober for recruiting me in his research group and for all his guidance and constructive criticism. It has been a pleasure to work with such an understanding, practical, inspiring and knowledgeable person, who is always bubbling with new ideas. He gave me exciting projects to work on and has made my years at Cornell, a wonderful learning experience.

Next, I would like to thank Intel Corporation for funding the supercritical CO_2 project, National Science Foundation (NSF) for funding the polymer brush work and Nanobiotechnology Center (NBTC) at Cornell for sponsoring the biosensor project. Without their financial support, this thesis would not have been possible. I would like to thank Prof. Héctor D. Abruña and Prof. Barbara A. Baird for sitting on my thesis committee and for all the invaluable discussions and words of encouragement. I have really enjoyed interacting with them and thank them for being patient with me while I was tying to grasp the concepts of electrochemistry and immunology.

I gratefully acknowledge Prof. Juan J. de Pablo (University of Wisconsin, Madison) and Dr. Richard Schenker, Dr. Michael Leeson and Dr. Alan Myers (Intel Corporation) for all their advice on the supercritical CO_2 work. I acknowledge Prof. Judith Appleton and Prof. Theodore Clark for their help with the biosensor project. I like to thank Prof. Dotsevi Y. Sogah and Prof. Tyler McQuade (Florida State University) for all their help during coursework.

I am extremely thankful to Dr. Manabu Tanaka (Yamanashi University) and Marvin Paik (Ober group) for being such wonderful collaborators and friends. Thanks for helping me with all my projects. Without the two of you, the ride to graduation would not have been so smooth. I will cherish all the moments that we have spent

together. I thank Dr. Sitaraman Krishnan (Clarkson University) and Dr. Dan Fisher for helping me understand the NEXAFS experiments performed at Brookhaven National Labs. I would also like to thank Robert Riggleman and Gregory Toepperwein for being great collaborators on the supercritical CO_2 project. Thanks for sharing some concepts of computational chemistry with me. For the biosensor work, I would like to thank Norah Smith, Lisa Blum, Yelena Bisharyan, Dr. Nicolas Da Mota and Michele Tague for being excellent collaborators. I thank Suddhasattwa Nad for all his help in preparing me for my candidacy exam and for working closely with me on the biosensor project.

I am thankful to all the past and present "obergroup" members especially Dr. Ramakrishna Ayothi, Dr. Sitaraman Krishnan, Dr. Yi Yi, Shalin Jhaveri, Nelson Felix, Anuja de Silva, Craig Weinman, Katy Bosworth, Rong Dong, Jing Sha, Evan Schwartz, Drew Forman, Marie Krysak, Liz Welch, Eisuke Murotani, Dr. Young Jin Cho, Dr. Youyong Xu & Dr. Harihara Subramanian for all the fun and discussions in lab and during group meetings. I wish you all the best in life. I thank the tool managers at Cornell Nanoscale Science & Technology Facility (CNF) and at NBTC for training me on the various tools to pattern and characterize my polymer coated surfaces. I also thank Vicki Conner, Carol Armstrong, Sharon Calhoun, Dolores Dewbury, Theresa Peck & Verne Thalheimer for taking care of all the administrative work for me.

I am extremely grateful to all my friends in Ithaca, who have made these seemingly never-ending years of graduate school, go by so fast. A special thanks to Kalyanaraman Krishnamoorthy, Lekha Gupta, Deepti Gadi, Jaya Bhatnagar, Debamita Paul & Dr. Garima Singh for providing me a "home outside home". Thanks for the countless meals that I have had at your places over the past five years. It is beyond my ability to express the deep sense of gratitude that I feel for you all. Thank you for throwing all the great parties to celebrate my success and for your moral and

emotional support during the hard times. I will cherish the time spent with each one of you for the rest of my life. I wish you good luck in all your future endeavors and I hope we will keep in touch. I also thank Anandroop , Arithro, Biki, Anand & Amit for the many games of badminton and table tennis (ping pong). It has been a lot of fun.

Finally, I would like to thank my parents without whom I would not be here to say these words. Thanks for having faith in me and for all your love and encouragement. I thank my sister, Ashita for her love and support. I would like to thank my family members especially Payal didi, Ronny jijaji, Amit Bhaiya, Meenal bhabhi, Guddu bhaiya, Komal bhabhi, Ammu didi, Hitesh jijaji, Parul didi and Chetan jijaji, who have taken good care of me and have always motivated me to move forward. And, I would like to thank my loving and caring wife, Kruti for being extremely patient and supportive. In the words of a materials chemist, I would like to thank all of you for catalyzing the process of transforming me from an incoming graduate student to a successful Ph.D. holder.

TABLE OF CONTENTS

LIST OF FIGURES

CHAPTER 1

CHAPTER 4

LIST OF SCHEMES

LIST OF TABLES

CHAPTER 1

HIGH RESOLUTION PATTERNING OF POLYMER THIN FILMS

Abstract

Patterning of polymer thin films is of great importance in many areas of modern science and technology. This chapter highlights recent advances in the micro- and nanopatterning of two different types of polymer films. The recent success in the lithographic patterning of fluorine and siloxane containing polymers and standard commercial polymeric photoresists using supercritical carbon dioxide as a developer is described. In this case, the polymer film is spun coated and is physically attached to the surface. This chapter also introduces the concept of "polymer brushes". These are functional, high-tech coatings wherein the polymer film is chemically attached to the surface via chemical bonds. The different methods for the preparation of polymer brushes have been described. Patterned polymer brushes have a wide variety of applications. Finally, this chapter highlights recent advances in top-down and bottom-up patterning of polymer brushes using photolithography, printing techniques and direct writing techniques.

1.0 Polymer Thin Films

The surface properties of substrates can be changed dramatically by application of polymer thin films. Although corrosion protection is certainly the most basic application of surface coatings, thin organic polymer films are also applied in a large number of high-tech research fields including cell-biology, tissue engineering, medical sciences and in the development of microelectronic devices.[1-6] Polymer films even when only a few nanometers thick, can influence the surface properties of a

material so strongly that the chemical nature of the underlying material becomes completely hidden. Depending on the type of interaction between the molecules of the film and the substrate that is to be modified, two different strategies for the formation of thin polymer films can be distinguished. In one case, the molecules of the film interact with the substrate by physical forces and in the other the molecules are attached to the surface via chemical bonds.

Some of the technologically important coating techniques where the polymer film is physically adsorbed on the substrate include droplet evaporation, spray coating, spin coating, dip coating, doctor blading and the Langmuir-Blodgett technique.[7] In all these processes the polymer film is deposited from solution and the solvent evaporates leaving behind the polymeric material. Processes such as spin coating and dip coating allow the deposition of extremely thin polymer films with essentially no upper limit to film thickness. The alternate approach that allows the formation of polymer films with long term stability even in very adverse environments consists of polymers attached to the substrate via chemical bonds. These systems, referred to as polymer brushes consist of polymers attached through one end to a surface or an interface.[8] This tethering is sufficiently dense that the polymer chains are forced to stretch away from the surface to avoid overlapping. Such polymer brush systems can be prepared using the ”grafting to” or the “grafting from” approach. A detailed description of the two approaches is summarized in section 1.5.

Recent past decades have witnessed the rapid development of a broad range of strategies used to pattern polymer surfaces. Patterned polymer films are comprised of surfaces with polymeric material in well-defined regions. A great deal of interest in polymer patterning has originated due to the application of polymer-patterned surfaces in the production of integrated circuits, information storage devices, light-emitting displays (LEDs), micro-electromechanical systems (MEMS), miniaturized sensors,

microfluidic devices, biochips, micro-optical components such as gratings and photonic crystals and in bio-related and medicinal research including the study of cell-surface interactions and tissue engineering.[4, 9, 10]

These following sections describe the high resolution patterning of two different types of polymer thin films: standard spun coated polymer photoresist thin films and polymer brushes prepared by the "grafting from" approach. Environmentally benign processes are now being considered as promising alternatives to current industrial practices due to the increasing awareness of environmental issues and the economic benefits of shifting to "greener" routes. Supercritical fluids have been investigated as alternatives to conventional solvents for this purpose. Carbon dioxide is considered a "green" solvent as it is nontoxic, nonflammable and unreactive under most conditions.[11] Supercritical carbon dioxide ($scCO_2$) is a widely used solvent that can enhance the processing performance in photolithography, especially in the development step.[12] In sections 1.1 and 1.2, we first understand the properties of $scCO_2$ and describe the different thermodynamic variables affecting polymer solubility in $scCO_2$. Highlights in the area of environmentally benign development of polymer photoresists in $scCO_2$ are summarized in section 1.3.

Polymer brushes are well suited for the fabrication of nano- or micropatterned arrays with control over chemical functionality, shape and feature dimensions. These characteristics make polymer brushes attractive for a variety of applications in biological sciences and microelectronics. The concept of polymer brushes is introduced in section 1.1. The various methods of preparing polymer brushes surfaces or interfaces are described in section 1.5. In final section 1.6, we highlight recent advances in the top-down and bottom-up patterning of polymer brushes using various photolithographic techniques, printing techniques and direct writing techniques.

1.1 Supercritical Carbon Dioxide: An Introduction

Rapid technology advances and rapid growth have historically been the basis for the success of the semiconductor industry. Over the last 30 years the industry has enjoyed a growth rate (~ 15 %) which far exceeds the growth rate of the U.S. economy overall (~ 4 %).[13] To ensure that this rapid growth can be sustained into the future, it is important that the industry makes efficient use of the available natural resources and minimizes its impact on the environment. A typical semiconductor processing line produces more than 1 L of waste solvent and 1 L of contaminated rinse water to process one silicon wafer.[14, 15] The use of any replacement solvent that would make the lithography process more environmentally benign would be highly desirable.

Carbon dioxide is often promoted as a sustainable solvent as CO_2 is non-flammable, relatively non-toxic, relatively inert and is naturally abundant. The use of carbon dioxide as a solvent has been investigated somewhat continuously in academia and industry since the 1950s. The PVT properties of CO_2 have been known since the 1930s and extensive data is available in the literature in the form of correlations of density, viscosity, dielectric constant etc as functions of temperature and pressure.[16]

Carbon dioxide is non-flammable, a significant safety advantage in using it as a solvent. It is also naturally abundant, with a TLV (threshold limit value for airborne concentration at 298 K to which a worker may be repeatedly exposed without adverse effects) of 5000 ppm. Hence, CO_2 is much less toxic than many other organic solvents such as acetone (TLV of 750 ppm), pentane (TLV of 600 ppm) and chloroform (TLV of 10 ppm).[16] Another process and environmental advantage of using CO_2 is that it is relatively inert towards reactive compounds. Hence byproducts due to side reactions with CO_2 are relatively rare. CO_2 is a naturally abundant material. Like water, CO_2 can be withdrawn from the environment, employed in a process and then returned to the environment.

Over the past decade there has been a growing interest in using supercritical fluids (SCFs) as environmentally benign solvents for the synthesis and processing of polymeric materials.[17-19] This has been due to the unique properties of supercritical fluids, such as high diffusivities, comparable to those of gases, their liquid like densities and also the ability to control their densities and hence their solvating powers by the simple manipulation of pressure and temperature.

A supercritical fluid is defined as a substance at a temperature and pressure above its thermodynamic critical values. The pressure-temperature phase diagram for a pure component showing the SCF region is illustrated in Figure 1.1. Darr and Poliakoff offer a more practical definition whereby a supercritical fluid is described as "any substance, the temperature and pressure of which are higher than their critical values, and which has a density close to or higher than its critical density".[19] Close to the critical density, SCFs display properties that are to some extent intermediate between those of a liquid and a gas. A comparison of typical values for density, viscosity and diffusivity of liquids, gases and SCFs is presented in Table 1.1.[20] Under supercritical conditions, these substances exhibit properties such as high diffusivity, zero surface tension and can be tuned to achieve the desired density and solvent properties. Figure 1.2 (a) shows a graph of the variation in density of pure CO_2 at 35 °C. At this temperature there is a rapid but continuous increase in density near the critical pressure. Figure 1.2 (b) is a schematic representation of the change from liquid-gas equilibrium ($T < T_c$) to supercritical fluid conditions ($T \geq T_c$) as a substance is heated above its critical temperature at a pressure above P_c. Supercritical carbon dioxide ($scCO_2$) has the added advantage of having an easily accessible critical point (T_c =31.1 °C, P_c = 72.8 atm).

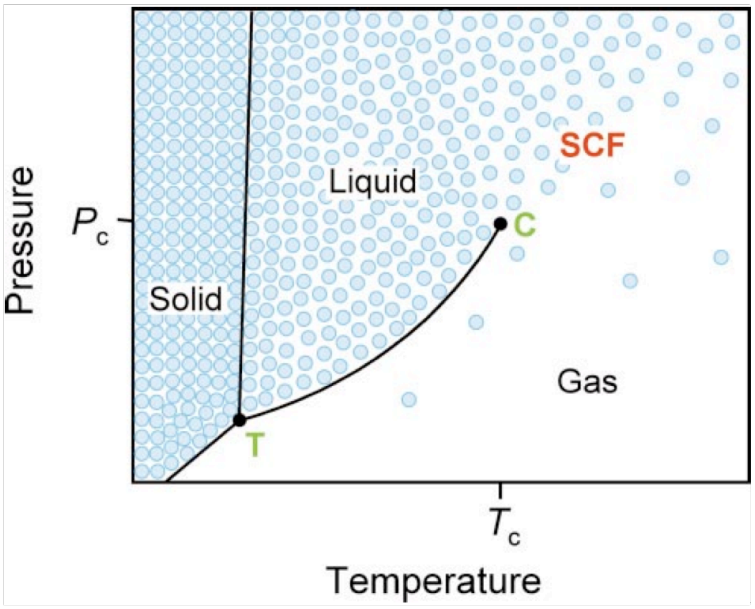

Figure 1.1 Schematic pressure-temperature phase diagram for a pure component showing the supercritical fluid (SCF) region. The triple point (T) and critical point (C) are marked. The blue circles represent the variation in density of the substance in the different regions of the phase diagram. Note that the density varies continuously between the liquid state and the gas state, providing that the liquid-gas equilibrium line (T-C) is not crossed. (Reprinted from Ref. # 19 with permission from the Royal Society of Chemistry)

Table 1.1 Comparision of physical and transport properties of gases, liquids and SCFs. (Reprinted from Ref. # 20 with permission from Dr. Edit Székely)

	Density (kg/m^3)	**Viscosity (μPa•s)**	**Diffusivity (mm^2/s)**
Gases	1	10	1-10
SCFs	100-1000	50-100	0.01-0.1
Liquids	1000	500-1000	0.001

$scCO_2$ has been used for several years in the food and fragrance industries for numerous separation processes, including decaffeination of coffee.[21, 22] More recently, $scCO_2$ has proved to be useful as a reaction medium for polymer synthesis and for the delivery of coating materials, in the fabrication of biomaterials for drug delivery and tissue engineering and as a processing solvent in the field of microelectronics.[12, 18, 19, 23]

1.2 Solubility of Polymers in $scCO_2$

In spite of all the advantages of using $scCO_2$, it remains a challenge to predict the solvent properties of CO_2 quantitatively. While CO_2 is a good solvent for many non-polar (and some polar) molecules with low molecular weights, it is a very poor solvent for most high molecular weight polymers under readily achievable conditions. The only polymers shown to have good solubility in pure CO_2 under mild conditions are certain amorphous fluoropolymers and silicones.[24-30] To form a stable polymer-SCF solvent solution at a given temperature and pressure, the Gibbs free energy must be negative and at a minimum. The Gibbs free energy of mixing is

$$\Delta G_{mix} = \Delta H_{mix} - T\Delta S_{mix} \qquad (1.0)$$

where ΔH_{mix} and ΔS_{mix} are the change in enthalpy and entropy, respectively, on mixing. Generally, the combinatorial entropy always promotes the mixing of a polymer with a solvent since this is usually associated with an increase in entropy. The polymer will dissolve only if the energetics of polymer-segment interactions outweigh polymer segment-segment and solvent-solvent interactions.[31] The interchange energy of mixing i–j pairs, ω, is given by

$$\omega = z[\Gamma_{ij}(r,T) - \frac{1}{2}(\Gamma_{ii}(r,T) + \Gamma_{jj}(r,T))] \qquad (1.1)$$

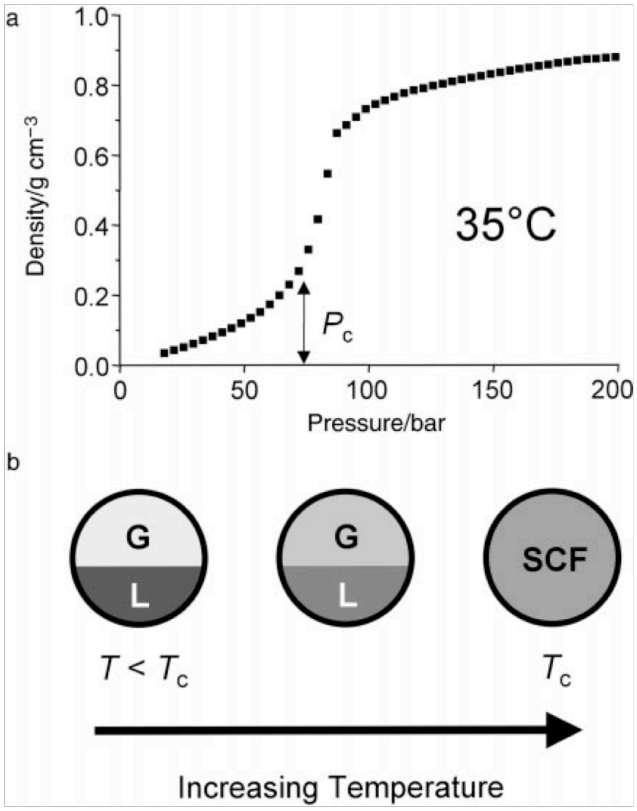

Figure 1.2. (a) Graph showing the variation in density of pure CO_2 at 35 °C. At this temperature (*i.e.*, close to T_c for CO_2) there is a rapid but continuous increase in density near the critical pressure (P_c). (b) Schematic representation of the change from liquid-gas equilibrium ($T < T_c$) to supercritical fluid ($T \geq T_c$) conditions as a substance is heated above its critical temperature at a pressure in excess of P_c. (Reprinted from Ref. # 20 with permission from the Royal Society of Chemistry)

where z is the coordination numbers or number of different pairs in solution, r is the distance between the two molecules and T is the absolute temperature.

The pressures and temperatures needed to dissolve a polymer in CO_2 depend on the intermolecular forces in operation between solvent-solvent, solvent-polymer segment, polymer segment-segment pairs in solution and on the free volume difference between the polymer and CO_2. McHugh and co-workers have used approximate expressions that reveal the important physical properties of both the polymer and CO_2 that govern whether a polymer will polymer will dissolve in CO_2.[32] The following simplified expression shows how the intermolecular potential energy of an i–j pair of segments and molecules, Γ_{ij}, depends on the physical properties of the polymer and the solvent.

$$\Gamma_{ij}(r,T) \approx -C_1\frac{\alpha_i\alpha_j}{r^6} - C_2\frac{\mu_i^2\mu_j^2}{r^6kT} - C_3\frac{Q_i^2Q_j^2}{r^{10}kT} - C_4\frac{\mu_i^2Q_j^2}{r^8kT} - C_5\frac{\mu_j^2Q_i^2}{r^8kT} + complex\ \ formation \qquad (1.2)$$

where subscripts i and j represent CO_2 and a segment of the polymer, respectively. The equation suggests that the intermolecular interaction depends on the polarizabilities (α), the dipole moments (μ) and on the quadrupole moments (Q) of the two interacting molecules. The dispersion interactions, dipole interactions and quadrupole interactions contribute to the overall interaction energy between CO_2 and the polymer. The last term in equation 1.2 represents complex formation. In this equation k is the Boltzmann's constant and $C_{1\text{-}5}$ are fixed constants. The interested reader is referred to a more comprehensive discussion of polymer solubility in $scCO_2$ in a review article by Kirby and McHugh.[33]

Carbon dioxide has a low dielectric constant and its polarizability is close to gases such as methane, perfluoromethane and fluoroform.[19] Due to its symmetric structure, CO_2 does not have a dipole moment, but it does have a substantial quadrupole moment that operates over a much shorter distance than dipole interactions. It has been argued that the solvent properties of CO_2 may be compared to those of toluene, acetone and hexanes.[34, 35] Spectroscopic techniques have been used to characterize the interactions between CO_2 and polymers.[36] This work has demonstrated that polymers possessing electron donating functional groups like carbonyl groups, show specific interactions with CO_2. It is believed that this complex formation is most probably a Lewis acid-base type interaction, where the carbon atom of CO_2 acts as an electron acceptor and the carbonyl oxygen in the polymer as an electron donator.[37] The strength of this CO_2-segment complex is shown to be less than 1 kcal/mol. Hence introduction of a degree of polarity in the polymer chains tends to increase the solubility in $scCO_2$, however, high pressures and temperatures are required to dissolve non-fluorinated materials. It has been shown that fluorinated groups play an important role in polymer solubility. This is attributed to the preferential clustering of CO_2 near the fluorine atom of the C–F bonds, which are more polar than C–H bonds.[36, 38] It is proposed that the fluorinated side groups help shield the hydrocarbon main chain from interacting with the $scCO_2$ solvent. The solubility of silicones has been attributed to the flexible nature of these polymers.[33] These flexible polymers result in a large entropy of mixing with much larger free volumes in comparison to other polymers.

Several different equations of state have been developed and used to calculate polymer-SCF solvent phase behavior. These models help simulate and predict the changes in phase behavior observed as a function of solvent quality or as a function of polymer architecture with a minimum number of fitted parameters. Two widely used

equations in polymer solution thermodynamics are Sanchez-Lacombe Equation of State[39, 40] and the Statistical Associating Fluid Theory (SAFT)[41]. The description of these equations is beyond the scope of this thesis. For an elaborate discussion on this topic, readers are referred to the many articles cited in the review paper by Kirby and McHugh.[33]

1.3 Processing of Patterned Polymers in $scCO_2$

As lithography in the industry progresses to the 45 nm node and smaller, overcoming the inherent challenges at such small dimensions becomes more difficult. Many of the conventional photoresists of today are based on similar chemistries that render them exclusively positive tone using aqueous base development. However, negative tone patterning has the appeal of reducing overall exposure flare, an effect that becomes more pronounced at smaller dimensions.[42] It would therefore be appealing to be able to transform the positive working, high resolution chemically amplified photoresists into a negative tone system.

As a very selective, non-polar solvent, $scCO_2$ is an ideal fit for developing existing photoresist platforms as negative tone systems. Supercritical CO_2 is environmentally benign and has been explored for multiple aspects of device fabrication including drying, cleaning, deposition and etching.[43-46] Several authors have demonstrated the benefit of a final $scCO_2$ development step in avoiding pattern collapse.[47] These studies that combined both theory and experiment showed that the supercritical properties of CO_2 were ideal for development of small scale structures without suffering from the very strong capillary forces that lead to pattern destruction or distortion. Another important problem faced by lithographers is that of line edge roughness (LER). LER is typically 10 % of the critical dimension. Hence, as we move to the 32 nm node and below, the improvement or elimination of LER becomes a big

challenge. LER may be attributed to a number of factors including aerial image contrast, resist molecular size, acid segregation and acid diffusion.[48] The problem of LER is intimately associated to that of finite-size behavior and anti-plastification. As a solvent that can readily plasticize or conceivably antiplasticize glassy substrates, $scCO_2$ presents itself as a possible tool to smooth inherent LER during development. This can be done by fine tuning the development conditions to plasticize the outer skin alone of the photoresist line during and after development. The use of $scCO_2$ as a processing solvent effectively combines the development and drying steps and can also be used in photoresist stripping processes.

Another key issue for sustainable growth of the semiconductor industry is water conservation. Based on water usage data for 23 fab from 1999 to 2001, the average 8 inch wafer fab consumes 1.8 million gallons of water per day.[13] This is equivalent to the daily water consumption of approximately 6000 single family homes. As the computer chip complexity has increased, the rising number of metal layers require more cleaning steps. Currently, there is great interest in the application of $scCO_2$ for photoresist removal in the backend of the process. While these processes are still being perfected, they promise to replace the use of organic solvents with carbon dioxide. In the remaining section, the development of fluorine- and siloxane containing polymers in $scCO_2$ has been highlighted. We also discuss the development of non-fluorinated standard photoresists in $scCO_2$ using CO_2 compatible salts. It must be noted that, although CO_2 is strongly implicated in global climate warming, in the application discussed here, CO_2 is *not being generated*, but simply captured and employed.

Siloxane-containing polymers were one of the very first $scCO_2$ processable photoresists. An early attempt to construct photoresists that could be processed in $scCO_2$ was based on the oxidation of poly(silanes) to poly(siloxanes), by the

photoinduced insertion of oxygen. These insoluble polymers transformed to being soluble in $scCO_2$ and were successfully imaged as positive tone photoresists.[49] Ober et al. reported several imageable copolymers as negative tone $scCO_2$ developable photoresists produced from a combination of t-butyl methacrylate (t-BMA) with 3-methylacryloxy propylpentamethyldisiloxane (SiMA) or pentafluoropropyl methacrylate (PFM).[50] Although poly(t-BMA) homopolymer is insoluble in $scCO_2$, the copolymers of t-BMA with SiMA and PFM showed good solubility in the supercritical solvent. The authors compared random copolymers of PFM and t-BMA with random copolymers of SiMA and t-BMA and the corresponding SiMA/t-BMA block copolymers. The structures of some of the polymers used are shown in Scheme 1.1. It was also observed that the solubility of SiMA/t-BMA copolymers in $scCO_2$ increased with an increase in the weight fraction of SiMA in the copolymer, indicating that composition plays an important role in $scCO_2$ solubility. The block copolymers (having 57 and 70 wt % SiMA) demonstrated excellent sensitivity and good contrast with 6 wt % of triphenylsulfonium hexafluoro antimonate as photoacid generator (PAG) after development in $scCO_2$. Sundararajan *et al.* utilized the high solubility of fluorinated block copolymers to develop an environmentally friendly lithographic process using $scCO_2$. Block polymers of tetrahydropyranyl methacrylate (THPMA) and perfluorinated methacrylate were synthesized using group transfer polymerization.[51] Chemical amplification using acid-cleavable tetrahydropyranyl groups was used to effect the polarity change in $scCO_2$. The imaging mechanism of these polymers is shown in Figure 1.3 (a). The block copolymers containing a very non-polar fluoropolymer block are soluble in $scCO_2$. After exposure to radiation, the THPMA block converts to a more polar methacrylic acid, which is insoluble in $scCO_2$. Using these polymers negative tone patterns as small as 0.2 μm could be obtained in $scCO_2$ at temperatures < 80 °C and pressures < 7000 psi. Figure 1.3 (b) shows the

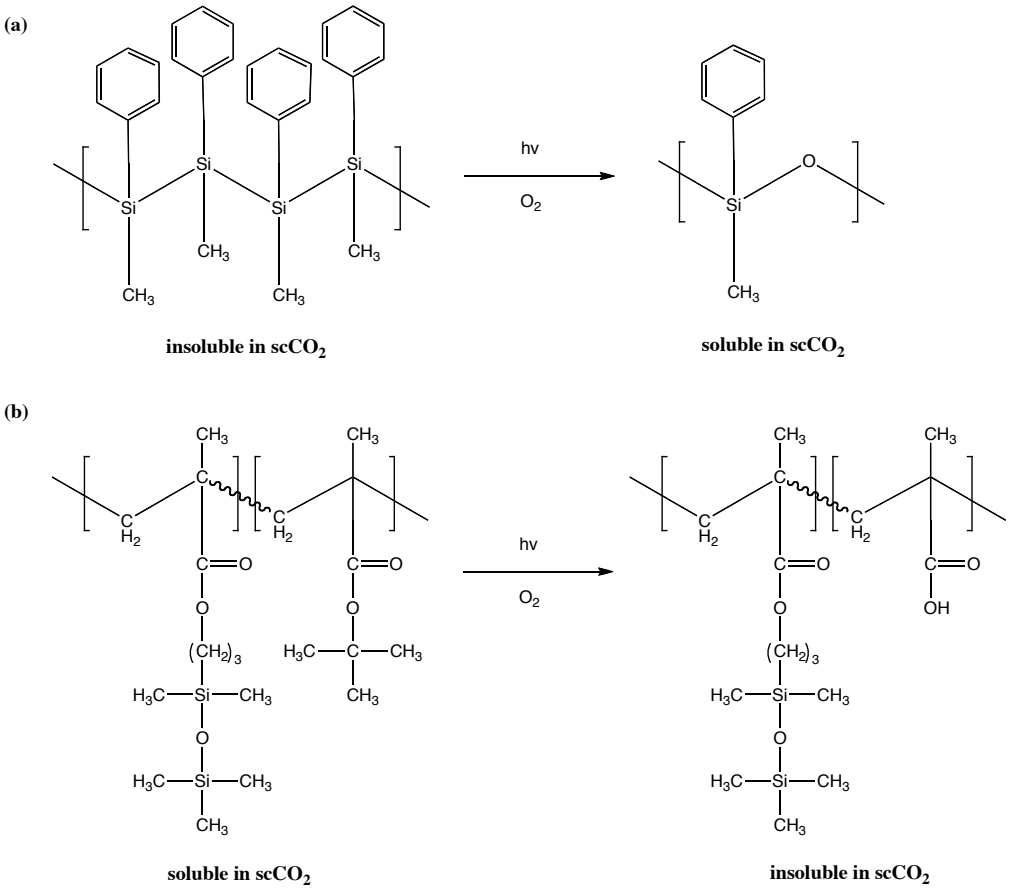

Scheme 1.1 Mechanism of solubility change of (a) polysilane and (b) poly(t-BMA-b-SiMA) by photoinduced reactions. PAG stands for photoacid generator. (Adapted from Figure 1 of Ref. # 50).

features resolved using THPMA-b-F7MA using 193 nm exposure and $scCO_2$ development. The authors also noted that the polarity of the PAG affects the sensitivity of the polymer photoresist. With a polar PAG such as bis(tert-butyl phenyl) iodonium triflate (t-BIT) the sensitivity of THPMA-b-F7MA was 4 mJ/cm^2 . The sensitivity of the same polymer with a non-polar PAG such as 2,6-dimethyl-4-(bromophenyl) perfluorooctyl sulfonate was 23 mJ/cm^2. This has been attributed to the reduction in effective concentration of the PAG due to the preferential aggregation of the non-polar PAG in the fluoroblock microdomains.

Using the same block copolymer system, Pham et al. described a method to create a positive tone photoresist by in situ chemical modification of THPMA-b-F7MA through silylation.[52] Exposure at 248 nm of these block copolymers containing PAG resulted in the generation of acids in the exposed regions. During the post-exposure bake, the acid cleaved the tetrahydropyranyl protecting groups, resulting in methacrylic acid with significantly decreased solubility in $scCO_2$. During subsequent silylation, hexamethyldisilazane (HMDS) or tetramethyldisilazane (TMDS) vapors diffused into the film to react with the free carboxylic acid groups, forming $O{-}Si(CH_3)_3$. This functionalization rendered the polymer soluble in $scCO_2$ due to the favorable interaction between the organosilicon groups and CO_2. On subsequent UV flood exposure, THP protecting groups were cleaved everywhere except in the originally patterned regions to render the exposed polymer insoluble in $scCO_2$. Therefore, with silylation and subsequent UV flood exposure, positive tone patterns down to 400 nm lines/spaces could be obtained. The lithographic performance of the photoresist was improved by using TMDS instead of HMDS. It was suggested that the enhanced diffusion and better interaction of TMDS with the polar carboxylic acids resulted in remarkable improvement in performance. The negative and positive tone images of THPMA-F7MA random copolymer photoresist patterned by 248 nm

(a)

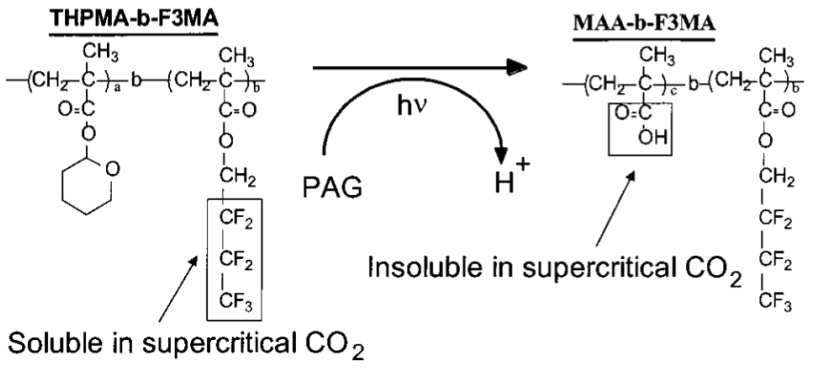

(b)

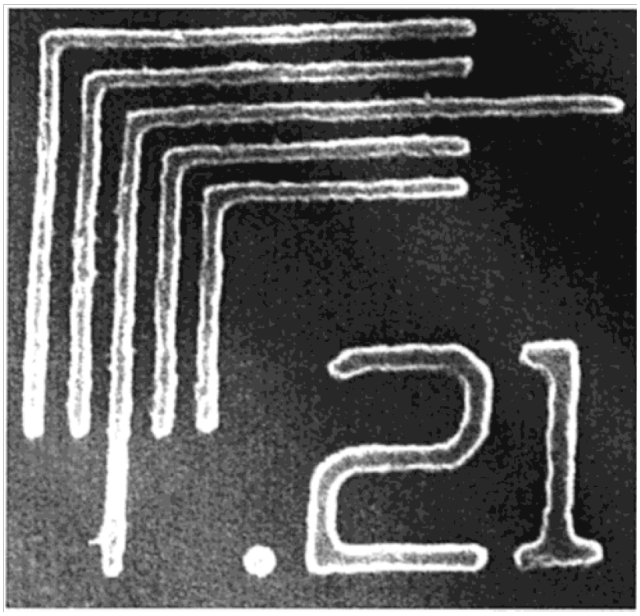

Figure 1.3 (a) Imaging process of the negative tone $scCO_2$ developable photoresists. (b) Features resolved using THPMA-F7MA copolymers using 193 nm exposure and $scCO_2$ development. (Reprinted from Ref. # 51 with permission from the American Chemical Society)

exposure are shown in Figure 1.4.

Though successful, the above mentioned fluorinated methacrylate polymers lack the adequate plasma etch resistance needed to protect the underlying substrate. It has been reported that copolymers of 1H,1H-perfluorooctyl methacrylate and THPMA etch at 2.5 times the rate of the commercially available, Shipley 1813 Novolac photoresist in the presence of an oxidizing plasma.[53] DeSimone and co-workers examined norbonene based polymers with highly fluorinated side groups. The allicyclic backbone of norbornene polymers were predicted to be more etch resistant based on the Ohnishi parameter and the ring parameter.[53] Addition copolymers of (Norbornyl)-1H,1H-perfluorooctyl acrylate (NBFOA) and (Norbornyl)-1,1,1-trifluoro-2-tri-(fluoromethyl)propan-2-ol (NBHFA) were synthesized using an allylpalladium dimmer catalyst. Scheme 1.2 shows the synthesis of the fluorinated addition copolymers. The hydroxyl groups were protected with a chemically amplified protecting t-butoxycarbonate (t-boc) group. Lithographic images were obtained using a 193 nm exposure, followed by development in $scCO_2$ at 135 bar for 5 min with a dynamic flow of CO_2 through a backpressure regulator, set at 20 psi. Using this approach, dense lines as small as 3 μm could be resolved. Images smaller than 3 μm had significant LER. There have been lots of efforts to tailor make $scCO_2$ processable polymer photoresists.

The examples presented above are some of the many efforts towards the use of polymer photoresists tailored towards $scCO_2$ development. Recently, several researchers have reported the ability to develop conventional polymeric photoresists in $scCO_2$. Mao *et al.* demonstrated the use of hydrocarbon alcohols and acetone as cosolvents, combined with $scCO_2$ to process standard photoresists. This work involved chemical vapor deposition (CVD) for applying photoresists on substrates. Patterning of CVD thin films using $scCO_2$ development was first explored in the CVD of

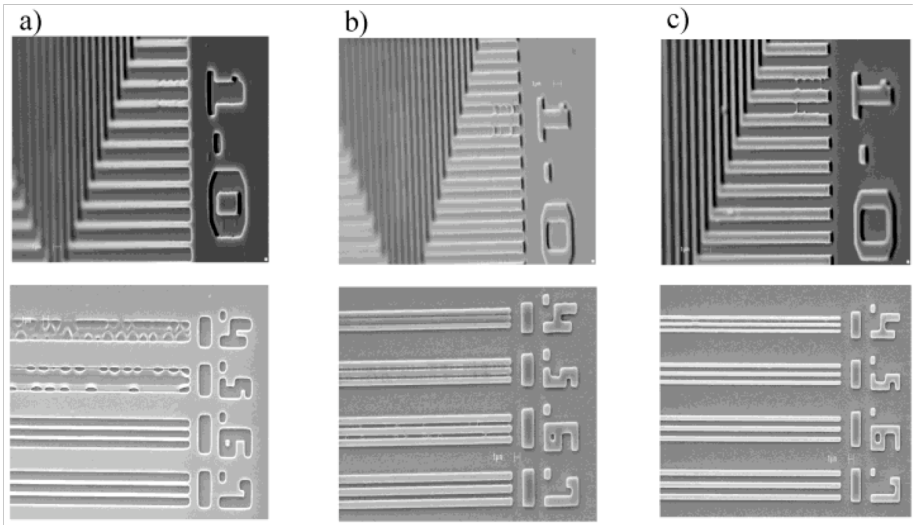

Figure 1.4 THPMA-F7MA random copolymer photoresist patterned by 248 nm exposure: (a) $scCO_2$ processed negative tone images, (b) positive tone images processed after silylation with HMDS and (c) positive tone images processed after silylation with TMDS. (Reprinted from Ref # 52 with permission from the American Chemical Society).

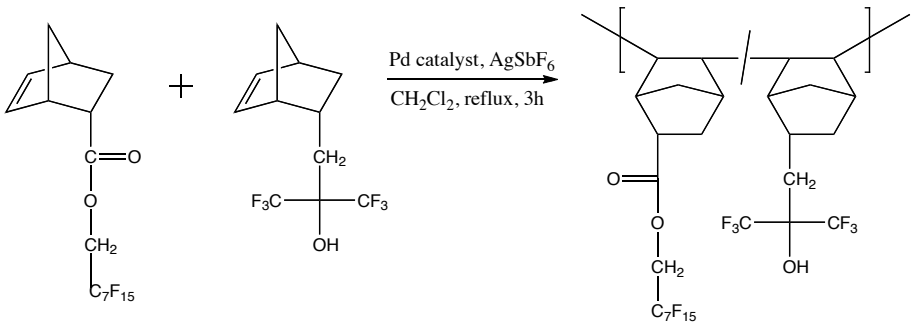

Scheme 1.2. Synthesis of fluorinated addition copolymer of (norbornyl)perfluorooctyl acrylate (NBFOA) and (norbornyl)-1,1,1-trifluoro-2-tri(fluoromethyl)propan-2-ol (NBHFA). (Adapted from Scheme 1 of Ref # 53)

poly(tetrafluoroethylene) (PTFE) thin films.[54] Using e-beam lithography, followed by $scCO_2$ development, lines/spaces patterns of 1 μm could be obtained. However, the dosage required for development of PTFE (6000 $\mu C/cm^2$) was two orders of magnitude higher than the dosage of common e-beam resists. $scCO_2$ developable e-beam photoresists of higher sensitivity were prepared by initiated chemical vapor deposition (iCVD). iCVD can facilitate reactions under mild processing conditions by thermal decomposition of an initiator and subsequent addition reaction of monomers. Copolymerization of glycidyl methacrylate (GMA) with 2,2,3,3,4,4,5,5,6,6,7,7-dodecafluoroheptyl acrylate (DFHA) gave a negative tone photoresist.[55] The crosslinking chemistry of epoxy groups in poly(GMA-DFHA) thin films created a negative tone contrast. Using this polymer, features down to 300 nm lines could be obtained after $scCO_2$ development with 2 vol. % ethanol added as a cosolvent. Positive tone patterning with 300 nm resolution could be obtained through anhydride stabilized chain-scission reactions in post-annealed copolymers of methacrylic acid (MMA) and perfluoroalkylethyl methacrylate (PFEMA).[55]

More recently, Carbonell and co-workers showed that the inclusion of certain surfactants into $scCO_2$ imparts solubility to otherwise insoluble polymeric resists. They reported the use of a CO_2 compatible salt (CCS) in homogeneous $scCO_2$ solution to dissolve the unexposed portions of a positive tone EUV photoresist obtained from Tokyo Ohka Kogya (TOK), resulting in reverse image development.[56-58] The authors propose that the salts enter both the exposed and unexposed regions of the photoresist, but the presence of deprotected acid groups inhibits dissolution in the exposed regions, thereby leading to negative tone development in $scCO_2$. Most of these surfactants are based on fluorinated salts. Using this approach they developed standard EUV photoresists with CCS in $scCO_2$. Figure 1.5 (a) shows the SEM images comparing line/space (L/S) feaures of standard EUV resist developed with TMAH (A) and CCS

in $scCO_2$ (B). Image A shows 160 nm patterned L/S features that were developed with the standard TMAH process to a critical dimension (CD) of 123 nm and image B shows 130 nm patterned features developed with CCS in $scCO_2$ to a CD of 61 nm. The sample developed with TMAH showed pattern collapse at an aspect ratio of 4.5, while the sample developed in CCS/$scCO_2$ showed no pattern collapse with an aspect ratio of 9. Figure 1.5 (b) shows SEM images to compare the EUV photoresist development with standard TMAH process (A & B) with CCS/$scCO_2$ development (C & D). The difference between normal positive tone development and reverse image development was clearly observed when comparing the same isolated features developed with TMAH (A) and CCS/$scCO_2$ (C). Images (B) and (D) are patterned 200 nm L/S features. The kinetics of the CCS/ $scCO_2$ development was modeled using simplified rate equations. The authors used a high pressure quartz crystal microbalance to study the effects of temperature, mass transfer, pressure and CCS concentration on the photoresist removal rate.[56] In a recent report, Felix and Ober reported a polymeric material free from fluorinated or silicone containing groups, based on acid catalyzed cleavage of acetal linkages.[59] The polymer photoresist was synthesized by stepwise addition of the dihydroxy(bisphenol) compounds and a divinyl ether compound to form acetal linkages. The exposed films were developed in $scCO_2$ at 40 °C and 140 bar for 5 min. These polymers were successfully patterned down to 200 nm lines in $scCO_2$.

A lot of progress has been made in the last couple of decades in the processing of polymers in $scCO_2$ in lithographic procedures. Some of the recent reports mentioned above suggest that the use of $scCO_2$ as a processing solvent presents a range of interesting opportunities in materials chemistry.

(a)

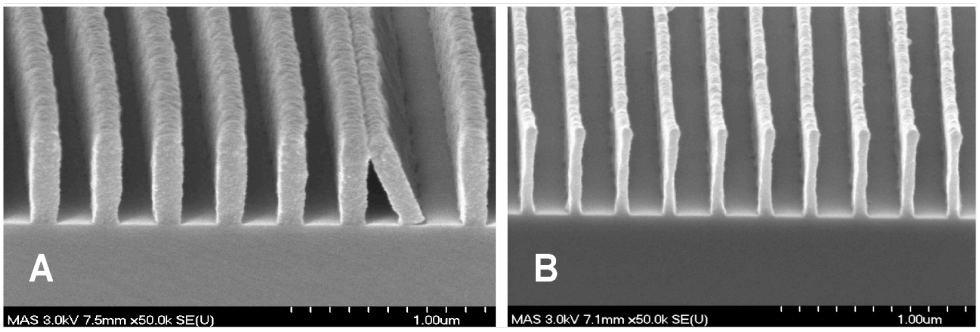

(b)

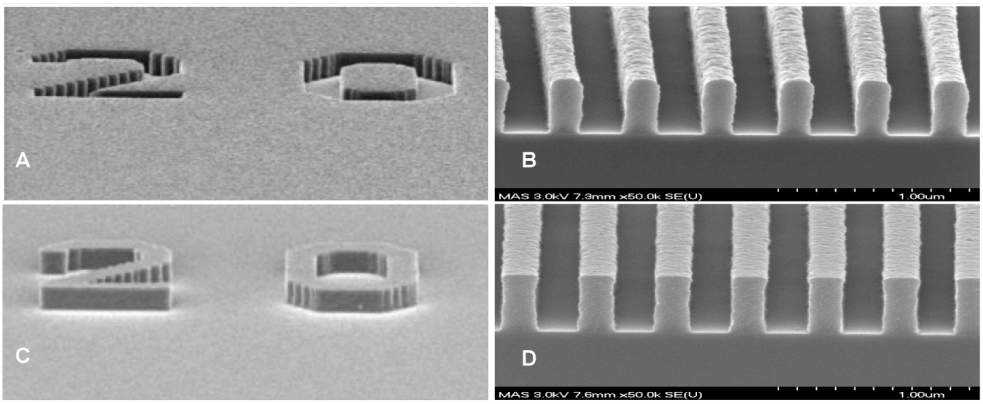

Figure 1.5 (a) SEM images comparing L/S features of a standard EUV photoresist developed with TMAH (A) and CCS/$scCO_2$ solution (B). Image A shows 160 nm patterned L/S features with a CD of 123 nm. Image B shows 130 nm patterned features with CD of 61 nm. (b) SEM images comparing EUV resist developed with standard TMAH process (A,B) and with CCS chemistry in $scCO_2$ (C,D). The difference between normal positive tone development and reverse image development is observed in A and C. Images B and D are patterned 200 nm L/S features development of standard EUV photoresist in $scCO_2$ using CCS makes EUV lithography a more viable process for next generation lithography. (Reprinted from Ref. # 56 with permission from the American Chemical Society)

1.4 Introduction to Polymer Brushes

Polymer brushes refer to an assembly of polymer chains that are tethered by one end or with a few anchor points to a surface or an interface.[2, 8, 60] This tethering is sufficiently dense that the polymer chains are crowded and forced to stretch away from the surface to avoid overlapping. The stretched polymer chains look like bristles of a brush, hence the name. These stretched configurations are observed without any confined geometry or an external field. Depending on the grafting density of the polymer chains, different possible conformations of the surface attached polymers are observed. Figure 1.6 is a schematic representation of the "mushroom", "pancake" and "brush" conformations of surface attached polymers. If the distance between two points of attachment is larger than the size of the attached polymers, the polymer segments behave like single chains. In this case there is minimal or no interaction between the polymer segments. If the polymer chains tend to get adsorbed strongly to the surface they form a "pancake" like conformation. However, if the interaction between the polymer and substrate is weak, then the polymer chains form a random coil that is attached to the surface by one end. This is called the "mushroom" conformation. A very different conformation is observed if the polymer chains are attached close to each other such that the polymer chains tend to overlap. In order to minimize the polymer segment-segment interaction, the polymers stretch away from the surface perpendicular to the surface. This is called the "brush" conformation.

A theoretical description of polymer brushes has been done using self-consistent field calculations and by computer simulation. Alexander and de Gennes did some pioneering work on the theoretical analysis of end tethered polymers on flat surfaces.[61-64] The polymer chains comprising a polymer brush system are often considered deformed. This deformation of densely tethered polymer chains reflects a balance between the interaction energy of the statistical segments (F_{int}) and the elastic

free energy (F_{el}).The high density of attached polymers forces a strong overlap between the polymer chains. This results in an increase in interaction energy. Stretching lowers the interaction energy per chain at the price of a high elastic free energy. It is the interplay between these two terms that determines the equilibrium thickness of the polymer brush. A simplified equation using the Alexander model[61] for the free energy of per chain is given as

$$F = F_{int} + F_{el} \tag{1.3}$$

A more precise expression for the free energy is obtained using the "Flory approximation" that estimates the reduction in entropy from results for an ideal random walk chain, constrained to travel from the surface to the outer edge of the polymer brush.[65] Based on this method, the free energy per chain is expressed as

$$\frac{F}{kT} \approx \frac{\nu\varphi^2 d^2 L}{a^3} + \frac{L^2}{R_0^2} \tag{1.4}$$

here, a is the diameter of the polymer segment, d is the average distance between two tethering points, L is the distance of the outer edge of the brush from the grafting surface, R_0 is the radius of an ideal coil and ν is a dimensionless volume parameter. These theoretical considerations demonstrate that the equilibrium thickness of the polymer brush varies linearly with the degree of polymerization, a novel behavior of tethered polymers. The polymer chains exhibit deformed configuration, irrespective of whether the polymer brush is in the presence of a good solvent, theta solvent or a bad solvent. More sophisticated models have been developed to describe the segment density profile of the brushes. For a more detailed description on this topic, the reader is referred to the review article by Zhao and Brittain.[2]

Based on their chemical composition, polymer brushes can divided into

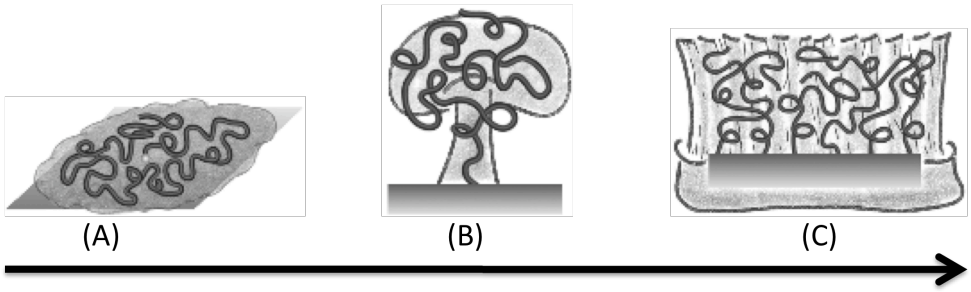

Figure 1.6. Schematic representation of the formation of (A) "pancake", (B) "mushroom" and (C) "brush" conformations of surface attached polymers with increase in grafting density. (Adapted from Ref # 83 with permission from Wiley-VCH Verlag GmbH & Co. KGaA, Weinheim)

homopolymer brushes, mixed homopolymer brushes, block copolymer brushes and random copolymer brushes. Homopolymer, random copolymer and block copolymer brushes are named according to the type of polymers attached to the surface. Mixed homopolymer brushes comprise of two or more types of homopolymers on the surface. Homopolymer brushes can be further categorized into neutral polymer brushes and charged polymer brushes. Depending on the rigidity of the polymer chains, polymer brushes are classified as flexible, semi-flexible and liquid crystalline polymer brushes.

One of the very first applications of polymer brushes, realized in the 1950s was for the stabilization of colloidal particles. Over the years, polymer brushes have found use in a number of applications such as in the development of new adhesive materials[66, 67], biosurfaces (implants, biomaterials, biosensors)[68-70], nonfouling biosurfaces[71, 72] and in chromatographic separation,[73] membranes,[74] polymer stabilization and compatiblization.[75] Recently, they have been used to prepare surfaces for electronics and in micro- and nanofluidic devices.[76] Figure 1.7 is a cartoon representation of three different types of polymer brushes. Amphiphilic polymer brushes are used as nonbiofouling coatings. Dendrimeric polymer brushes have shown potential to be used in the development of drug delivery systems and liquid crystalline brushes may be used to design nematic display devices. Thus, the impact of polymer brushes on future applications holds great promise.

1.5 Synthesis of Polymer Brushes

Based on the type of attachment between the polymer chains and the surface, there are generally two ways to fabricate polymer brushes: physisorption and covalent attachment. Polymer brushes synthesized by physisorption of polymers generally consist of diblock copolymers, where one part strongly adheres to the surface. An

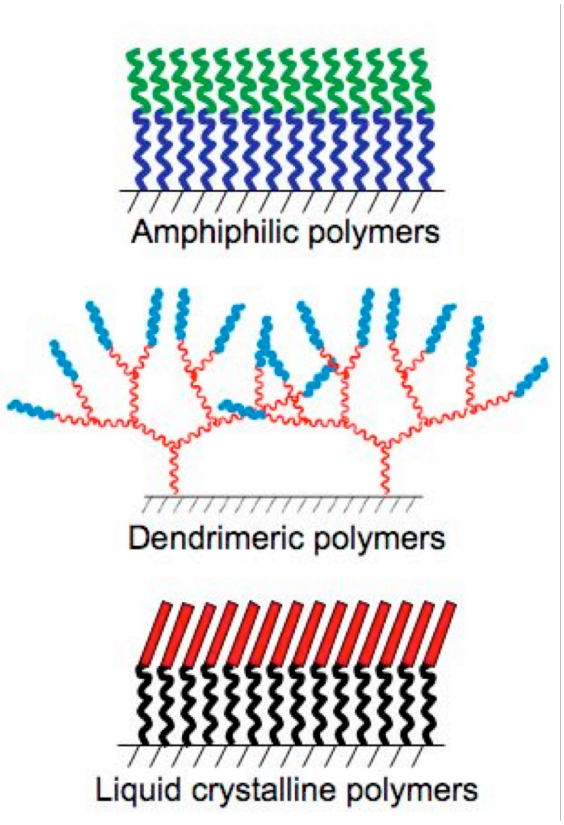

Figure 1.7. Schematic representation of an amphiphilic diblock copolymer brush, a dendrimeric polymer brush and a liquid crystalline polymer brush. Different polymer brush structures find applications in a wide range of applications.

ideal solvent is chosen which is a bad solvent for the block that forms the anchor layer and a good solvent for the other block that forms polymer brushes. Some examples of this type of polymer brushes are poly(styrene-b-2-vinyl pyridine) adsorbed silica, alumina or mica in toluene.[77] Here, poly(2-vinyl pyridine) (PVP) forms the anchor layer while poly(styrene) (PS) blocks formed a brush. In another example, poly(styrene-b-ethylene oxide) adsorbed onto silicon and quartz surface, more polar poly(ethylene oxide) (PEO) showed stronger adsorption on the surface than the nonpolar PS.[78]

Physisorption is a reversible process. There is very little control on the grafting density and the polymer brush thickness. The polymer brush structure depends on the solvent, the length of each block of the copolymer and on the interaction between the blocks and the surface. Polymer brushes synthesized using this approach exhibit thermal and solvolytic instabilities. If these polymer films are heated above the glass transition temperature (T_g) of the polymer, dewetting occurs due to formation of polymer droplets.[79]

There is lot more control over the synthesis of homogeneous polymer brushes by covalently grafting chains either by the "grafting to" or the "grafting from" technique. In the "grafting to" technique, preformed polymers are allowed to tether to the surface via a chemical bond between the polymer end group and the active site on the surface. The various polymerization methods give polymers with narrow molecular weight distributions which allow the formation of a uniform polymer brush. The "grafting to" technique gives a polymer brush with low grafting density and low brush thickness. This characteristic occurs because steric hindrance inhibits the diffusion of large polymer chains through the existing polymer film to reach the reactive sites on the surface. Several papers have been published describing the synthesis of polymer brushes using the "grafting to" approach.[2, 80-83] The limitations of

the "grafting to" technique can be overcome with the "grafting from" approach. This approach is also known as surface-initiated polymerization (SIP). SIP has gained considerable interest in recent years and is now the method of choice for the preparation of dense, thick polymer brushes. This approach now involves the immobilization of an initiator containing self-assembled monolayers (SAM)[84] on the surface. Then the desired monomer is polymerized from the surface to obtain the polymer brush. Figure 1.8 is an illustration of the different approaches to attach polymers on surfaces. Early work involved the immobilization of the initiator on the surface by treating the surface with plasma or glow discharge treatment.[85, 86] Rühe and coworkers reported a new strategy of immobilizing initiator on the surface in a single step from initiator solution.[87] Since then, this has been the widely accepted method of preparing initiator coated surfaces.

The grafting density (σ, chains per nm^2) of polymer brushes is calculated using the following equation:

$$\Gamma = h \times \rho$$

$$\sigma = \frac{(6.023\Gamma \times 100)}{M_n} \qquad (1.5)$$

where Γ is the surface coverage in mg m^{-2}, h is the polymer brush thickness and ρ is the density of the polymer.[88] The study of polymer brushes extends into the field of physics, chemistry and materials science and engineering. Thousands of papers have been published on polymer brushes and their applications. There are several examples of surface initiated polymerization using group transfer polymerization (GTP), conventional radical polymerization,[89] iniferter,[90] ring-opening,[91] cationic,[92] anionic,[93]

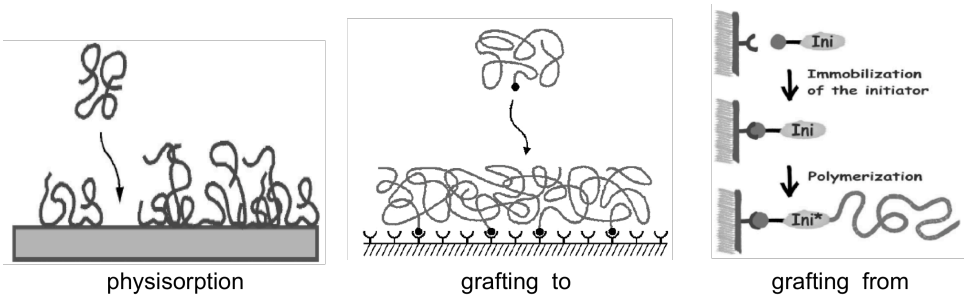

Figure 1.8 Schematic illustration of different processes used for the attachment of polymers to surfaces: physisorption, "grafting to" and "grafting from" techniques. (Adapted from Ref # 83 with permission from WILEY-VCH Verlag GmbH & Co. KGaA, Weinheim)

aminoxyl mediated,[94] radical addition fragmentation chain transfer (RAFT)[95] and atom transfer radical polymerization (ATRP)[96] reactions.

1.6 Patterning of Polymer Brushes

The fabrication of patterned polymer brushes is of great importance in the emerging field of nanotechnology. The requirement for a successful lithographic process varies substantially depending on the application. This section provides a review of the various techniques for patterning of polymer brushes. This section does not aim to cover in depth all the technical details of the patterning techniques. A very selective overview of recent advances in patterned brush surfaces is presented. Figure 1.9 shows the range of features sizes that have been demonstrated for each type of patterning technique.[97]

For the past couple of decades, photolithography has been the most established method to generate patterned brush surfaces. In photolithography, a photosensitive film (photoresist) is first patterned by exposure to UV light. Irradiation of the photoresist causes a photo-induced chemical reaction that can give rise to photopolymerization, photocrosslinking, functionalization and decomposition reactions. Rühe and coworkers prepared patterned polymer brushes by photolithography before, during and after polymeriation.[98] The immobilized azo initiators were decomposed in selected areas. Thermally induced radical polymerization in the unexposed areas gave patterned brushes. Using photolithography, Imanishi and coworkers obtained micropatterned azidophenyl-derivatized poly(acrylic acid) immobilized on a polystyrene film.[99] Hawker and coworkers reported the preparation of a continuous polymer brush, patterned into chemically distinct regions by combining photolithographic techniques with surface initiated polymerization.[100] They used TEMPO-mediated radical polymerization to

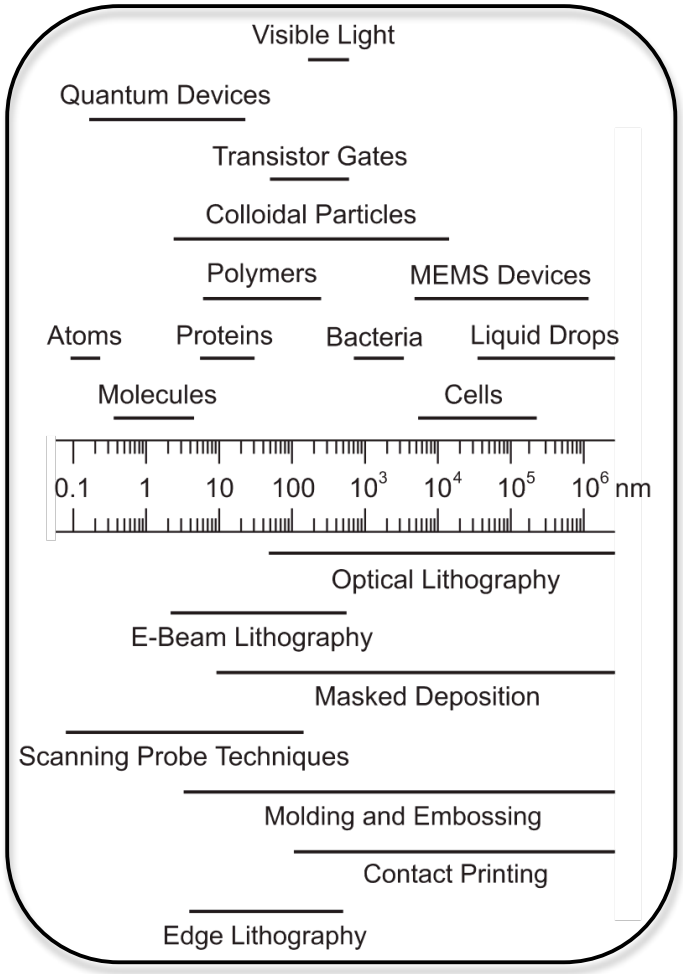

Figure 1.9 Patterning on various length scales. The scale bar indicates the range of dimensions for a specific object and the range of feature sizes that have been demonstrated for each type of patterning technique. (Reprinted from Ref. # 97 with permission from WILEY-VCH Verlag, GmbH & Co. KGaA, Weinheim)

prepare a poly(t-butyl acrylate) brush. A polystyrene film containing bis(t-butylphenyl)iodonium triflate was spun onto the brush. Photolithography caused generation of acid, which converted poly(t-butyl acrylate) to poly(acrylic acid) brushes. Using this approach, 10 μm features in a continuous brush showing regions of poly(t-butyl acrylate) (hydrophobic) and poly(acrylic acid) (hydrophilic) brushes could be obtained. Figure 1.10 shows the scheme for patterning a polymer brush using a sacrificial photoresist layer and lithographic imaging. Zhou *et al.* fabricated patterned poly(methyl methacrylate) (PMMA) brushes as a thin dielectric and etch resistant layer.[101] A PMMA brush was directly exposed to UV light through a transmission electron microscopy (TEM) grid mask. The exposed area was completely removed after an exposure time of 6 h, giving rise to UV patterned PMMA brushes. This approach was extended further to prepare binary polymer brush patterns of poly(2-hydroxyethyl methacrylate)/poly(methyl methacrylate) brushes.[102] PHEMA was first passivated by reaction with NaN_3 and then etched with UV irradiation through a TEM grid. Initiator was again immobilized on the exposed sites to grow the second polymer brush. Andruzzi *et al.* reported the micropatterning of polymer brushes grown via the nitroxide mediated polymerization of styrenic monomers containing oligo(ethylene glycol) moieties.[103] In this case, polymer brushes were patterned using a modified photolithographic process involving the chemical vapor deposition of parylene. The parylene was deposited, coated with photoresist by spin-casting, exposed, developed and reactive ion etched. Parylene acts as a protective layer between the polymer brush modified surface and the photoresist layer. After reactive ion etch, the parylene was peeled from the substrate. Figure 1.11 is a schematic of the parylene patterning carried out on the polymer brush modified surface. More recently, Rong *et al.* used photolithography to prepare patterned poly(acrylic acid) brushes.

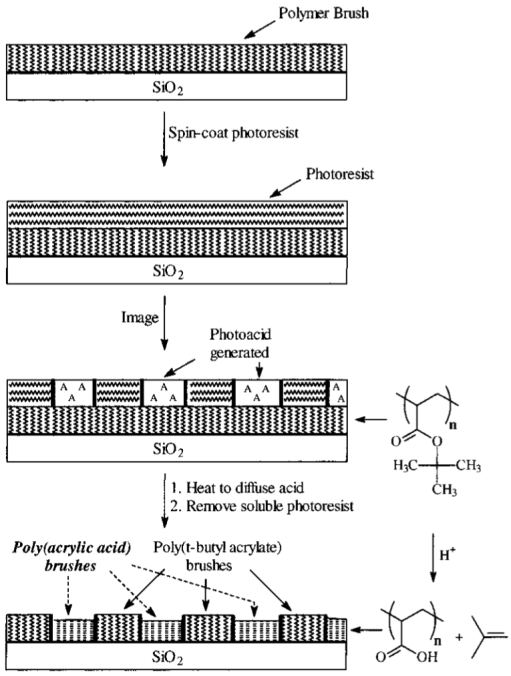

Figure 1.10 Scheme of strategy for patterning of a polymer brush using a sacrificial photoresist layer and lithographic imaging. (Reprinted from Ref. # 100 with permission from the American Chemical Society)

Patterns down to 2μm stripes could be prepared by immobilizing ATRP initiator in the patterned regions, followed by surface initiated polymerization.[104]

Whitesides and coworkers introduced the concept of microcontact printing (μCP) to prepare patterned SAMs.[105, 106] In μCP, a rigid or elastic stamp is used to transfer an 'inked' material to the substrate. The conformal contact between the substrate and the raised regions of the stamp provides high fidelity when transferring an 'ink' to the surface. This method has been extended to pattern polymer brushes. Site-specific polymerization is accomplished by selective deposition of an initiator containing SAM or monomer to a pre-patterned surface. Abbott and coworkers used μCP to prepare patterned polymer brushes via surface initiated ring opening polymerization of ε-caprolactone from the functionalized areas of the patterned SAM.[106] Using patterned di(ethyl glycol) containing SAMs ($HO(CH_2CH_2O)_2(CH_2)_{11}SH$), patterned brushes with 10 μm lines could be obtained. Figure 1.12 shows the strategy for amplification of a patterned SAM prepared by μCP into a patterned polymer brush. Similarly, several monomers such as methyl methacrylate, hydroxyethyl methacrylate, t-butyl methacrylate, isobornyl methacrylate, ((dimethylamino)ethylmethyl acrylate), N-isopropylacrylamide (PNIPAm), glycidyl methacrylate and oligo(ethylene glycol) methyl methacrylate have been polymerized from initiators patterned by microcontact printing to obtain patterned polymer brushes for various applications.[68, 107-114] Hamelinck and Huck reported the use of μCP to obtained patterned liquid crystalline polymer brushes to use as alignment layers for liquid crystal displays.[115] A reactive mesogen RM488 (Merck Chemicals Ltd.) was polymerized vi ATRP on patterned initiators. Han and coworkers combined μCP with the "grafting to" approach to prepare patterned self-adaptive mixed polymer brushes of poly(2-vinyl pyridine) and polystyrene. These

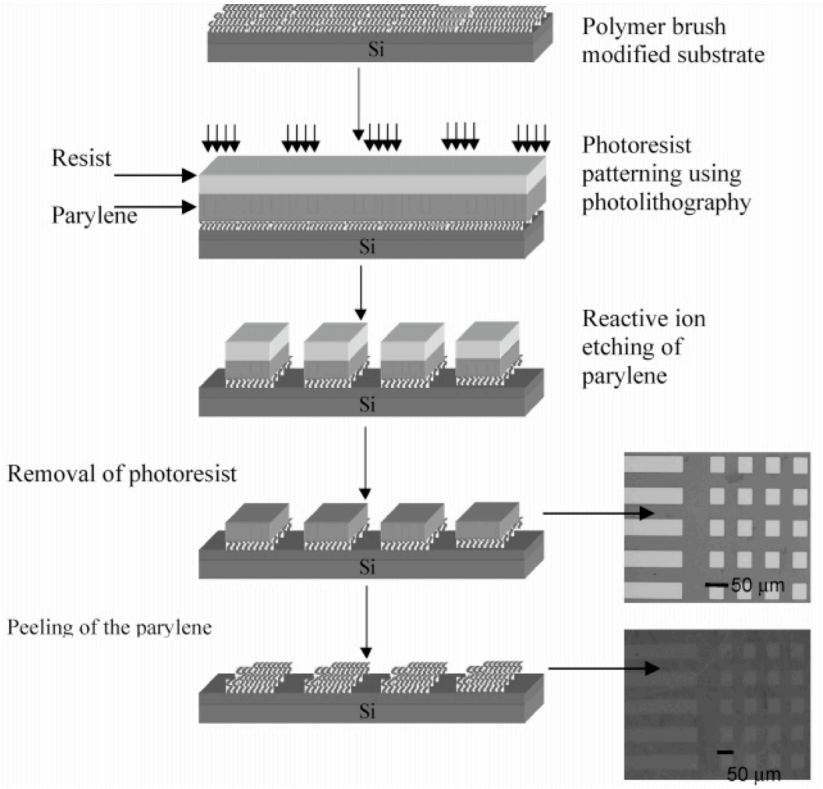

Figure 1.11 Schematic of the parylene patterning process to obtain patterned polymer brushes. (Reprinted from Ref. # 103 with permission from the American Chemical Society)

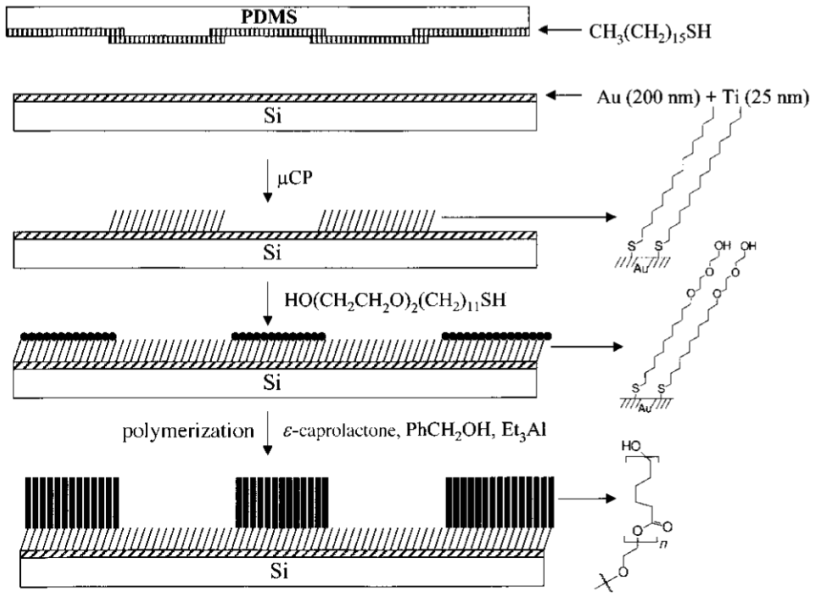

Figure 1.12 Schematic representation of amplification of a patterned SAM prepared by microcontact printing into a patterned polymer brush. (Reprinted from Ref. # 106 with permission from WILEY-VCH Verlag, GmbH & Co. KGaA, Weinheim)

mixed brushes showed reversible switching behavior upon exposure to selective solvents for different components.

Huck and coworkers described a general synthetic route to laterally distinctive multicomponent polymer brushes on gold.[116] First, polymer brushes were grown off patterned initiator layers by microcontact printing, surface initiated ATRP and subsequent passivation of the "living" chain end with NaN_3. The next initiator SAM was then contact printed onto the same surface, and the second brush was grown in those areas that were in contact with the stamp and had not previously been modified with a polymer brush. These steps were repeated to grow different patterned polymer brushes on the same surface. Using this approach, poly(methacrylic acid) (PMAA), poly(methacryloylethylphosphate) (PMEP), PNIPAm and poly(N,N′-dimethylamino ethyl methacrylate) (DMAEMA) brushes were grown in the same substrate. The procedure for obtaining multiple patterned polymer brushes is shown in Figure 1.13 (A). An overview of different regions (1-8) obtained on the surface after three partially overlapping printing steps and four brush growth cycles (PMAA/PMEP/ PNIPAm/ PDMAEMA) are shown in Figure 1.13 (B) More recently, Zauscher and coworkers used microphase separation of a binary mixture of alkanethiols during μCP to yield initiator-gradient patterns that were amplified to PNIPAm brush microstructures.[108] The μCP technique has been used in combination with other patterning techniques to make major advances in surface sciences. Although patterning with sub-100 nm resolution is feasible, most of the patterns generated using this method have features in the micrometer size range. For a detailed discussion of the various soft lithographic techniques, the reader is referred to an excellent review.[105]

Another common method for patterning polymer brushes is using direct writing techniques. Zauscher and coworkers reported the fabrication of nanopatterned

(A)

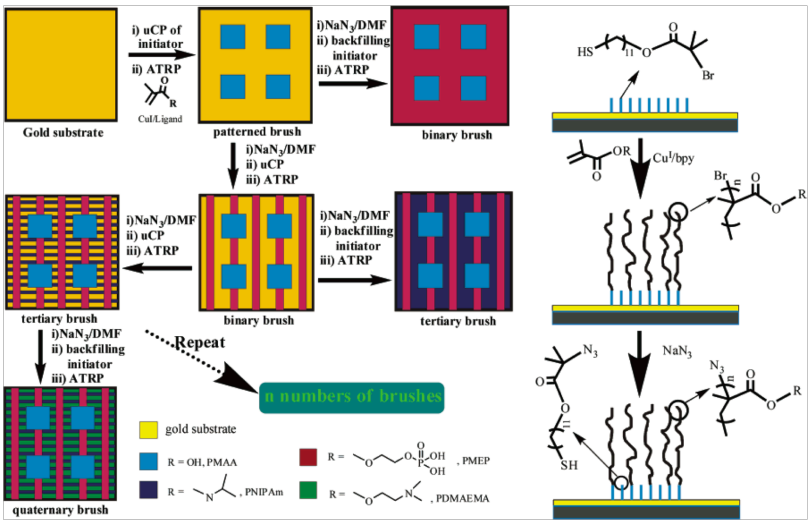

(B)

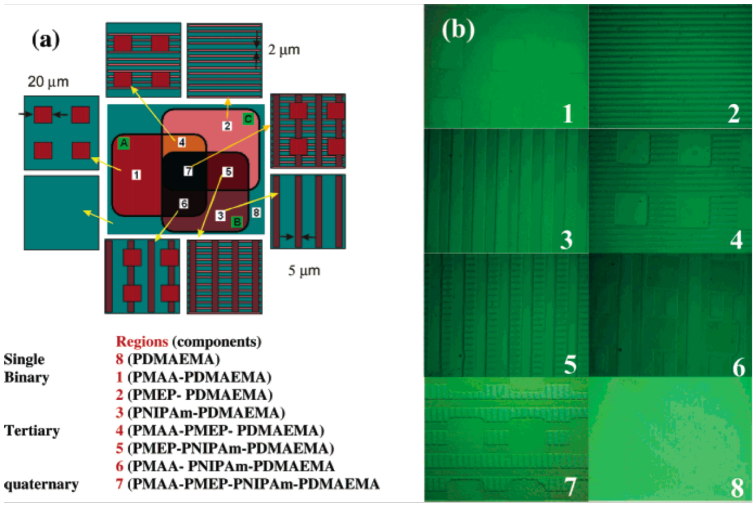

Figure 1.13 (A) Outline procedure for grafting multiple patterned polymer brushes and ATRP passivation. (B) (a) Overview of different regions (1-8) obtained on the surface after partially overlapping printing steps and surface initiated polymerization of four monomers. (b) Images taken from different areas of a single surface show in 2(a). (Reprinted from Ref. # 116 with permission from the American Chemical Society)

polymer brushes by scanning probe lithography.[117, 118] This writing scheme involves the mechanical displacement or modification of a material on the surface of a substrate in a spatially controlled manner. First, a gold substrate precoated with a SAM of methyl-terminated 1-octadecanethiol (ODT) was patterned using an AFM tip. The AFM tip was used as a nanomechanical tool to selectively remove the "thiol resist" at a scanning speed of ~ 20 μm/s with a normal force of 50 nN. The exposed gold surface was back filled with thiol initiator and nanopatterned PNIPAm brushes (line widths of 300-500 nm) were prepared by ATRP.[118]

Another "direct writing" method of patterning is using a focused beam of electrons across the surface of a susceptible material. These techniques have really high resolution capabilities due to the extremely short wavelengths (< 0.1 nm) combined with large depths of focus. The practical resolution is determined by the spot size of the e-beam and other scattering effects. Ulman and coworkers reported the fabrication of patterned polystyrene brushes by e-beam irradiation of SAMs of 4′-nitro-1,1′-biphenyl-4-thiol (NBT) in spatially defined regions.[119] E-beam exposure caused the reduction of the nitro functionalities to amino groups, while the aromatic biphenyl layer is crosslinked. The amino groups were derivatized to initiate the surface initiated polymerization of styrene. Using this approach 70 nm isolated lines of polystyrene brushes could be obtained. The reaction scheme starting with SAMs of NBT to patterned polystyrene brushes is shown in Figure 1.14. One drawback is that the required electron dose for the successful irradiation of SAMs was 50 eV with an electron dose of 20,000 μC/cm^2 or 300 eV with an electron dose of 40,000 μC/cm^2.

Similarly, several papers on fabrication of patterned polymer brushes using e-beam lithography have been reported.[120-124] The general procedure involves the selective removal/modification of a SAM layer or patterning of a polymer resist using

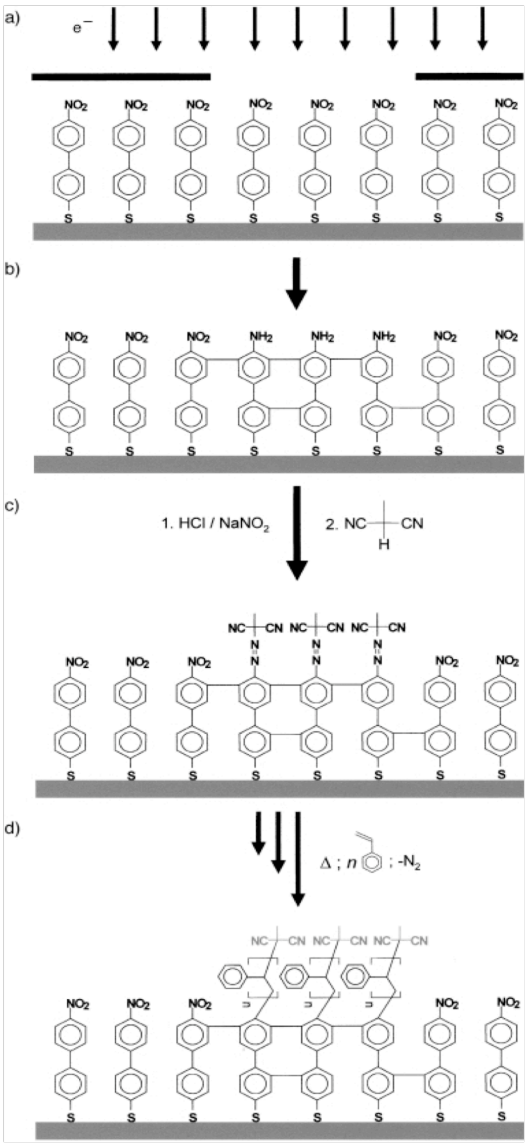

Figure 1.14 Reaction scheme starting from SAMs of NBT on Au (111) to the fabrication of patterned polystyrene brushes. (a) exposure of NBT-SAMs to e-beam (b) nitro group are reduced to amino groups and phenyl groups are crosslinked (c) derivatization of the amino groups for free radical polymeriztion (d) radical polymerization of syrene at 80 °C results in the patterned brush. (Reprinted from Ref. # 119 with permission from WILEY-VCH Verlag, GmbH & Co. KGaA, Weinheim)

e-beam lithography, followed by surface initiated polymerization to give patterned brush surfaces.

More recently, Jordan and coworkes reported the self-initiated photografting and photopolymerization (SIPGP) of styrene, methyl methacrylate and t-butyl methacryate on e-beam crosslinked ω-functionalized biphenylthiols SAMs on gold.[125] The polymer brushes were formed in selective regions on the crosslinked SAMs by placing in bulk monomer with benzophenone (BP) as photosensitizer and irradiation with UV light (λ = 300-400 nm). Patterns down to 50 nm polystyrene patterns could be obtained.

In addition to the techniques mentioned above, some less common methods for the fabrication of patterned polymer brushes has been reported using CVD polymerization [126], imprint lithography of photopolymer resins containing embedded initiator groups,[127] contact molding followed by aminoxyl mediated polymerization,[128] dip pen lithography (DPL),[107] AFM anodization lithography,[117] capillary force lithography[129, 130] and microelectrochemical patterning.[131, 132]

1.7 Conclusions

It is an exciting time for the field of high resolution patterning of polymer thin films. There is a growing need for patterned polymer thin films in many areas of research including microelectronics and biotechnology. Various patterning techniques have emerged for the high resolution patterning of standard spun coated polymer photoresist thin films and polymer brushes. As the semiconductor industry continues to keep pace with Moore's Law, environmentally benign processes are being considered as promising alternatives to current industrial practices due to the increasing awareness of environmental issues and the economic benefits. $scCO_2$ has proven to be useful in the development of polymeric photoresists and is now a subject

of intense research. Both tailor-made as well as commercially available standard photoresists have been developed in $scCO_2$. Chapter 2 describes the synthesis and use of CO_2 compatible quaternary ammonium salts as dissolution aids for the processing of standard polar polymers used as photoresist materials.

The patterning of polymer brushes with high fidelity and enhanced resolution has gained a lot of attention in the past decade. Some techniques such as photolithography, microcontact printing (soft lithography) and e-beam lithography have emerged as attractive tools for exploratory research. Chapter 3 describes the direct patterning of polymer brushes in a single step using e-beam lithography. Using this single step approach, polymer brush patterns down to 50 nm could be obtained. Chapter 4 combines the concept of direct patterning of brushes with environmentally benign development in $scCO_2$. Patterned poly(2,2,2-trifluoroethyl methacrylate) brushes were successfully developed in $scCO_2$ to obtain 150 nm patterns. In the future, to achieve improved patterning efficiency and cost effectiveness, a combination of patterning techniques will be used. Examples of this are starting to appear in the literature.

Polymer brushes have also been utilized for the development of biosensors. Chapters 5 and 6 describe the role of poly(acrylic acid) brushes in the development of an electrochemical biosensor. Polymer brushes were grown off a new modified ATRP initiator to prevent non-specific adsorption and control the immobilization the antigenic groups on the sensor surface.

REFERENCES

1. Van der Waarden, M., *J. Colloid Sci.* **1950,** 5, 317.

2. Zhao, B.; Brittain, W. J., *Prog. Polym. Sci.* **2000,** 25, 677.

3. Krishnan, S.; Weinman, C. J.; Ober, C. K., *J. Mater. Chem.* **2008,** 18, (29), 3405.

4. Senaratne, W.; Andruzzi, L.; Ober, C. K., *Biomacromolecules* **2005,** 6, (5), 2427.

5. Takei, Y. G.; Aoki, T.; Sanui, K.; Ogata, N.; Sakurai, Y.; Okano, T., *Macromolecules* **1994,** 27, (6163).

6. Ito, Y.; Park, Y. S.; Imanishi, Y., *J. Am. Chem. Soc.* **1997,** 119, 2739.

7. Advincula, R. C.; Brittain, W. J.; Caster, K. C.; Ruhe, J., *Polymer Brushes*. WILEY-VCH Verlag GmbH & Co.: Weinheim, 2004.

8. Milner, S. T., *Science* **1991,** 251, 905.

9. Dong, R.; Krishnan, S.; Baird, B. A.; Lindau, M.; Ober, C. K., *Biomacromolecules* **2007,** 8, 3082.

10. Nie, Z.; Kumacheva, E., *Nature Materials* **2008,** 7, 277.

11. Beckman, E. J., *Ind. Eng. Chem. Res.* **2003,** 42, 1598.

12. Sha, J.; Ober, C. K., *Polym. Int.* **2009,** 58, 302.

13. Miller, C.; Worth, W., *J. Vac. Sci. Technol. A* **2003,** 21, (4), 1139.

14. Wells, S. L.; DeSimone, J., *Angew. Chem. Int. Ed.* **2001,** 40, 518.

15. Williams, E. D.; Ayres, R. U.; Heller, M., *Environ. Sci. Technol.* **2002,** 36, 5504.

16. Beckman, E. J., *J. Supercrit. Fluids* **2004,** 28, 121.

17. Ajzenberg, N.; Trabelsi, F.; Recasens, F., *Chem. Eng. Technol.* **2000,** 23, 829.

18. McCluskey, G. E.; Lee, J. K.; Sha, J.; Ober, C. K.; Watkins, S. E.; Holmes, A. B., *MRS Bulletin* **2009,** 34, 108.

19. Cooper, A. I., *J. Mater. Chem.* **2000,** 10, 207.

20. BUTE-CEPE, S. g. http://sfe.vemt.bme.hu/angol/supercritical.html

21. Brennecke, J. F., *Chem. Ind.* **1996**, 831.

22. Rizvi, S. S. H.; Benado, A. L.; Zillweg, J. A.; Daniels, J. A., *Food Technol.* **1986,** 40, 55.

23. Krishnan, S.; Kwark, Y. J.; Ober, C. K., *The Chemical Record* **2004,** 4, 315.

24. McHugh, M. A.; Krukonis, V. J., *Supercritical Fluid Extraction, 2nd edition*. Butterworth-Heinermann: Boston, MA, 1994.

25. Hoefling, T. A.; Enick, R. M.; Beckman, E. J., *J. Phys. Chem.* **1991,** 95, 7127.

26. Hoefling, T. A.; Stofesky, D.; Reid, M.; Beckman, E. J.; Enick, R. M., *J. Supercrit. Fluids* **1992,** 5, 237.

27. Zhao, X.; Watkins, R.; Barton, S. W., *J. Appl. Pol. Sci.* **1995,** 55, 773.

28. Xiang, Y.; Kiran, E., *Polymer* **1995,** 36, 4817.

29. DeSimone, J. M.; Maury, E. E.; Menceloglu, Y. Z.; McClain, J. B.; Romack, T. J.; Combles, J. R., *Science* **1994,** 265, 356.

30. Hsiao, Y. L.; Maury, E. E.; DeSimone, J. M.; Mawson, S.; Johnston, K. P., *Macromolecules* **1995,** 28, 8159.

31. Prausnitz, J. M.; Lichtenthaler, R. N.; de Azevedo, E., *Molecular Thermodynamics of Fluid-Phase Equilibria, 2nd edition*. Prentice-Hall: Englewood Cliffs, NJ, 1986.

32. Rindfeisch, F.; DiNoia, T. P.; McHugh, M. A., *J. Phys. Chem.* **1996,** 100, 15581.

33. Kirby, C. F.; McHugh, M. A., *Chem. Rev.* **1999,** 99, 565.

34. Hyatt, J. A., *J. Org. Chem.* **1984,** 49, 5097.

35. Walsh, J. M.; Ikonomou, G. D.; Donohue, M. D., *Fluid Phase Equilib* **1987,** 33, 295.

36. Kazarian, S. G.; Vincent, M. F.; Bright, F. V.; Liotta, C. L.; Eckert, C. A., *J. Am. Chem. Soc.* **1996,** 118, 1729.

37. O'Shea, K. E.; Kirmse, K. M.; Fox, M. A.; Johnston, K. P., *J. Phys. Chem.* **1991,** 95, 7863.

38. McHugh, M. A.; Garach-Domech, A.; Park, I. H.; Li, D.; Barbu, E.; Graham, P.; Tsibouklis, J., *Macromolecules* **2002,** 35, (17), 6479.

39. Sanchez, I. C.; Lacombe, R. H., *J. Phys. Chem.* **1976,** 80, 2568.

40. Sanchez, I. C.; Lacombe, R. H., *Macromolecules* **1978,** 11, 1145.

41. Huang, S. H.; Radosz, M., *Ind. Eng. Chem. Res.* **1990,** 29, 2284.

42. Chandhok, M.; Lee, S. H.; Roberts, J.; Rice, B. J.; Cao, H. B., *J. Vac. Sci. Technol. B* **2006,** 24, (1), 274.

43. Weibel, G. L.; Ober, C. K., *Microelectronic Engineering* **2003,** 65, 145.

44. Zong, Y.; Watkins, J. J., *Chem. Mater.* **2005,** 17, (3), 560.

45. Shan, X.; Watkins, J. J., *Thin Solid Films* **2006,** 496, (2), 412.

46. Wahlbrink, T.; Kuepper, D.; Bolten, J.; Moeller, M.; Lemme, M. C.; Kurz, H., *Microelectronic Engineering* **2007,** 84, (5-8), 1045.

47. Namatsu, H.; Yamazaki, K.; Kurihara, K., *JVST B* **2000**
, 18, (2), 780.

48. Saeki, A.; Kozawa, T.; Tagawa, S.; Cao, H. B., *Nanotechnology* **2006,** 17, 1543.

49. Gallagher-Wetmore, P.; Wallraff, G. M.; Allen, R. D., *Proceedings of SPIE* **1995,** 2438, 694.

50. Ober, C. K.; Gabor, A. H.; Gallagher-Wetmore, P.; Allen, R. D., *Adv. Mater.* **1997,** 9, 1039.

51. Sundararajan, N.; Yang, S.; Ogino, K.; Valiyaveettil, S.; Wang, J. G.; Zhou, X.; Ober, C. K.; Obendorf, S. K.; Allen, R. D., *Chem. Mater.* **2000,** 12, 41.

52. Pham, V. Q.; Ferris, R. J.; Hamad, A.; Ober, C. K., *Chem. Mater.* **2003,** 15, 4893.

53. Boggiano, M. K.; Vellenga, D.; Carbonell, R. G.; Ashby, V. S.; DeSimone, J. M., *Polymer* **2006,** 47, 4012.

54. Lewis, H. P. G.; Weibel, G. L.; Ober, C. K.; Gleason, K., *Chem. Vap. Deposition* **2001,** 7, 195.

55. Mao, Y.; Felix, N. M.; Nguyen, P. T.; Ober, C. K., *Chemical Vapor Deposition* **2006,** 12, (5), 259.

56. Zweber, A. E.; Wagner, M.; DeYoung, J.; Carbonell, R. G., *Langmuir* **2009,** 25, (11), 6176.

57. Zweber, A. E.; Wagner, M.; Carbonell, R. G., *Proc. of SPIE* **2007,** 6519, 651948-1.

58. Wagner, M.; DeYoung, J.; Harbinson, C., *Proc. of SPIE* **2006,** 6153, 615311-1.

59. Felix, N.; Ober, C. K., *Chem. Mater.* **2008,** 20, 2932.

60. Edmondson, S.; Osborne, V. L.; Huck, W. T. S., *Chem. Soc. Rev.* **2004,** 33, 14.

61. Alexander, S. J., *J. Phys (Paris)* **1977,** 38, 977.

62. de Gennes, P. G., *J. Phys (Paris)* **1976,** 37, 1443.

63. de Gennes, P. G., *Macromolecules* **1980,** 13, 1069.

64. Cantor, R., *Macromolecules* **1981,** 14, 1186.

65. Flory, P. J., *Principles of Polymer Chemistry*. Cornell University Press: Ithaca, NY, 1981.

66. Gutowski, W. S.; Sheng, L.; Filippou, C.; Hoobin, P.; Petinakis, S., *J. Adhesion* **2003,** 79, 483.

67. Deruelle, M.; Leger, L.; Tirrell, M., *Macromolecules* **1995,** 28, 7419.

68. de las Heras Alarcon, C.; Farhan, T.; Osborne, V. L.; Huck, W. T. S.; Alexander, C., *J. Mater. Chem.* **2005,** 15, 2089.

69. Pan, Y. V.; Wesley, R. A.; Luginbuhl, R.; Denton, D. D.; Ratner, D., *Biomacromolecules* **2001,** 2, 32.

70. Nath, N.; Chilkoti, A., *Anal. Chem.* **2003,** 75, 709.

71. Kim, G.; Park, S.; Jung, J.; Heo, K.; Yoon, J.; Kim, H.; Kim, I. J.; Kim, J. R.; Lee, J. I.; Ree, M., *Adv. Func. Mater.* **2009,** 19, (10), 1631.

72. Li, L.; Yan, G.; Wu, J., *J. Appl. Polym. Sci.* **2009,** 111, (4), 1942.

73. Kawai, T.; Saito, K.; Lee, W., *J. Chromatogr. B.* **2003,** 790, 131.

74. Sevick, E. M.; Williams, D. R. M., *Macromolecules* **1994,** 27, 5285.

75. Ballauff, M., *Macromol. Chem. Phys.* **2003,** 204, 220.

76. Culbertson, C. T.; Ramsey, R. S.; Ramsey, J. M., *Anal. Chem.* **2000,** 72, 2285.

77. Parsonage, E.; Tirrell, M.; Watanabe, H.; Nuzzo, R., *Macromolecules* **1987,** 24, 1987.

78. Fytas, G.; Anastasiadis, S. H.; Seghrouchi, R.; Vlassopoulos, D.; Li, J.; Factor, B. J.; Theobald, W.; Toprakciolu, C., *Science* **1996,** 274, 2041.

79. Zerushalmi-Royen, R.; Klein, J.; Fetters, L., *Science* **1994,** 263, 793.

80. Murthy, R.; Shell, C. E.; Grunlan, M. A., *Biomaterials* **2009,** 30, 2433.

81. Yu, K.; Cong, Y.; Fu, J.; Xing, R.; Zhao, N.; Han, Y., *Surface Science* **2004,** 572, 490.

82. Ebata, K.; Furukawa, K.; Matsumoto, N., *J. Am. Chem. Soc.* **1998,** 120, 7367.

83. Advincula, R. C.; Brittain, W. J.; Caster, K. C.; Ruhe, J., *Polymer Brushes: Synthesis, Characterization, Applications*. Wiley-VCH: Weinheim, Germany, 2004.

84. Ulman, A., *Chem. Rev.* **1996,** 96, 1533.

85. Ito, Y.; Park, Y. S.; Imanishi, Y., *Macromol. Rapid. Commun.* **1997,** 18, 221.

86. Suzuki, M.; Kishida, A.; Iwata, H.; Ikada, Y., *Macromolecules* **1986,** 19, 1804.

87. Prucker, O.; Ruhe, J., *Macromolecules* **1998,** 31, 592.

88. Henn, G.; Bucknall, D. G.; Stamm, M.; Vanhoorne, P.; Jerome, R., *Macromolecules* **1996,** 29, 4305.

89. Prucker, O.; Ruhe, J., *Langmuir* **1998,** 14, 6893.

90. de Boer, B.; Simon, H. K.; Werts, M. P. L.; van der Vegte, E. W.; Hadziioannou, I., *Macromolecules* **2000,** 33, 349.

91. Weck, M.; Jackiw, J. J.; Rossi, R. R.; Weiss, P. S.; Grubbs, R. H., *J. Am. Chem. Soc.* **1999,** 121, 4088.

92. Zhao, B.; Brittain, W. J., *Macromolecules* **2000,** 33, 342.

93. Jordan, R.; Ulman, A.; Kang, J. F.; Rafailovich, M. H.; Sokolov, J., *J. Am. Chem. Soc.* **1999,** 121, 1016.

94. Husseman, M.; Malmstrom, E. E.; McNamara, M.; Mate, M.; Mecerreyes, O.; Benoit, D. G.; Hedrick, J. L.; Mansky, P.; Huang, E.; Russell, T. P.; Hawker, C. J., *Macromolecules* **1999,** 32, 1424.

95. Li, C.; Benicewicz, B. C., *Macromolecules* **2005,** 38, (14), 5929.

96. Matyjaszewski, K.; Miller, P. J.; Shukla, N.; Immaraporn, B.; Gelman, A.; Luokala, B. B.; Siclovan, T. M.; Lickelbick, G.; Vallant, T.; Hoffmann, H.; Pakula, T., *Macromolecules* **1999,** 32, 8716.

97. Geissler, M.; Xia, Y., *Advanced Materials* **2004,** 16, (15), 1249.

98. Ruhe, J., *Macromol. Symp.* **1997,** 126, 215.

99. Chen, G.; Ito, Y.; Imanishi, Y., *Macromolecules* **1997,** 30, 7001.

100. Husemann, M.; Morrison, M.; Benoit, D.; Frommer, J.; Mate, C. M.; Hinsberg, W. D.; Hedrick, J. L.; Hawker, C. J., *J. Am. Chem. Soc.* **2000,** 122, 1844.

101. Zhou, F.; Liu, W.; Hao, J.; Xu, T.; Chen, M.; Xue, Q., *Adv. Funct. Mater.* **2003,** 13, (12), 938.

102. Zhou, F.; Jiang, L.; Liu, W.; Xue, Q., *Macromol. Rapid Commun.* **2004,** 25, 1979.

103. Andruzzi, L.; Senaratne, W.; Hexemer, A.; Sheets, E. D.; Ilic, B.; Kramer, E. J.; Baird, B. A.; Ober, C. K., *Langmuir* **2005,** 21, 2495.

104. Dong, R.; Krishnan, S.; Baird, B.; Lindau, M.; Ober, C. K., *Biomacromolecules* **2007,** 8, 3082.

105. Xia, Y.; Whitesides, G. M., *Angew. Chem. Int. Ed.* **1998,** 37, 550.

106. Husemann, M.; Mecerreyes, D.; Hawker, C. J.; Hedrick, J. L.; Shah, R.; Abbott, N. L., *Angew. Chem. Int. Ed.* **1999,** 38, 647.

107. Ma, H.; Hyun, J.; Stiller, P.; Chilkoti, A., *Adv. Mater.* **2004,** 16, (4), 338.

108. Chen, T.; Zhang, J.; Chang, D. P.; Garcia, A.; Zauscher, S., *Adv. Mater.* **2009,** 21, 1.

109. Edmondson, S.; Huck, W. T. S., *Adv. Mater.* **2004,** 16, (15), 1327.

110. Tingey, M. L.; Sondgrass, E. J.; Abbott, N. L., *Adv. Mater.* **2004,** 16, (15), 1331.

111. Shah, R. R.; Merreceyes, D.; Husemann, M.; Rees, I.; Abbott, N. L.; Hawker, C. J.; Hedrick, J. L., *Macromolecules* **2000,** 33, 597.

112. Jones, D. M.; Smith, J. R.; Huck, W. T. S.; Alexander, C., *Adv. Mater.* **2002,** 14, (16), 1130.

113. Tu, H.; Heitzman, C. E.; Braun, P. V., *Langmuir* **2004,** 20, 8313.

114. Farhan, T.; Huck, W. T. S., *Eur. Polym. J.* **2004,** 40, 1599.

115. Hamelinck, P. J.; Huck, W. T. S., *J. Mater. Chem.* **2005,** 15, 381.

116. Zhou, F.; Zheng, Z.; Yu, B.; Liu, W.; Huck, W. T. S., *J. Am. Chem. Soc.* **2006,** 128, 16253.

117. Lee, W. K.; Caster, K. C.; Kim, J.; Zauscher, S., *Small* **2006,** 2, (7), 848.

118. Kaholek, M.; Lee, W.; LaMattina, B.; Caster, K. C.; Zauscher, S., *Nano Letters* **2004,** 4, 373.

119. Schmelmer, U.; Jordan, R.; Geyer, W.; Eck, W.; Golzhauser, A.; Grunze, M.; Ulman, A., *Angew. Chem. Int. Ed.* **2003,** 42, (5), 559.

120. Chen, J. K.; Chen, Z. Y.; Lin, H. C.; Hong, P. D.; Chang, F. C., *ACS Appl. Mater. Interfaces* **ASAP article**.

121. Kaholek, M.; Lee, W.; Feng, J.; LaMattina, B.; Dyer, D. J.; Zauscher, S., *Chem. Mater.* **2006,** 18, 3660.

122. Ahn, S. J.; Kaholek, M.; Lee, W.; LaMattina, B.; LaBean, T. H.; Zauscher, S., *Adv. Mater.* **2004,** 16, 2141.

123. Chen, J. K.; Hsieh, C. Y.; Huang, C. F.; Li, P. M.; Kuo, S. W.; Chang, F. C., *Macromolecules* **2008,** 41, 8729.

124. Schilp, S.; Ballav, N.; Zharnikov, M., *Angew. Chem. Int. Ed.* **2008,** 47, 6786.

125. Steenackers, M.; Kuller, A.; Stoycheva, S.; Grunze, M.; Jordan, R., *Langmuir* **2009,** 25, 2225.

126. Lahann, J.; Langer, R., *Macromol. Rapid Commun.* **2001,** 22, (12), 968.

127. Jhaveri, S. B.; Beinhoff, M.; Hawker, C. J.; Carter, K. R.; Sogah, D. Y., *ACS Nano* **2008,** 2, 719.

128. von Werne, T. A.; Germack, D. S.; Hagberg, E. C.; Sheares, V. V.; Hawker, C. J.; Carter, K. R., *J. Am. Chem. Soc.* **2003,** 125, 3831.

129. Liu, Y.; Luzinov, I., *J. Am. Chem. Soc.* **2006,** 128, 8106.

130. Zdyrko, B.; Hoy, O.; Kinnan, M. K.; Chumanov, G.; Luzinov, I., *Soft Matter* **2008,** 4, 2213.

131. Slim, C.; Tran, Y.; Chehimi, M. M.; Garraud, N.; Roger, J. P.; Combellas, C.; Kanoufi, F., *Chem. Mater.* **2008,** 20, 6677.

132. Hauquier, F.; Matrab, T.; Kanoufi, F.; Combellas, C., *Electrochem. Acta* **2009,** 54, 5127.

CHAPTER 2

FLUORINATED QUATERNARY AMMONIUM SALTS AS DISSOLUTION AIDS FOR POLAR POLYMERS IN ENVIRONMENTALLY BENIGN SUPERCRITICAL CARBON DIOXIDE*

Abstract

Environmentally benign supercritical carbon dioxide ($scCO_2$) has been utilized as an "ecologically responsible" solvent for a wide variety of applications. However, non-polar $scCO_2$ is generally a very poor solvent for polar polymers, which limits its use as a processing solvent in high resolution photolithography. This chapter describes the synthesis of fluorinated $scCO_2$ compatible additives and demonstrates their utility to help dissolve polar polymers in $scCO_2$. A series of quaternary ammonium salts (QAS) were designed and synthesized as $scCO_2$ additives. The ability of these salts to assist in the dissolution of model acidic and protected polar polymers has been compared. For this study we have chosen three different polar reference polymers. Addition of millimolar quantities of the QAS to the $scCO_2$ solvent helped to dissolve the protected model polymer under moderate supercritical conditions. To explicitly investigate the interactions between the QAS additive and the various functionalities

* Reproduced with permission from Manabu Tanaka, Abhinav Rastogi, Gregory N. Toepperwein, Robert A. Riggleman, Nelson M. Felix, Juan J. de Pablo and Christopher K. Ober. Fluorinated Quaternary Ammonium Salts as Dissolution Aids for Polar Polymers in Environmentally Benign Supercritical Carbon Dioxide. *Chemistry of Materials* (2009), 21(14), 3125-3135. Copyright 2009 American Chemical Society.

on the polymers, computational simulations were carried out using a fully atomistic force-field adapted from optimized potentials for liquid simulations (OPLS). These studies combining both theory and experiment show that the architecture of the cation and the basic nature and size of the anion are crucial in designing more efficient additives. Finally based on these findings the lithographic evaluation of a standard commercially available polymer photoresist was shown using an appropriate $scCO_2$ compatible QAS additive after development in $scCO_2$. Well-resolved, negative-tone patterns as small as 100 nm were obtained by e-beam exposure, indicating the excellent potential of using $scCO_2$ as the processing solvent in the presence of the QAS additives to form high-resolution structures.

Introduction

Environmentally benign processes are gaining renewed interest and are being considered as promising alternatives to current industrial practices due to increasing awareness of environmental issues and the economic benefits of shifting to "greener" routes. Carbon dioxide is considered a "green" solvent and since its first use in the 1950s it has attracted attention in academia and industry. Carbon dioxide is relatively nontoxic, nonflammable, inert under most conditions and is a potential candidate for a more environmentally friendly replacement for organic solvents in the area of polymer synthesis, coatings, biomaterials and microelectronic processing.[1, 2, 3] Like water, it is a naturally abundant material that can be removed from the environment, used in a process and then recycled.

Supercritical fluids have been heavily investigated as environmentally benign solvents. A supercritical fluid is a substance at a temperature and pressure above its thermodynamic critical point. Under these conditions, these substances exhibit properties such as high gas-like diffusivity, zero surface tension, ease of solvent

removal, the ability to be recycled and can be tuned to achieve the desired density and solvent properties. However, the critical temperatures (T_c) of possible solvents can be inconveniently high (T_c of water is 374.2°C, P_c = 221.2 atm). In contrast, supercritical carbon dioxide ($scCO_2$) has the advantage of having an easily accessible critical point (T_c = 31.1°C, P_c = 72.8 atm). It is inexpensive and environmentally benign, and it combines the best properties of both a gas and liquid which makes it easy to separate from solutes. These unique properties associated with supercritical fluids offer a range of possibilities in polymer chemistry. DeSimone *et al.* showed that high molar mass fluoropolymers could be synthesized by using homogeneous free radical polymerization methods in $scCO_2$.[4] Here $scCO_2$ helped circumvent the environmental concerns of chlorofluorocarbons. DuPont has prepared a range of fluoropolymers using $scCO_2$ as a reaction medium.[5] Several co-polymerizations via living free radical polymerization reactions (Reversible Addition Fragmentation Chain Transfer (RAFT) and Atom Transfer Radical Polymerization (ATRP)) have been successfully carried out in $scCO_2$.[6, 7] Supercritical CO_2 has also been used for the production of microcellular biodegradable composite materials. Mistele *et al.* described the ring opening metathesis polymerization (ROMP) of norbornene in $scCO_2$.[8] Bien Tan *et al.* developed a new approach for producing inexpensive and biodegradable polymer surfactants for use in $scCO_2$.[9] They synthesized CO_2-soluble surfactants from oligomeric poly(vinyl acetate) that produced stable CO_2-in-water emulsions, which were then used to produce emulsion templated materials. For a more detailed study of polymerizations in $scCO_2$, the reader is directed to the review article by Kendall *et al*.[10]

Over the last couple of decades the unique properties of $scCO_2$ have led to its application in the area of microelectronics. Industrial and academic researchers have shown that $scCO_2$ has been explored for multiple aspects of device fabrication

including drying, cleaning, deposition and etching.[11, 12, 13, 14] More recently $scCO_2$ has been used for the synthesis and processing of organic materials in the area of flexible electronics. Progress of the semiconductor industry is based on the ever increasing demand of miniaturization of devices as described by Moore's Law.[15] As microelectronic features progress to the 45 nm node and smaller, overcoming the inherent challenges at such small dimensions becomes more difficult. At these resolutions, development of photoresist images in aqueous-base can cause the pattern to collapse inwards due to high surface tension of the aqueous solution.[16, 17] As the rinse solution evaporates from the narrow openings, it pulls the features together. In addition, line edge roughness (LER) becomes increasingly problematic for sub-50 nm features as the acceptable tolerance of edge roughness of the patterns decreases with smaller features.[18, 19] Both these issues need to be addressed in lithography. Thus, the use of multiple layers of varied materials in organic electronics and high performance transistors requires a solvent system that is selective and benign in order to maintain the integrity of the device. It has been established that $scCO_2$ can be used for the development of small scale structures without suffering from the very strong capillary forces that lead to pattern distortion. In particular, Goldfarb *et al.* have explored in greater depth, the direct use of $scCO_2$ as a means of avoiding pattern collapse.[20, 21] Johnston and co-workers have reported the use of hydrocarbon surfactants to dry photoresists directly in $scCO_2$.[22] Development in $scCO_2$ can lead to a dramatic decrease in the glass transition temperature of resists. It has been shown by various methods that CO_2 is a good plasticizing agent for a host of polymeric materials even at moderate pressures.[23] This can help in reducing LER by surface treating the photoresist with $scCO_2$ during and after development. The plasticized photoresist may be subjected to a heating step to reflow the photoresist. Meagley *et al.* have predicted that such a reflow process may help reduce LER of the patterned, developed

photoresist.[24] Besides these technical issues of image collapse and LER, "wet" processes have high environmental implications and potentially pose an occupational risk for line workers. Williams *et al.* reported in 2002 that the production of a single 2-gram 32 MB DRAM microchip requires about 1600 g of secondary fossil fuels and 72 g of chemical inputs. About 32 kg of water and 700 g of elemental gases (mainly nitrogen) are used in the fabrication stage.[25] A solution to this problem is of utmost importance. The advantages of $scCO_2$ development over conventional aqueous base development are summarized in Figure 2.1.

Even though liquid and supercritical CO_2 have attracted much interest as an environmentally benign solvent, its practical use has been limited due to the low solubility of many materials, particularly the polar polymers used in high-resolution photoresists. Generally CO_2 is a good solvent for many non-polar molecules with low molecular weights. However, high CO_2 pressures are required to dissolve small amounts of polar, amphiphilic or high molecular weight polymers. This restricts the type of polymers that can be processed in $scCO_2$ to experimental photoresists. The current lithographic imaging process involves the acid-catalyzed cleavage of pendent protecting groups, such as the *tert*-butoxycarbonyl (t-boc) group, *tert*-butyl and methyl adamantyl groups to generate base-soluble acidic functionalities such as hydroxyl and carboxylic acid groups. This imaging mechanism has drawn a great deal of attention because it provides the basis of designing aqueous base developable positive photoresists. However, these polar polymer photoresists are generally insoluble in $scCO_2$, making it extremely difficult for the required solubility switch to be observed in the $scCO_2$ solvent. For pure $scCO_2$ processing, certain fluorinated or silicone containing classes of polymers are typically used.[26] It is believed that the presence of fluorine creates molecules with weak self-interaction, thus increasing the solubility in

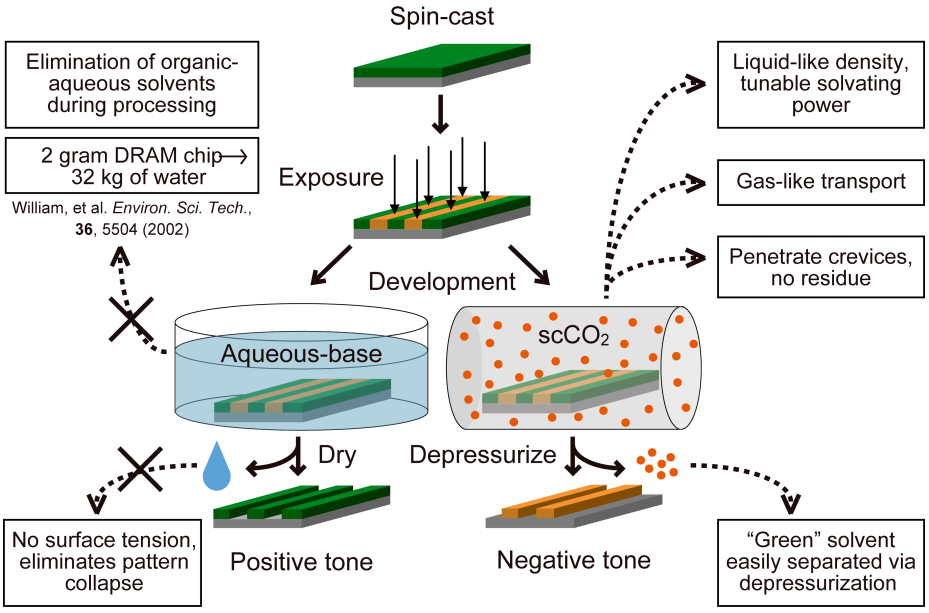

Figure 2.1. Comparison between conventional aqueous-base processing and $scCO_2$ processing. Processing in $scCO_2$ has several environmental and lithographical benefits.

$scCO_2$. Previously our group has demonstrated the ability to develop custom polymeric photoresists in pure $scCO_2$ using otherwise conventional photoresist chemistries with the inclusion of fluorinated moieties to impart $scCO_2$ solubility.[27] Unfortunately, the fluorination of polymers to achieve CO_2 solubility is relatively expensive and the high content of fluorine has an adverse effect on the etch resistance of the polymer matrix.[28] Due to this characteristic, commercial photoresists generally do not have fluorinated components. Examining the possibility to process fluorine free photoresists, the ability to develop a variety of small molecule, molecular glass resists in pure $scCO_2$ with easily achievable resolution down to 50 nm have been demonstrated.[29, 30] Felix *et al.* have reported a new type of acid-catalyzed, chain scission polymeric system based on main-chain acetal linkages to produce high-resolution, $scCO_2$ processed positive tone patterns. Excellent solubility contrasts and feature sizes below 200 nm were obtained with this system.[31]

Recently, several researchers have reported the ability to develop conventional polymeric resists in $scCO_2$ using cosolvents or tailored soluble additives. Mao *et al.* have shown that the addition of selected cosolvents such as acetone or alcohols allows for the development of fluorinated and non-fluorinated photoresists in $scCO_2$.[32, 33] In addition, other researchers have shown that the inclusion of certain surfactants into $scCO_2$ imparts solubility to otherwise insoluble polymers.[34] Wagner *et al.* at Micell Integrated Systems have recently reported a solution to the solubility of polar polymers in $scCO_2$ by use of surfactants they call CO_2 compatible salts.[35] They used these salts to get highly effective images with $scCO_2$ processing of a standard EUV photoresist. This technique has shown impressive contrast and dense L/S features with aspect ratios > 12.[36] These results encouraged us to study $scCO_2$ compatible quaternary ammonium salt additives. The mechanism of dissolution of polymers in $scCO_2$ in the presence of nitrogen containing additives is clearly at an early stage of

understanding. In order to design highly efficient additives, it is crucial to understand the interactions that these additives have with the different functional groups on the chemical structures of the polar polymers commonly used as photoresist materials.

This chapter describes the synthesis of a series of fluorinated quaternary ammonium salts (QAS) as $scCO_2$ compatible additives and demonstrates their utility to help dissolve polar polymers in $scCO_2$. In particular, the effects of architecture (symmetric or asymmetric structure) of the cation and the effect of the basic nature and size of the counter anion of the salt, on the efficiency of the $scCO_2$ compatible additive were studied in detail. The solubility of each QAS was tested in $scCO_2$ at various concentrations, temperatures and pressures. The solubility enhancement parameter was calculated for each salt using computational methods. The effect of these salts on the dissolution behavior of model polymers has been described. For this study, three different protected acidic polymer systems. Poly(4-t-butoxycarbonyloxystyrene) (PBOCST), poly(hydroxystyrene-co-styrene-co-*t*-butylacrylate) (PHS-co-PS-co-PtBA) and poly(methyladamantane methylacrylate-co-α-methacryloxy-γ-butyrolactone) (PMAMA-co-PGBLMA) each have structures similar to what one would find in a chemically amplified photoresist were chosen. Without the QAS additive, all of the polar polymers showed no dissolution in $scCO_2$ in the protected or deprotected acidic form. Addition of millimolar quantities of the QAS to the $scCO_2$ developer helped dissolve the protected polymers under moderate supercritical conditions. To explicitly investigate the interactions between the polymers, QAS additives and the $scCO_2$ solvent computational simulations were carried out using a fully atomistic force-field adapted from optimized potentials for liquid simulations (OPLS). Based on the experimental and computational results the interactions between the QAS additive and different functional groups on the

solubilized polymer were identified. Understanding these interactions is important if superior additives are to be designed.

Finally based on these findings, the lithographic evaluation of a standard commercially available polymer photoresist has been reported using an appropriate $scCO_2$ compatible QAS additive in $scCO_2$. Well-resolved, negative tone patterns as small as 100 nm were obtained by e-beam lithography, indicating the potential of using $scCO_2$ as a process solvent for polar polymers in the presence of the QAS additives.

Experimental Section

Materials. All chemicals except resists were purchased from Sigma-Aldrich unless otherwise stated and were used without further purification. High purity carbon dioxide and argon were purchased from Airgas and used as received. Poly(4-*t*-butoxycarbonyloxystyrene] (PBOCST) was prepared by protecting poly(4-hydroxystyrene) (M_n = 8000) with di-*t*-butyldicarbonate. Poly(hydroxystyrene-co-styrene-co-*t*-butylacrylate) (PHS-co-PS-co-PtBA) and Poly(methyladamantane methacrylate-co-a-methacryloxy-g-butyrolactone) (PMAMA-co-PGBLMA) polymers were obtained from DuPont Electric polymers Inc. and Mitsubishi Rayon America Inc., respectively. A commercial photoresist used for lithographic evaluation was donated by Tokyo Ohka Kogyo (TOK) Co. Ltd.

Characterization. ^{1}H NMR spectra were recorded on a Varian Inova-400 (400 MHz) or Mercury-300 (300 MHz) spectrometer at room temperature, using the chemical shift of a residual protic solvent (chloroform at δ 7.24 ppm or acetonitrile at 2.10 ppm) as an internal reference. All shifts are quoted in parts per million (ppm) relative to chloroform or acetonitrile, and coupling constants *J* are measured in hertz. The multiplicity of the signal is indicated as follows: s (singlet), d (doublet), t (triplet),

q (quartet), and m (multiplet). ^{19}F NMR spectra were recorded on a Varian Mercury-300 (300 MHz) spectrometer.

Synthesis of 1,1,1,2,2,3,3,4,4,5,5,6,6-tridecafluoro-9-iodononane (1). 4,4,5,5,6,6,7,7,8,8,9,9,9-tridecafluorononan-1-ol (25 g, 66.1 mmol, purchased from SynQuest), triphenyl phosphine (26.0 g, 99.2 mmol), and imidazole (26.0 g, 99.2 mmol) were dissolved in 300 ml of anhydrous THF and cooled to -78 °C. Iodine (25.2 g, 99.2 mmol) was then added slowly to the solution at -78 °C. The mixture was stirred for 1 h at -78 °C and allowed to warm up to room temperature. After stirring for 2 h at room temperature, the mixture was quenched by adding 100 ml of water. The product was extracted with diethyl ether three times and washed with water. The solvent was evaporated, and then 300 ml of fresh diethyl ether was added to precipitate the by-product, phosphonium oxide. After the precipitate was filtrated off, the product was purified by the distillation under vacuum. The product was obtained as a colorless viscous liquid (27.1 g, yield = 79.3%); ^{1}H NMR (300 MHz, $CDCl_3$): d = 3.24 (t, J = 6.3 Hz, 2H, -CF_2-C$\underline{H}_2$-), 2.20 (m, 2H, -C$\underline{H}_2$-), 2.15 (t, J = 6 Hz, 2H, -C$\underline{H}_2$-I). ^{19}F NMR (300 MHz, $CDCl_3$): d = -82.0 (s, 3F, C$\underline{F}_3$-), -114.7 (s, 2F, CF_3-C$\underline{F}_2$-), -122.8 (s, 2F, -C$\underline{F}_2$-), -123.8 (s, 2F, -C$\underline{F}_2$-), -124.5 (s, 2F, -C$\underline{F}_2$-), -127.1 (s, 2F, -C$\underline{F}_2$-CH_2-).

Synthesis of *N*-ethyl-4,4,5,5,6,6,7,7,8,8,9,9,9-tridecafluoro-*N*-methylnonan-1-amine (2)., Ethyl methyl amine (5.5 g, 92.2 mmol) was added dropwise to a mixture of **1** (10g, 20.5 mmol) and pyridine (20 ml). The mixture was stirred for 4 hours at 80 °C after which the lower phase (yellow liquid) of the mixture solution was collected. The remaining upper phase (red liquid) was washed with 10 wt% NaOH aqueous solution for 1h at 50 °C and allowed to stand. The lower phase was collected and combined to the previous yellow liquid. The collected liquid was washed with a 10 wt% NaOH aqueous solution and dried with magnesium sulfate. After distillation

under vacuum, the product was obtained as colorless viscous liquid (6.29 g, yield = 73.2%); ^{1}H NMR (300 MHz, $CDCl_3$): *d* = 2.42 (t, *J* = 7.4 Hz, 2H, -C$\underline{H}_2$-N-), 2.39 (t, *J* = 7.8 Hz, 2H, -N-C$\underline{H}_2$-), 2.20 (s, 3H, -N-C$\underline{H}_3$), 2.09 (m, 2H, -CF_2-C$\underline{H}_2$-), 1.75 (m, 2H, -CH_2-C$\underline{H}_2$-CH_2-), 1.04 (t, *J* = 7.2 Hz, 3H, -CH_2-C$\underline{H}_3$). ^{19}F NMR (300 MHz, $CDCl_3$): *d* = -81.3 (s, 3F, C$\underline{F}_3$-), -114.7 (s, 2F, CF_3-C$\underline{F}_2$-), -122.4 (s, 2F, -C$\underline{F}_2$-), -123.4 (s, 2F, -C$\underline{F}_2$-), -124.0 (s, 2F, -C$\underline{F}_2$-), -126.7 (s, 2F, -C$\underline{F}_2$-CH_2-).

Synthesis of *N*-ethyl-4,4,5,5,6,6,7,7,8,8,9,9,9-tridecafluoro-*N*-methyl-*N*-(4,4,5,5,6,6,7,7,8,8,9,9,9-tridecafluorononyl)nonan-1-aminium iodide (QAS-3). A mixture of **1** (9.06 g, 18.6 mmol) and **2** (6.77 g, 16.2 mmol) was stirred for 24 h at 80 °C. After the reaction, the crude product was washed with copious amount of diethyl ether to remove remaining reactants, and then dried under vacuum. The product was obtained as a white powder (11.8 g, yield = 80.4%); ^{1}H NMR (300 MHz, acetonitrile-3d): *d* = 3.39-3.29 (m, 6H, -N-C$\underline{H}_2$-), 3.00 (s, 3H, -N-C$\underline{H}_3$), 2.31 (m, 4H, -C$\underline{H}_2$-), 2.05 (m, 4H, -C$\underline{H}_2$-), 1.32 (t, *J* = 6.9 Hz, 3H, -CH_2-C$\underline{H}_3$). ^{19}F NMR (300 MHz, acetonitrile-3d): *d* = -81.9 (s, 6F, C$\underline{F}_3$-), -115.0 (s, 4F, CF_3-C$\underline{F}_2$-), -122.8 (s, 4F, -C$\underline{F}_2$-), -123.8 (s, 4F, -C$\underline{F}_2$-), -124.5 (s, 4F, -C$\underline{F}_2$-), -127.1 (s, 4F, -C$\underline{F}_2$-CH_2-).

Synthesis of QAS-1 – QAS-10. The general synthetic procedure for QAS is described with the synthesis of **QAS-4** and **QAS-7** given in detail as representative. **QAS-5** – **QAS-10** were prepared using similar synthetic procedures as **QAS-7**, with their corresponding counter anion sodium salts. **QAS-1** was obtained from **1** and triethylamine. **QAS-2** was prepared using diethylamine instead of ethylmethylamine.

QAS-4. An acetic acid/water mixture solution (25 ml/25ml) of **QAS-3** (0.50 g, 0.55 mmol) was passed slowly through an ion-exchange column filled with 500 g of an anion exchange resin (Dowex® 1X4 chloride form, 20-50 mesh), which was converted to acetate form using acetic acid/water before usage. After passing the **QAS-3** solution, the column was washed with 500 ml of acetic acid/water. The

aqueous solution was concentrated and fully dried at 80°C under vacuum to yield **QAS-4** as a white solid (0.46 g, yield = 99.4%); ^{1}H NMR (300 MHz, acetonitrile-3d): *d* = 3.40-3.31 (m, 6H, -N-C$\underline{H}_2$-), 3.02 (s, 3H, -N-C$\underline{H}_3$), 2.32 (m, 4H, -C$\underline{H}_2$-), 2.19 (s, 3H, C$\underline{H}_3$-COO$^-$), 2.03 (m, 4H, -C$\underline{H}_2$-), 1.32 (t, *J* = 6.9 Hz, 3H, -CH$_2$-C$\underline{H}_3$). ^{19}F NMR (300 MHz, acetonitrile-3d): *d* = -82.0 (s, 6F, C$\underline{F}_3$-), -114.9 (s, 4F, CF$_3$-C$\underline{F}_2$-), -122.8 (s, 4F, -C$\underline{F}_2$-), -123.8 (s, 4F, -C$\underline{F}_2$-), -124.4 (s, 4F, -C$\underline{F}_2$-), -127.1 (s, 4F, -C$\underline{F}_2$-CH$_2$-).

QAS-7. To an acetonitrile solution (5 ml) of **QAS-3** (1.5 g, 1.65 mmol), an aqueous solution (50 ml) of sodium perfluoropropionate (15.4 g, 82.7 mmol) was added. After stirring the mixture solution for 7 -10 days to ensure complete ion exchange, the solvent was removed under vacuum. The crude product was washed with 5×200 ml of water to remove excess amount of sodium perfluoropropionate, and then dried under vacuum. The product was obtained as a white solid (1.09 g, yield = 69.8%); ^{1}H NMR (300 MHz, acetnitrile-3d): *d* = 3.42-3.35 (m, 6H, -N-C$\underline{H}_2$-), 3.03 (s, 3H, -N-C$\underline{H}_3$), 2.31 (m, 4H, -C$\underline{H}_2$-), 2.04 (m, 4H, -C$\underline{H}_2$-), 1.32 (t, *J* = 6.9 Hz, 3H, -CH$_2$-C$\underline{H}_3$). ^{19}F NMR (300 MHz, aetnitrile-3d): *d* = -82.1 (s, 6F, C$\underline{F}_3$-), -83.8 (s, 3F, C$\underline{F}_3$-), -115.1 (s, 4F, CF$_3$-C$\underline{F}_2$-), -120.1 (s, 2F, CF$_3$-C$\underline{F}_2$-COO$^-$), -122.9 (s, 4F, -C$\underline{F}_2$-), -123.9 (s, 4F, -C$\underline{F}_2$-), -124.6 (s, 4F, -C$\underline{F}_2$-), -127.2 (s, 4F, -C$\underline{F}_2$-CH$_2$-).

QAS-1. Yield = 62.3%; ^{1}H NMR (300 MHz, acetonitrile-3d): δ = 3.61-3.48 (m, 8H, -N-C$\underline{H}_2$-), 2.42 (m, 2H, -C$\underline{H}_2$-), 2.18 (s, 3H, C$\underline{H}_3$-COO$^-$), 2.14 (t, 2H, -C$\underline{H}_2$-), 1.46 (t, *J* = 6.9 Hz, 9H, -CH$_2$-C$\underline{H}_3$). ^{19}F NMR (300 MHz, acetonitrile-3d): δ = -81.3 (s, 3F, C$\underline{F}_3$-), -114.3 (s, 2F, CF$_3$-C$\underline{F}_2$-), -122.4 (s, 2F, -C$\underline{F}_2$-), -123.4 (s, 2F, -C$\underline{F}_2$-), -124.0 (s, 2F, -C$\underline{F}_2$-), -126.7 (s, 2F, -C$\underline{F}_2$-CH$_2$-).

QAS-2. Yield = 54.7%; ^{1}H NMR (300 MHz, acetonitrile-3d): δ = 3.34-3.19 (m, 8H, -N-C$\underline{H}_2$-), 3.02 (s, 3H, -N-C$\underline{H}_3$), 2.32 (m, 4H, -C$\underline{H}_2$-), 2.17 (s, 3H, C$\underline{H}_3$-COO$^-$), 1.96 (m, 4H, -C$\underline{H}_2$-), 1.27 (t, *J* = 6.9 Hz, 3H, -CH$_2$-C$\underline{H}_3$). ^{19}F NMR (300 MHz,

acetonitrile-3d): δ = -81.3 (s, 6F, C$\underline{F}_3$-), -114.2 (s, 4F, CF_3-C$\underline{F}_2$-), -122.4 (s, 4F, -C$\underline{F}_2$-), -123.4 (s, 4F, -C$\underline{F}_2$-), -123.9 (s, 4F, -C$\underline{F}_2$-), -126.6 (s, 4F, -C$\underline{F}_2$-CH_2-).

QAS-5. Yield = 7.6%; ^{1}H NMR (300 MHz, acetonitrile-3d): δ = 3.42-3.31 (m, 6H, -N-C$\underline{H}_2$-), 2.99 (s, 3H, -N-C$\underline{H}_3$), 2.30 (m, 4H, -C$\underline{H}_2$-), 2.23 (m, 2H, -C$\underline{H}_2$-COO^-), 2.03 (m, 4H, -C$\underline{H}_2$-), 1.56 (m, 2H, -C$\underline{H}_2$-), 1.30 (m, 9H, -CH_2-C$\underline{H}_3$, -C$\underline{H}_2$-), 0.90 (t, 3H, -C$\underline{H}_3$).

QAS-6. Yield = 61.4%; ^{1}H NMR (300 MHz, acetonitrile-3d): δ = 3.43-3.37 (m, 6H, -N-C$\underline{H}_2$-), 3.05 (s, 3H, -N-C$\underline{H}_3$), 2.32 (m, 4H, -C$\underline{H}_2$-), 2.05 (m, 4H, -C$\underline{H}_2$-), 1.32 (t, J = 6.9 Hz, 3H, -CH_2-C$\underline{H}_3$). ^{19}F NMR (300 MHz, acetonitrile-3d): δ = -75.8 (s, 3F, C$\underline{F}_3$-COO^-), -82.1 (s, 6F, C$\underline{F}_3$-), -115.0 (s, 4F, CF_3-C$\underline{F}_2$-), -122.9 (s, 4F, -C$\underline{F}_2$-), -123.8 (s, 4F, -C$\underline{F}_2$-), -124.5 (s, 4F, -C$\underline{F}_2$-), -127.1 (s, 4F, -C$\underline{F}_2$-CH_2-).

QAS-8. Yield = 79.3%; ^{19}F NMR (300 MHz, acetonitrile-3d): δ =-82.0 (s, 9F, C$\underline{F}_3$-), -114.9 (s, 4F, CF_3-C$\underline{F}_2$-), -116.5 (s, 2F, CF_3-C$\underline{F}_2$-), -122.8 (s, 4F, -C$\underline{F}_2$-), -123.1 (s, 2F, -C$\underline{F}_2$-), -123.8 (s, 6F, -C$\underline{F}_2$-), -124.5 (s, 6F, -C$\underline{F}_2$-), -127.1 (s, 6F, -C$\underline{F}_2$-CH_2-).

QAS-9. Yield = 87.6%; ^{1}H NMR (300 MHz, acetonitrile-3d): δ = 3.41-3.29 (m, 6H, -N-C$\underline{H}_2$-), 3.00 (s, 3H, -N-C$\underline{H}_3$), 2.48-2.21 (m, 10H, -C$\underline{H}_2$-), 2.02 (m, 4H, -C$\underline{H}_2$-), 1.30 (t, J = 6.9 Hz, 3H, -CH_2-C$\underline{H}_3$). ^{19}F NMR (300 MHz, acetonitrile-3d): δ = -81.9 (s, 9F, C$\underline{F}_3$-), -114.9 (s, 4F, CF_3-C$\underline{F}_2$-), -116.3 (s, 2F, CF_3-C$\underline{F}_2$-), -122.8 (s, 4F, -C$\underline{F}_2$-), -123.8 (s, 4F, -C$\underline{F}_2$-), -124.5 (s, 4F, -C$\underline{F}_2$-), -126.9 (s, 4F, -C$\underline{F}_2$-CH_2-), -128.9 (s, 2F, -C$\underline{F}_2$-CH_2-).

QAS-10. Yield = 79.3%; ^{1}H NMR (300 MHz, acetonitrile-3d): δ = 7.01 (t, J = 7.8 Hz, 2H, Ph), 7.01 (d, J = 8.1 Hz, 2H, Ph), 6.45 (t, J = 6.6 Hz, 1H, Ph), 3.38-3.21 (m, 6H, -N-C$\underline{H}_2$-), 2.96 (s, 3H, -N-C$\underline{H}_3$), 2.28 (m, 4H, -C$\underline{H}_2$-), 2.04 (m, 4H, -C$\underline{H}_2$-), 1.29 (t, J = 7.1 Hz, 3H, -CH_2-C$\underline{H}_3$). ^{19}F NMR (300 MHz, acetonitrile-3d): δ =-82.0 (s, 6F, C$\underline{F}_3$-), -114.9 (s, 4F, CF_3-C$\underline{F}_2$-), -122.8 (s, 4F, -C$\underline{F}_2$-), -122.9 (s, 4F, -C$\underline{F}_2$-), -123.8 (s, 4F, -C$\underline{F}_2$-), -124.6 (s, 4F, -C$\underline{F}_2$-), -127.2 (s, 4F, -C$\underline{F}_2$-CH_2-).

Lithographic Procedure. A typical procedure is described as follows using PHS-co-PS-co-PtBA as an example. A 10 wt% solution of the resist and triphenylsulfonium perfluoro-1-butane sulfonate (5 wt% w.r.t. photoresist) was prepared in propylene glycol monomethyl ether acetate (PGMEA). The solution was then spun-coat onto a HMDS-primed silicon wafer after being filtered through a 0.2 mm filter. The film (approximately 100 or 400 nm) was baked at 130 °C for 90 s. Parts of the wafers were exposed using an ABM mask aligner with 254 nm light source (7.1 mW/cm^2) for various times from 0.1 to 20 s. High resolution patterning was done using a Leica VB6B-HR e-beam lithography system operated at 100 kV. After exposure, post exposure bake was performed at 115 °C for 30 s.

Supercritical Carbon Dioxide Development. A series of films were developed in QAS/$scCO_2$ solutions using a $scCO_2$ dissolution-rate monitor apparatus, as described in previous papers.[37, 38] Briefly, a piece of silicon wafer coated with polymer resist film was placed into a 25 ml observation vessel, which was aligned with a HeNe laser (632.8 nm wavelength) and fitted with a quartz glass observation window for the laser beams to pass through. A known amount of QAS was dissolved in a 25 ml preheating vessel that connects the observation vessel and the CO_2 pump. CO_2 was introduced into the preheating vessel and kept for 15 min at the desired temperature and pressure to dissolve QAS into $scCO_2$ with stirring. Then, the QAS/$scCO_2$ solution was quickly introduced into the observation vessel. The reflected intensity of the laser on the film was continuously monitored until complete dissolution. The dissolution rate was calculated from the dissolution time and the film thickness. After development with QAS/$scCO_2$ solution, pure CO_2 was injected into each vessel to flush out the dissolving polymer photoresist and QAS.

Metrology. Tencor P10 profilometer was used to measure the film thickness of each polymer photoresist before and after development. Optical microscopy and

scanning electron microscopy (SEM) imaging were performed using the Nikon Digital Sight DS-5M-L1 and the Zeiss Ultra 55 SEM, respectively.

Computational Simulation. A fully atomistic model of the photoresists was adapted from the optimized potentials for liquid simulations (OPLS) force field. Optimization of the model by calculating local charges for each species was performed using quantum mechanical calculations with the Gaussian simulation package. Thin films of each resist were equilibrated and simulated in GROMACS.

Results and Discussion

Design and Synthesis of the QAS. The fluoroalkyl-substituted quaternary ammonium salt (QAS) was designed as a $scCO_2$ compatible additive to dissolve standard protected acidic polymers in $scCO_2$. The rationale behind the design is that the additive should favorably interact with either the unexposed (protected) or exposed (acidic) photoresist and solubilize it into the $scCO_2$ phase. This solubility switch forms the basis of creating three-dimensional patterns in the resist film. The ammonium cation center has high affinity for the polar moieties of the polymer photoresist and the fluoroalkyl chain is expected to impart solubility to the salt itself in $scCO_2$. These electrostatic interactions between the additive and the polymer can assist in the dissolution of the polymer in $scCO_2$. For these QAS, the architecture of the salt and the ion pair energy are important factors to be considered. QAS with symmetrical and unsymmetrical cations were synthesized and their solubility performance was compared. The basic nature of the counter anion also plays an important role in controlling the solubility of the salt and the strength of the ion pair energy, which determines the interaction between QAS and photoresists. Figure 2.2 shows a series of QAS with various combinations of cations and anions that were synthesized and used for this study. Scheme 2.1 shows a typical synthetic route of QAS using **QAS-4** as an

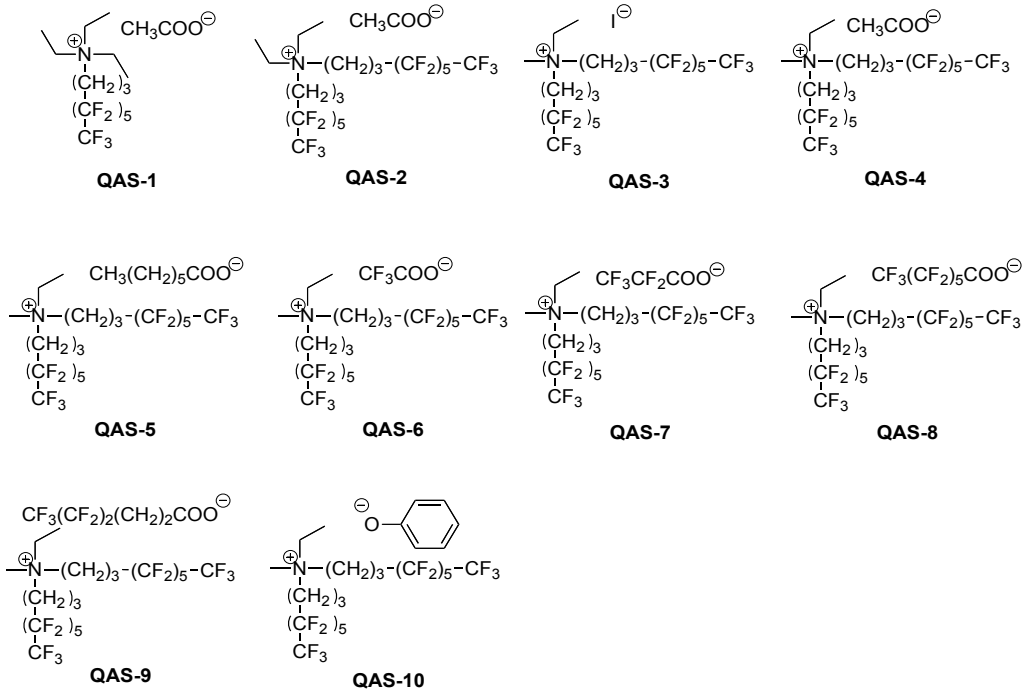

Figure 2.2. A series of synthesized QAS with asymmetric and symmetric cations and different counter anions.

example. Amination of fluoroalkyl iodide **1**, which was synthesized in three steps with a total yield of 40%, using ethylmethylamine yielded tertiary amine **2**. Reaction of the tertiary amine **2** and the fluoroalkyl iodide **1** formed quaternary ammonium salt with iodide anion (**QAS-3**). An acetic acid/water solution of **QAS-3** when passed through an ion-exchange yielded the anion-exchanged salt (**QAS-4**). To ensure complete conversion, the ion exchange column was washed with 500 mL of 50% acetic acid solution. Other salts were obtained from their corresponding counter anion sodium salts; for example **QAS-2** was synthesized using diethylamine instead of ethylmethylamine, and **QAS-7** bearing a fluorocarboxylate anion was prepared using the corresponding sodium perpropionate. The structure of each compound was characterized by ^{1}H- and ^{19}F-NMR.

Solubility of a series of QAS in $scCO_2$ was examined at various temperatures and pressures. Most of the QAS were highly soluble in $scCO_2$ under moderate conditions. In particular **QAS-4** and **QAS-7** showed good solubility in $scCO_2$ over a wide range of temperature and pressure (50-70 °C and 5000-7000 psi). These salts dissolved at concentrations up to 5 mM at 50 °C and 5000 psi. On the other hand, some of the QAS (**QAS-1**, **QAS-2**, **QAS-3**, and **QAS-5)** showed poor solubility in $scCO_2$ even at high temperature and pressure (70 °C, 7000 psi). These experimental observations were confirmed using computational simulations. The quaternary ammonium salts are amphiphilic as they have a polar ammonium cation and a relatively non-polar fluoroalkyl chain. It is expected that these salts form a reverse micelle structure in non- polar $scCO_2$ with the polar headgroups at the center and the fluoroalkyl chains facing outwards (water-in-oil micelle). The shape and size of a micelle depends on the architecture of its surfactant molecules and the solution conditions such as surfactant concentration, temperature and ionic strength. **QAS-1** was insoluble in $scCO_2$. This is somewhat expected due to the lower content of

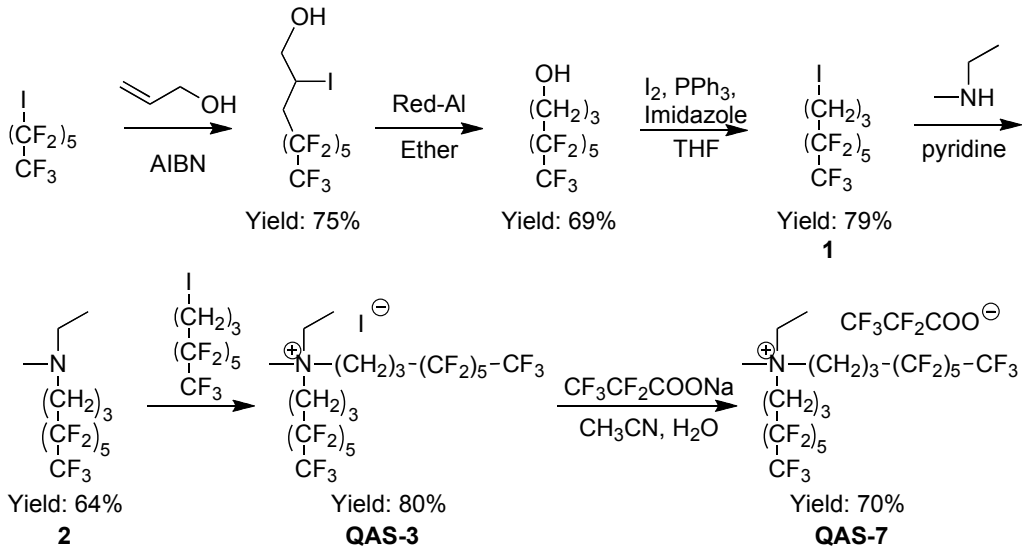

Scheme 2.1. Synthesis of the **QAS-4** additive. Other QAS were obtained similarly.

fluorine in the molecule. Psathas et al. have reported simulation results that also show that quaternary ammonium salts with a perfluoropolyether (PFPE) tail and a cationic trimethylammonium acetate head group form micelles in $scCO_2$.[39]

Fluorination is known to impart solubility in $scCO_2$. Modification of the **QAS-1** by adding another fluoroalkyl chain gave new salts with improved solubilities. However, **QAS-2** showed much lower solubility than **QAS-4** which is attributed to the symmetric molecular structure of **QAS-2**. Such symmetric molecules can aggregate and stratify onto each other, preventing the formation of micelles. The poor solubility of **QAS-3** and **QAS-5** can be explained by the fact that they both have rigid and bulky anions. The iodide and the heptanoate anions have low mobility in the solvent. This decreased mobility of the anions coupled with their steric hindrance prevents the micelle formation. The asymmetric salts, **QAS-4** and **QAS-7** showed high solubility in $scCO_2$. Thus the micelle formation in $scCO_2$ depends on the molecular architecture of the cation and size of the anion. Generally, it was observed that QAS with asymmetric cations are more easily soluble in $scCO_2$ compared to salts with symmetric cations.

These solubility properties of QAS were also studied using molecular simulations, where five QAS molecules were placed in a dense $scCO_2$ phase to examine micelle formation and determine solubility parameters. At the beginning of the simulation, the QAS molecules were widely spaced out in the simulation box; for **QAS-4** and **QAS-7**, the molecules quickly diffused towards each other and formed micelles. These micelles were stable for the duration of the simulation, corresponding to at least 1.5 ns. Other salts exhibiting relatively poor solubility in $scCO_2$, such as **QAS-1**, were slow to come together, and were unable to form stable micelles. The solubilities in $scCO_2$ can be quantified from a simulation by calculating the solubility enhancement factor, Γ.

$$\Gamma = \rho \int_0^\infty (g(r) - 1) 4\pi r^2 dr \quad (2.1)$$

where r is the density, and g(r) is the pair distribution function calculated between the QAS and $scCO_2$ molecules. Γ represents the solubility of the species relative to a mixture of ideal gases, and large positive values of Γ indicate good solubility while large negative values indicate poor solubility. For **QAS-4** and **QAS-7**, Γ was calculated to be 1.01 and 1.24, respectively; these values are consistent with the stable micelles observed in the simulations. **QAS-1**, on the other hand, had Γ = -1.44 and did not form long-lived, stable micelles.

Solubility Test of Reference Polymers in $scCO_2$ with QAS. Chemically amplified photoresists invented in the early 1980s enabled lithography to decrease the smallest accessible features of semiconductor devices. Today's advanced photoresists are exclusively built on the acid-catalyzed deprotection mechanism. Thus, three different acidic reference polymer systems namely poly(4-*t*-butoxycarbonyloxystyrene) (PBOCST), poly(hydroxystyrene-co-styrene-co-*t*-butylacrylate) (PHS-co-PS-co-PtBA) and poly(methyladamantane methylacrylate-co-α-methacryloxy-γ-butyrolactone) (PMAMA-co-PGBLMA) were chosen, that mimic many of the characteristics of a modern photoresist. In addition to these three model systems, the effect of our QAS additives on a commercial photoresist was also examined. The solubility of these spin-cast photoresist films shown in Figure 2.3 was tested in $scCO_2$ without any salts using a dissolution rate monitor. All these polymers were completely insoluble in $scCO_2$ before and after exposure without the addition of any additive.

The $scCO_2$-soluble QAS was put into the preheating vessel to help dissolve the polymer films into $scCO_2$. The solubilization of the polymer films (ca. 300 nm) was

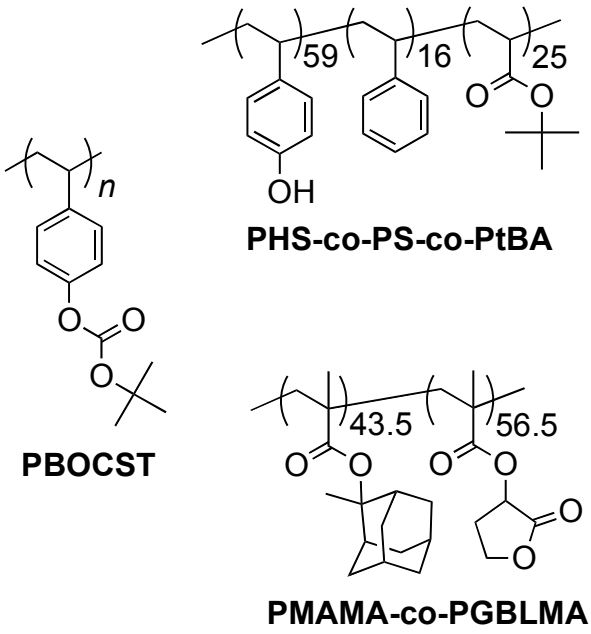

Figure 2.3. Chemical structures of PBOCST, PHS-co-PS-co-PtBA, and PMAMA-co-PGBLMA reference polymers.

monitored using laser interferometry. PBOCST and PHS-co-PS-co-PtBA with **QAS-4** dissolved in $scCO_2$ and showed changes in laser reflected intensity that corresponds to the film thickness change. After keeping the film in a QAS/$scCO_2$ solution for a short period, the laser reflected intensity increased slowly and reached a constant value corresponding to the value of the silicon surface itself, indicating that the entire film dissolved in $scCO_2$. The dissolution rates of polymer films were calculated by dividing the film thickness (nm) by the total time (s) until full dissolution of the films occur. The dissolution rates of PBOCST and PHS-co-PS-co-PtBA polymers in 1.25 mM **QAS-4**/$scCO_2$ solution at 50 °C and 5000 psi were ca. 40 and 25 nm/min, respectively. Profilometry and optical microscopy also support the bulk removal of these polymer films into $scCO_2$ after development. On the other hand, PMAMA-co-PGBLMA in the **QAS-4**/$scCO_2$ solution showed no change in reflected intensity value, suggesting the insolubility of this polymer in $scCO_2$. Table 2.1 shows the dissolution results of representative combinations of QAS and the selected polymers. The **QAS-7** did not help dissolve PBOCST, PHS-co-PS-co-PtBA or PMAMA-co-GBLMA into $scCO_2$, in contrast to **QAS-4** which solubilizes PHS-co-PS-co-PtBA and PBOCST in $scCO_2$. Other combinations of QAS and reference polymers were also examined: most of the other QAS including **QAS-6**, **QAS-8**, **QAS-9**, and **QAS-10** helped dissolve PBOCST in $scCO_2$, but they had no effect on PHS-co-PS-co-PtBA and PMAMA-co- PGBLMA. The exposed (deprotected) polymers were also developed in the QAS/$scCO_2$ solutions. The PHS-co-PS-co-PtBA copolymer became insoluble in the **QAS-4**/$scCO_2$ solution after exposure at doses of 0.71 to 14.2 mJ/cm^2. The deprotected PBOCST films showed very slow dissolution at 1-4 nm/min, which is much slower than that of the corresponding unexposed polymers. These results indicate that PBOCST and PHS-co-PS-co-PtBA have the potential to be utilized as negative-tone photoresists, processable

Table 2.1. Summary of dissolution of the reference polymers in 1.25 mM **QAS-4**/$scCO_2$ and **QAS-7**/$scCO_2$ solutions. The choice of counter anion is crucial to the QAS design. The basic nature and size of the counter anion is important. **QAS-4** with acetate anion helped dissolve polar protected polymers.

QAS	Resist	Unexposed	Exposed	Note
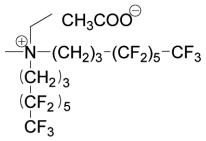 **QAS-4**	PBOCST	Dissolution (40 nm/min)	Slow dissolution (1-4 nm/min)	*Negative tone resist*
	PHS-co-PS -co-PtBA	Dissolution (25 nm/min)	No dissolution	*Negative tone resist*
	PMAMA-co-PGBLMA	No dissolution	No dissolution	
	TOK resist	Dissolution (15 nm/min)	Slow dissolution (1-2 nm/min)	*Negative tone resist*
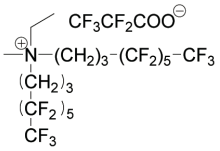 **QAS-7**	PBOCST	No dissolution	No dissolution	
	PHS-co-PS -co-PtBA	No dissolution	No dissolution	
	PMAMA-co-PGBLMA	No dissolution	No dissolution	
	TOK resist	Dissolution (45 nm/min)	Slow dissolution (<1 nm/min)	*Negative tone resist*

in $scCO_2$. The PMAMA-co-PGBLMA copolymer however, did not show any solubility in 1.25 mM **QAS-4**/$scCO_2$ solution at 50 °C and 5000 psi after a processing for 30 min. It is worth mentioning that the salt may be recovered from the QAS/$scCO_2$ solution by depressurizing $scCO_2$.

Computational Simulation. A number of polymers were simulated as thin films and exposed to various QAS additives in concert with this experimental work to provide a molecular level view of the systems and help elucidate the underlying mechanism at work. In that work, a fully atomistic model of the PHS-co-PS-co-PtBA and the PBOCST photoresists was adapted from the OPLS force field. In addition, the model was further optimized by calculating local charges for each species using quantum mechanical calculations with the Gaussian simulation package. The model of Harris and Yung was used for the $scCO_2$.[40] Thin films of each polymer were equilibrated and simulated in GROMACS. Each polymer was first equilibrated in the bulk, thenexposed to $scCO_2$ to form a thin film. This film was further equilibrated at a constant density of 817 kg/m^3 (Figure 2.4). After equilibration, production runs were performed in the NVT ensemble at 340K for 2ns. Forces on each atom were recorded during the simulations. Due to the high fluctuations on force during the course of a simulation, exact values at given positions were not statistically meaningful. However, by integrating the average force of each chain as a function of its position in the film, free energy curves for the removal of a polymer chain from the film in the presence of different QAS additives were obtained. The uncertainty in the energy at the surface of the film is less than 4 kT for all values shown. For further details on the molecular simulations, the reader is referred to another article.[41]

Proposed mechanism of dissolution of polymers in $scCO_2$. Here the interactions that the QAS have with the functional groups on the polymer have been

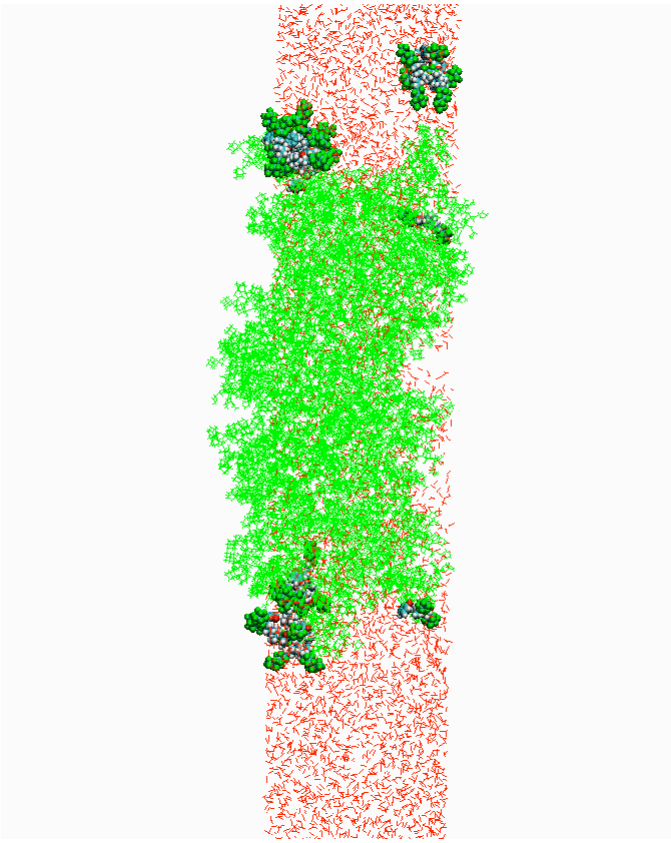

Figure 2.4. Example of equilibrated polymer film: PMAMA-co-PGBLMA with **QAS-10** in $scCO_2$. Box has periodic boundaries. Red lines are $scCO_2$, green lines are PMAMA-co-PGBLMA and spheres are **QAS-10**.

discussed to help them dissolve in $scCO_2$. As both **QAS-4** and **QAS-7** showed good solubility in $scCO_2$ but showed opposite effects on the dissolution of the reference polymers, these salts have been used to explain the interactions involved in the dissolution process. It is known that standard polar photoresist polymers are generally insoluble in non-polar $scCO_2$ solvent. The solubility of acidic and protected polar polymers in the presence of additives was examined and it was observed that the protected polymer is more soluble in $scCO_2$ than the acidic, deprotected polymer. The interactions between the QAS and the polymers depend on the ion pair energy, the shape and size and the mobility of the ions. Protected PBOCST showed very good solubility in $scCO_2$ in the presence of most of QAS because the electro-negative oxygen atom in the carbonate group can easily interact with the electro-positive ammonium center of QAS to provide a CO_2-friendly environment. This allows the fluorinated $scCO_2$ soluble salt to pull the polymer into the $scCO_2$. Simulation of PBOCST also predicted dissolution in **QAS-4** and **QAS-7**. It was found that as polymer chains dissolved into the $scCO_2$ phase from the film, each chain formed its own spherical globule with the *tert*-butyl tails of each monomer creating a non-polar outer shell for the chain. The QAS molecules bind to the surface of the polymer film, but have limited interactions with the dissolved species. However, such micelles do not freely form in the absence of QAS, indicating that the QAS interactions stabilize the formation of these micelles by an unknown mechanism. E-beam exposure of the PBOCST polymer in the presence of an onium acid generator, causes the deprotection of the acid labile *tert*-butoxycarbonyl groups to phenolic acid. Removal of the acid cleavable *t*-BOC group greatly increases polymer-polymer dipole interactions by the resulting hydroxy groups. This lowers the interaction with the QAS additive and the solubility in $scCO_2$ sharply decreases.

In the case of the unexposed PHS-co-PS-co-PtBA polymer, oxygen atoms in the hydroxyl group and carbonyl group can undergo electrostatic interaction with ammonium cations. **QAS-7**/$scCO_2$ solution did not dissolve the PHS-co-PS-co-PtBA polymer in contrast to **QAS-4**/$scCO_2$ solution. This result is attributed to the ion pair energy of the salt, which depends on the basic nature of the anion. The fluoroalkyl carboxylate anion in **QAS-7** is less basic than the carboxylate anion in **QAS-4** due to the inductive effect of the fluorine substitution. Therefore the anion in **QAS-7** is weak enough to deprotonate the hydroxyl groups and has weak electrostatic interaction with the electropositive carbon atom of the carbonyl group in the polymer. Simulations of this polymer provided results consistent with the experiments suggesting dissolution in the presence of **QAS-4**, but not with **QAS-7** (Figure 2.5). While resist at any given position may tend more towards dissolution or stability, it is only the energy value at the surface of the film, denoted by the termination of the line, as compared to the center that determines thermodynamic stability. Note that values reported at a higher distance from the center are averaged over more data, and are thus more accurate. Our molecular simulations show the carbonyl group of PHS-co-PS-co-PtBA plays a much smaller role than the hydroxyl group. Contact analysis confirms that charged **QAS-4** anions bind strongly to the hydroxyl groups and that multiple hydroxyl groups coalesce around a single **QAS-4**. These structures are stable on time scales exceeding 500ps.[39] Additionally, the **QAS-4** salt ions dissociate as additive penetrates into the polymer phase. **QAS-7** has a weaker interaction with this polymer on the film surface and a substantial fraction of the additive remains in the $scCO_2$ phase. Thus, it is unable to shield the hydroxyl groups of PHS-co-PS-co-PtBA from the non-polar $scCO_2$, causing the polymer to be insoluble in the solvent. This polymer has *tert*-butyl protecting groups, which are cleaved on deprotection. This deprotection reaction results in a more polar deprotected polymer bearing carboxylic acids and phenols that

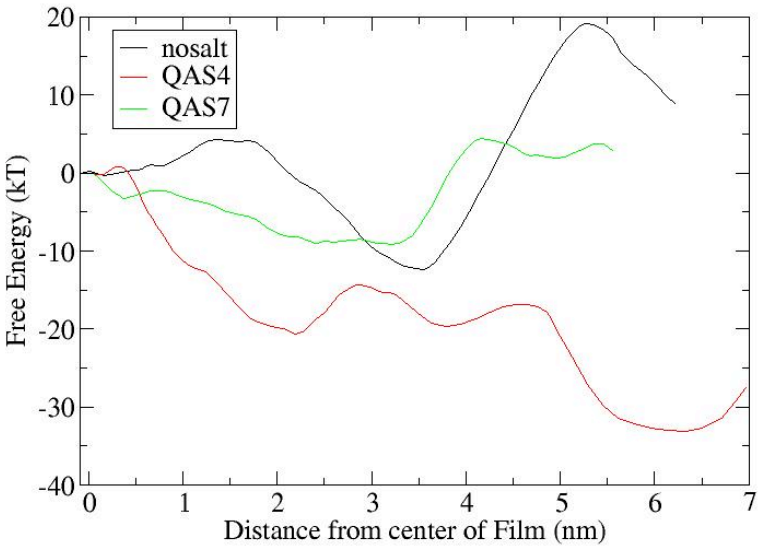

Figure 2.5. Free energy curves for $scCO_2$ system with and without QAS additives. Solid black, red and green lines represent PHS-co-PS-co-PtBA systems without an additive, with **QAS-4** and with **QAS-7** respectively. Results averaged over 1.0 ns. The free energy for **QAS-4** system is lower at the interface of the film (end of the line) than at the center of the film, indicating a net driving force for polymer dissolution. The other lines show an opposite trend, indicating that the polymer remains insoluble in $scCO_2$.

does not dissolve in $scCO_2$.

QAS-4 turned out to be the best salt for our work. This superior performance is because the ion pair energy of **QAS-4** is such that the ammonium cation can interact with the oxygen atoms of the resist material. Its acetate anion is strong enough to deprotonate the Brønsted acid groups. Based on the idea, **QAS-10** bearing phenolate anion was prepared as a new QAS bearing more basic anion. However, **QAS-10** allowed only PBOCST to dissolve in $scCO_2$ similar to the results of **QAS-7**. It is conceivable that the stronger ion pair prevented **QAS-10** from having any favorable interactions with the polymer. It is believed that a balance between the ion pair energy of the QAS and the basicity of the counter anion is important for the QAS to help dissolve the polymer. The protected PMAMA-co-PGBLMA polymer, which bears many ester groups and no carboxylic/phenol groups, was expected to dissolve in $scCO_2$ by using QAS. However, PMAMA-co-PGBLMA was fully insoluble in any QAS/$scCO_2$ solutions. Insolubility can be explained on the basis of steric effects. It is speculated that the bulky methyl adamantyl groups inhibit the polymer resist from interacting with the QAS. Simulation of PMAMA-co-PGBLMA in the presence of **QAS-10** also showed no solubility enhancement of the polymer. The QAS anion was bound immobile to the surface of the cation for the duration of the simulation. This is in contrast to other systems, whose QAS ions maintained some relative mobility, if not dissociating completely.

$scCO_2$ development of an e-beam patterned commercial resist. Based on these findings, a TOK polymer photoresist was used to evaluate the lithographic performance of this standard commercial polymer using an appropriate $scCO_2$ compatible QAS additive in $scCO_2$. This polymer works as a positive-tone photoresist in conventional aqueous base processing and is insoluble in $scCO_2$ without the use of

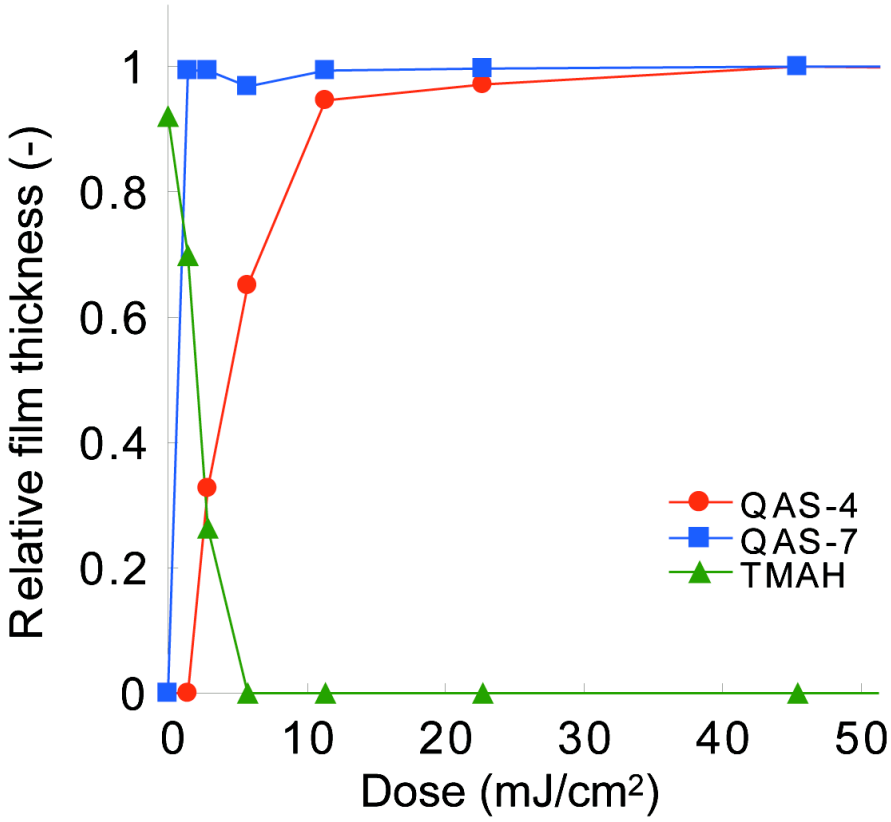

Figure 2.6. Contrast curves of the commercial TOK photoresist developed in $scCO_2$ with **QAS-4** or **QAS-7** (1.25 mM) at 50 °C, 5000 psi for 15 min, or developed in tetramethylammonium hydroxide (TMAH) aqueous solution (0.24 N) at room temperature for 30 sec.

the additive. Similar to the previously mentioned acidic polymers, the protected TOK polymer was processed in $scCO_2$ using the QAS additives. The protected polymer showed complete dissolution in scCO2 with either **QAS-4** or **QAS-7**. The dissolution rate monitor studies with the protected polymer film gave sine wave response, indicating a constant dissolution rate of 15 nm/min. Most of the other salts had no effect on the polymer. It is worth mentioning that the polymer swelled in the **QAS-10**/$scCO_2$ solution. This result has encouraged us to design QAS additives with substituted phenolate counter anions to be used as dissolution aids for such commercial polymers. The deprotected TOK polymer film showed very slow dissolution at 1 nm/min, which is much slower than the corresponding protected polymer. The contrast curves of the TOK resist were studied with development in both **QAS-4**/$scCO_2$ and 0.26 N tetramethylammonium hydroxide solutions. The dissolution test of the TOK resist in $scCO_2$ in the presence of **QAS-7** revealed a similar negative tone behavior (Figure 2.6).

New lithographic technologies and materials are being developed to meet the growing demand for higher resolution. Electron-beam lithography enables the fabrication of nanometer-scale patterns as small as 20 nm. The primary advantage of e-beam lithography over photolithography is that it is one of the ways to beat the diffraction limit of light. Here results of an e-beam patterned resist developed in QAS/$scCO_2$ have been shown. Figure 2.7 (a) is a SEM image of a TOK resist film (90 nm thick) that was patterned by e-beam lithography with an exposure dose of 107 mC/cm^2 and developed in the 1.25mM **QAS-4**/$scCO_2$ solution for 60 min at 50 ^oC and 5000 psi. In the same way, the **QAS-7**/$scCO_2$ development also gave negative-tone patterns with feature sizes down to 100nm (Figure 2.7 (b)).

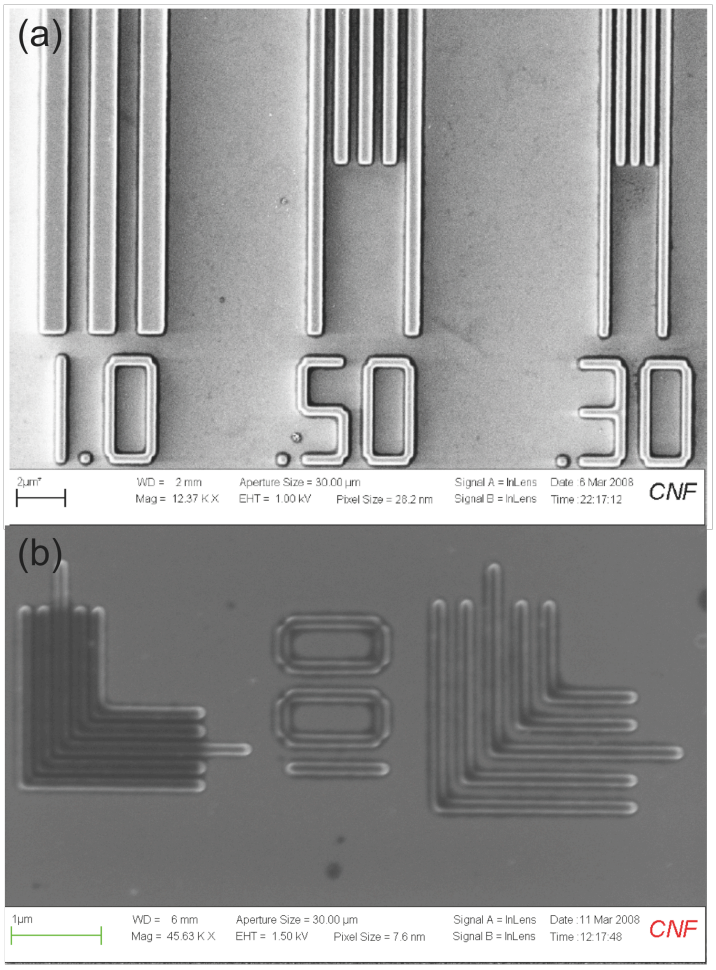

Figure 2.7. SEM images of the e-beam patterned commercial TOK polymer photoresist (a) exposed with 107 μC/cm^2, developed in 1.25 mM **QAS-4**/scCO_2 solution for 60 min at 50 °C and 5000 psi, (b) exposed with 20 μC/cm^2, developed in 1.25 mM **QAS-7**/scCO_2 solution for 60 min at 50 °C and 5000 psi.

Conclusion

A series of QAS were synthesized and examined as additives for $scCO_2$ to dissolve polar polymers in $scCO_2$. The chemical structures of QAS influence their solubility in $scCO_2$. QAS with higher fluorination, less sterically hindered anion and asymmetric structure of cation showed higher solubility. Such QAS proved to be very effective for dissolution of polar polymers in $scCO_2$. Addition of the $scCO_2$ compatible QAS greatly helped in the dissolution of polymers, especially PBOCST, PHS-co-PS-co-PtBA and a commercially used photoresist, under moderate conditions (50 °C and 5000 psi). Solubility of the polymers in $scCO_2$ was examined at various combinations of polymer and QAS additive by using a dissolution rate monitor to observe the change in film thickness during dissolution. The key interactions between the additive and the photoresist material were discussed by comparing the experimental results and computational simulations. Understanding these interactions is important and will help in designing more efficient additives for polymer dissolution.

Finally, based on these studies the lithographic performance of a polymer photoresist in $scCO_2$ development using an appropriate QAS was shown. As $scCO_2$ development has various advantages in terms of environmental and lithographic benefits, the success of photoresist development in $scCO_2$ using QAS additives is a significant result in the advancement of this environmentally friendly process.

Acknowledgments

Funding by Intel Corporation is gratefully acknowledged. Richard Schenker, Michael J. Leeson, Alan M. Myers (Intel Corporation), Jacob Adams and Roel Gronheid (Interuniversity Microelectronics Centre) are thanked for their helpful discussions. TOK is acknowledged for donating the commercial polymer photoresist.

The Cornell Nanoscale Science & Technology Facility (CNF) and the Cornell Center for Materials Research (CCMR) are thanked for use of their facilities and technical support. The author also acknowledges Grid Laboratory of Wisconsin (GLOW) for its computational resources.

REFERENCES

1. Cooper, A. I., *J. Mater. Chem.* **2000,** 10, 207.

2. Busby, D. C.; Glancy, C. W.; Hoy, K. L.; Kuo, A. C.; Lee, C.; Nielsen, K. A., *Surf. Coat. Int.* **1991,** 74, 362.

3. Ober, C. K.; Gabor, A. H.; GallagherWetmore, P.; Allen, R. D., *Adv. Mater.* **1997,** 9, 1039.

4. DeSimone, J. M.; Guan, Z.; Elsbernd, C. S., *Science* **1992,** 257, 945.

5. Wood, C. D.; Cooper, A. I.; DeSimone, J. M., *Curr. Opin. Solid State Mater. Sci.* **2004,** 8, 325.

6. Gregory, A. M.; Thurecht, K. J.; Howdl, S. M., *Macromolecules* **2008,** 41, 1215.

7. Villarroya, S.; Zhuo, J.; Duxbury, C. J.; Heis, A.; Howdle, S. M., *Macromolecules* **2006,** 39, 633.

8. Mistele, C. D.; Thorp, H. H.; DeSimone, J. M., *J. Macromol. Sci., Pure Appl. Chem.* **1996,** A33, 953.

9. Tan, B.; Lee, J. Y.; Cooper, A. I., *Macromolecules* **2007,** 40, 1945.

10. Kendall, J. L.; Canelas, D. A.; Young, J. L.; DeSimone, J. M., *Chem. Rev.* **1999,** 99, 543.

11. Wahlbrink, T.; Kuepper, D.; Bolten, J.; Moeller, M.; Lemme, M. C.; Kurz, H., *Microelectronic Engineering* **2007,** 84, (5-8), 1045.

12. Weibel, G. L.; Ober, C. K., *Microelectronic Engineering* **2003,** 65, 145.

13. Zong, Y.; Watkins, J. J., *Chem. Mater.* **2005,** 17, (3), 560.

14. Shan, X.; Watkins, J. J., *Thin Solid Films* **2006,** 496, (2), 412.

15. Bondyopadhyay, P. K., *Proc. of the IEEE* **1998,** 86, (1), 78.

16. Stoykovich, M. P.; Cao, H. B.; Yoshimoto, K.; Nealey, P. F., *Adv. Mater.* **2003,** 15, (14), 1180.

17. Yoshimoto, K.; Stoykovich, M. P.; Cao, H. B.; de Pablo, J. J.; Nealey, P. F.; Drugan, W., *J. Appl. Phys.* **2004,** 96, (4), 1857.

18. Bohme, T. R.; de Pablo, J. J., *J. Chem. Phys.* **2002,** 116, (22), 9939.

19. Fryer, D. S.; Nealey, P. F.; de Pablo, J. J., *Macromolecules* **2000,** 33, (17), 6439.

20. Goldfarb, D. L.; de Pablo, J. J.; Nealey, P. F.; Simons, J. P.; Moreau, W.; Angelopoulos, M., *J. Vac. Sci. Technol. B* **2001,** 19, (2), 600.

21. Goldfarb, D. L.; de Pablo, J. J.; Nealey, P. F.; Simons, J. P.; Moreau, W.; Anglelopoulos, M., *J. Vac. Sci. Technol. B* **2000,** 18, (6), 3313.

22. Zhang, X.; Pham, J. Q.; Ryza, N.; Green, P. F.; Johnston, K. P., *J. Vac. Sci. & Tech. B* **2004,** 22, (2), 818.

23. Chiou, J. S.; Barlow, J. W.; Paul, D. R., *J. Appl. Polym. Sci.* **1985,** 30, 2633.

24. Meagley, R.; Goodner, M.; Putna, S. E.; Clark, S.; Yueh, W. "Reducing Line Edge Roughness Using Chemically Assisted Reflow." US Patent WO/2005/038884, April 28, **2005**.

25. Williams, E. D.; Ayres, R. U.; Heller, M., *Environ. Sci. Technol.* **2002,** 36, 5504.

26. Krukonis, V., *Polymer News* **1985,** 11, 7.

27. Sundararajan, N.; Yang, S.; Ogino, K.; Valiyaveettil, S.; Wang, J. G.; Zhou, X.; Ober, C. K.; Obendorf, S. K.; Allen, R. D., *Chem. Mater.* **2000,** 12, 41.

28. Ito, H., *Adv. Polym. Sci.* **2005,** 172, 37.

29. Felix, N. M.; Tsuchiya, K.; Ober, C. K., *Adv. Mater.* **2006,** 18, (4), 442.

30. Tanaka, M.; Rastogi, A.; Kudo, H.; Watanabe, D.; Nishikubo, T.; Ober, C. K., *J. Mater. Chem.* **accepted**.

31. Felix, N.; Ober, C. K., *Chem. Mater.* **2008,** 20, 2932.

32. Mao, Y. e. a., *J. Vac. Sci. Technol. B* **2004,** 22, (5), 2473.

33. Mao, Y.; Felix, N. M.; Nguyen, P. T.; Ober, C. K., *Chemical Vapor Deposition* **2006,** 12, (5), 259.

34. Zweber, A. E.; Wagner, M.; Carbonell, R. G., *Proc. of SPIE* **2007,** 6519, 651948-1.

35. DeYoung, J.; Wagner, M.; Harbinson, C.; Miles, M.; Zweber, A. E.; Carbonell, R. G., *Proc. of SPIE* **2006,** 6153, 615345-1.

36. Wagner, M.; DeYoung, J.; Harbinson, C., *Proc. of SPIE* **2006,** 6153, 61531l-1.

37. Pham, V. Q.; Rao, N.; Ober, C. K., *J. Supercritical Fluids* **2004,** 31, 323.

38. Tanaka, M.; Rastogi, A.; Felix, N. M.; Ober, C. K., *J. Photopolym. Sci. Technol.* **2008,** 21, (3), 393.

39. Psathas, P. A.; Sander, E. A.; Lim, K. T.; Johnston, K. P., *J. Dispersion Sci. Tech.* **2002,** 23, (1-3), 65.

40. Harris, J. G.; Yung, K. H., *The Journal of Physical Chemistry* **1995,** 99, (31), 12021.

41. (a) Rastogi, A; Topperwein, G. N.; Tanaka, M.; Riggleman, R. A.; de Pablo, J. J.; Ober, C. K., Proceedings of SPIE 2009, 7273, 72734F-1. (b) Toepperwein, G. N.; Riggleman, R.; Rastogi, A.; Tanaka, M.; Ober, C. K.; de Pablo, J. J., **manuscript in preparation**.

CHAPTER 3

DIRECT PATTERNING OF INTRINSICALLY E-BEAM SENSITIVE POLYMER BRUSHES*

Abstract

The fabrication of patterned polymer brushes has attracted considerable attention as these structures can be exploited in devices on the nano- and microscale. Patterning of polymer brushes is typically a complex, multistep process. This chapter describes the direct patterning of poly(methyl methacrylate) (PMMA), poly(2-hydroxyethyl methacrylate) (PHEMA), poly(isobutyl methacrylate) (PIBMA), poly(neopentyl methacrylate) (PNPMA) and poly(2,2,2-trifluoroethyl methacrylate) (PTFEMA) brushes in a single step by electron beam lithography, to obtain nano-patterned polymer brush surfaces. PMMA, PHEMA, PIBMA, PNPMA and PTFEMA brushes were grown on silicon substrates via surface-initiated atom transfer radical polymerization. Surface analysis techniques including ellipsometry, contact angle goniometry, atomic force microscopy (AFM) and X-ray photoelectron spectroscopy (XPS) were used to characterize the thickness, hydrophilicity, roughness and chemical composition of the polymer brushes. Tapping-mode AFM imaging confirmed the successful electron beam patterning of these brushes. Using this direct patterning method, highly resolved nano-structured polymer brush patterns down to 50 nm lines were obtained. This direct patterning of brushes eliminates the need for complex

* This work done in collaboration with Marvin Y. Paik and Dr. Manabu Tanaka (Department of Materials Science & Engineering, Cornell University)

lithographic schemes. The sensitivity of these polymer brushes towards direct patterning with e-beam was studied and compared. The sensitivity curves indicate that the structure of the methacrylate polymer has a significant effect on the sensitivity of the polymer brush towards e-beam patterning. In particular, the effect of the functionality at the β-position to the methacrylate ester on the polymer brush sensitivity towards direct patterning was studied using groups of varying size and polarity.

Introduction

Stable and functional polymer brushes have been used as high tech coatings on flat or curved organic and inorganic substrates for a variety of applications. Polymer brushes in this chapter refer to an assembly of polymer chains tethered by one end to a surface. This tethering is sufficiently dense and due to this high steric crowding, the grafted chains extend from the surface, thus residing in an entropically unfavorable conformation.[1, 2] Generally, end-tethered polymer brushes, with covalent attachment of polymers on the substrate surface are assembled by either the "grafting to" or the "grafting from" approach. In the "grafting to" approach, pre-formed polymers are made to react with the reactive sites on the surface. The "grafting to" technique produces brushes with low grafting density and relatively low thickness due to the increased steric hindrance of grafted chains. This steric hindrance inhibits diffusion of large free polymer chains to diffuse to open surface reactive sites.[3] The "grafting from" approach, often referred to as surface-initiated polymerization, is attracting a lot of scientific interest mainly because it offers a way to assemble polymer brushes with tunable grafting density and brush thickness in a controllable fashion. Surface-initiated polymerization involves polymerizing a monomer from an immobilized monolayer of surface initiators. Several polymerization reactions such as conventional radical

polymerization,[4] iniferter,[5] ring-opening metathesis polymerization (ROMP),[6] cationic,[7] anionic,[8] aminoxyl mediated,[9] radical addition fragmentation chain transfer (RAFT)[10] and atom transfer radical polymerization (ATRP)[11] have been used to grow dense end-tethered polymer brushes.

The fabrication of patterned polymeric nanostructures has received significant interest because of its applications that range from the production of integrated circuits, information storage devices, light emitting displays to the fabrication of semiconductor microelectronics, micro-electromechanical systems (MEMS), miniaturized sensors, micro- or nanofluidic devices, biochips and for the production of optical components such as gratings and photonic crystals.[12-14] The past decade has witnessed the rapid development of a broad range of strategies used to pattern polymer brushes. Conventionally, patterned polymer brushes are produced from the initiator monolayer immobilized on patterned surfaces.[15-19] Here, the substrate is first patterned using complex lithographic schemes. Then a suitable initiator is immobilized in the patterned regions to grow polymer brushes in these confined regions. Patterned brushes have also been obtained via surface initiated polymerization from initiator containing self-assembled monolayers (SAMs) patterned by microcontact printing,[20-25] two-dimensional gradients,[26] contact molding,[27] scanning probe microscopy[28] or chemical lithography with electron irradiation[29-31] and subsequent surface initiated polymerization of a desired monomer. Kang and co-workers prepared self-assembled monolayers (SAMs) containing patterns of two different initiators, which they subjected to sequential orthogonal polymerization steps.[32] Zhou et al. prepared binary brushes of poly(methyl methacrylate) (PMMA) and poly(2-hydroxyethyl methacrylate) (PHEMA) via photoetching and reinitiation.[33] Andruzzi et al. have reported the patterning of polymer brushes using a modified photolithographic process involving the chemical vapor deposition of parylene.[34] In this method, the polymer

brushes were first grown off the silicon surface. The parylene was deposited, coated with photoresist by spin-casting, exposed, developed and reactive ion etched. Using this technique patterned brushes with 10 μm lines with 40 μm pitch size were prepared. Luzinov recently reported the use of an imprinted masking layer to form binary brushes.[35] New patterning methods such as nanografting, dip-pen nanolithography, contact lithography, atomic force microscopy lithography and microelectrochemical patterning have produced surface motifs with resolution down to tens of nanometers.[36-41] Most of these patterning methods require many steps in between and each of these steps may impose the possibility of losing information or pattern distortion.

This chapter describes the direct patterning of poly(isobutyl methacrylate) (PIBMA), poly(neopentyl methacrylate) (PNPMA) and poly(2,2,2-trifluoroethyl methacrylate) (PTFEMA) brushes using electron beam lithography. The polymer brushes were grown on silicon substrates via controlled atom transfer radical polymerization and patterned in a single step by degrading specific regions of the brush under an electron beam (Figure 3.1). Using this direct patterning method, highly resolved nano-structured polymer brush patterns down to 50 nm lines were obtained. This work concentrated on patterned polymer brushes on oxidized silicon wafers since silicon wafers are relatively more stable and smooth compared to gold coated surfaces. The silane/silicon interface is stronger than the thiol/gold interface. Additionally, patterning on oxidized silicon wafers may be compatible with integrated circuit technology.

It is well established that patterning of positive tone (meth)acrylate photoresists by e-beam exposure is based on the scission reactions that occur on the backbone chain.[42] The scission reaction leads to the degradation of polymers into smaller fragments. This study involved the use of different positive tone, e-beam

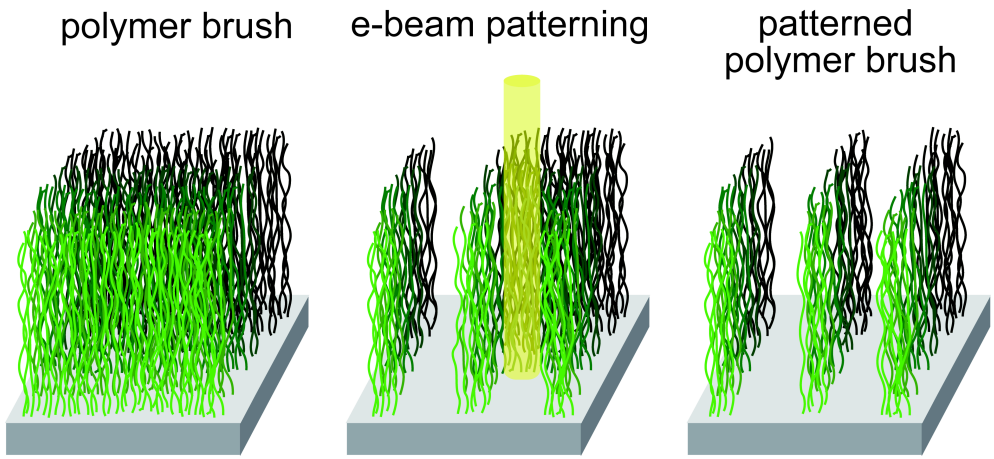

Figure 3.1. Schematic representation of the direct pattering of polymer brushes using electron beam lithography.

methacrylate polymer brush systems with varying functionalities β–position to the methacrylate ester. PMMA and PHEMA are classical positive tone photoresists for e-beam lithography. Recently, PMMA and PHEMA brushes were directly patterned, in a single step using e-beam lithography to achieve patterned brush surfaces with features down to sub-50 nm.[43] In this chapter, the sensitivity of PIBMA, PNPMA and PTFEMA brushes towards e-beam patterning was studied and compared to the sensitivity of PMMA and PHEMA brushes. The contrast curves obtained for these e-beam degradable polymeric systems indicates that a polymer brush that degrades to form a more stable main chain radical is more sensitive to e-beam irradiation. The order of sensitivity of the methacrylate polymer brush systems was evaluated and explained based on the trend of the molecular free energy values of the main chain radicals and R• radicals (Scheme 2). High quality quantitative predictions for the methacrylate systems were performed using *ab initio* methods.

Experimental Section

Materials and Chemical Reagents. Allyl-2-bromo-2-methylpropionate, chlorodimethyl- hydrosilane, Pt on activated carbon (10 wt %), triethylamine, copper (I) bromide, copper (II) dibromide, copper (I) chloride, 4,4′-dinonyl-2,2′-dipyridyl (dNnbpy), α,α,α-trifluorotoluene, 2,2′-bipyridine, inhibitor remover packing material, anhydrous toluene, isobutyl methacrylate (IBMA) (inhibited with 15 ppm monomethyl ether hydroquinone (MEHQ)), methyl methacrylate (MMA) (inhibited with 10-100 ppm MEHQ) and 2-hydroxyethyl methacrylate (HEMA) (inhibited with 200 ppm MEHQ) were purchased from Sigma Aldrich and used without purification unless stated otherwise. Neopentyl methacrylate (NPMA) (inhibited with 100 ppm MEHQ) and 2,2,2-trifluoroethyl methacrylate (TFEMA) (inhibited with 50 ppm MEHQ) were

purchased from Scientific Polymer Products, Inc. Monomers were purified by passing through a short column of MEHQ and HQ inhibitor remover packing material.

Deionized water with a resistivity of 18.2 MΩ•cm at 25 °C was obtained from Millipore's Milli-Q® Synthesis A10 system. All other solvents for rinsing and cleaning were purchased from Fisher Scientific. Doped silicon wafers were obtained from Montco Silicon Technologies, Inc.

Synthesis and Immobilization of the Surface Initiator. Hydrosilylation of allyl 2-bromo-2-methylpropionate was carried out using a literature procedure to obtain the ATRP silane initiator, 3-(chlorodimethylsilyl)propyl 2-bromo-2-methylpropionate.[44] Silicon wafers were diced into 3 cm x 1 cm pieces and cleaned by rinsing with acetone and dried under a nitrogen stream. To remove any organic residues on the surface, the substrates were further cleaned in Piranha solution (3:1 conc. H_2SO_4/30% H_2O_2 soln) for 30 minutes. (*Caution*: piranha solution reacts violently with organic materials and should be handled carefully). After rinsing with copius amounts of deionized water, the substrated were washed with dichloromethane and then dried in a vacuum oven for 10 min at 120 °C. The clean Si wafer pieces were immersed in a toluene solution of the silane initiator (2 mM) and triethyamine (0.05 mM) for 24 h. The wafers were then removed from the solution and washed with dichloromethane and left to stand in dichloromethane for 18 h. The initiator coated wafers were either used immediately or stored under standard conditions. No loss of activity was observed on storage for couple of weeks.

Preparation of PMMA & PHEMA Brushes. PMMA and PHEMA brushes were prepared using a literature procedure.[45]

Preparation of PIBMA Brushes. In a typical reaction, two initiator coated silicon substrates (3 cm x 1cm) were placed in a 25 mL Schlenk flask under an argon atmosphere. The flask was evacuated and back filled with argon three times. CuBr

(143 mg, 1.0 mmol), 2,2′-bipyridine (312 mg, 2.0 mmol) were taken in another 25 mL Schlenk flask equipped with a magnetic stir bar. The air in the flask was evacuated and replaced with argon three times. The solvent mixture (2 mL deionized water and 8 mL isopropanol) and purified IBMA (5 g, 35.2 mmol) were purged separately with argon for about an hour and cannulated into the flask containing the ligand and copper salts. The reaction mixture was stirred at room temperature for 10 min to ensure the dissolution of the monomer and the copper-ligand complex in the solvent. This solution was then transferred into the flask containing the silicon wafer pieces. Polymerization was carried out for a set reaction time at 32 °C. After polymerization, the substrates were removed from the flask and washed with isopropanol, acetone and gently sonicated in isopropanol for 5 min and dried under a stream of nitrogen.

Preparation of PNPMA Brushes. PNPMA brushes were prepared by surface initiated polymerization of NPMA (5 g, 32 mmol) via ATRP as described for PIBMA brushes. After polymerization, the substrates were removed from the flask and washed with isopropanol, acetone and gently sonicated in isopropanol for 5 min and dried under a stream of nitrogen.

Preparation of PTFEMA Brushes. PTFEMA brushes were prepared using a modified literature procedure.[47] In a typical reaction, two initiator coated silicon substrates (3 cm x 1cm) were placed in a 25 mL Schlenk flask under an argon atmosphere. The flask was evacuated and back filled with argon three times. CuCl (32 mg, 0.324 mmol), $CuBr_2$ (8mg, 0.0324 mmol) and dNnbpy (285.6 mg, 0.712mmol) were taken in another 25 mL Schlenk flask equipped with a magnetic stir bar. The air in the flask was evacuated and replaced with argon three times. The solvent (α,α,α-trifluorotoluene, 13 mL) and purified TFEMA (8 mL, 56 mmol) were purged separately with argon for about an hour and cannulated into the flask containing the ligand and copper salts. The reaction mixture was stirred at room temperature for 10

min to ensure the dissolution of the monomer and the copper-ligand complex in the solvent. This solution was then transferred into the flask containing the silicon wafer pieces. Polymerization was carried out for a set reaction time at 90 °C. After polymerization, the substrates were removed from the flask and washed with THF, acetone and gently sonicated in THF for 5 min and dried under a stream of nitrogen.

Characterization of Polymer Brushes. Polymer brushes were characterized by ellipsometry, water contact angle goniometry, atomic force microscopy (AFM) and X-ray photoelectron spectroscopy (XPS). Thicknesses of the polymer brushes were measured using a Woollam variable angle spectroscopic ellipsometer at a 70° angle of incidence. A Cauchy model (Cauchy layer/silicon substrate) was used to fit the data, in which the Cauchy layer was representative of the polymer brush. Water contact angles were measured using a VCA optima XE goniometer. Dynamic water contact angles measurements were performed by addition and retraction of a drop of water on the surface. At least three sample spots were taken on each surface. Surface topography was analyzed and the root-mean-square (RMS) roughness was measured using a Veeco Dimension 3100 scanning probe microscope. Olympus tapping mode etched silicon probes were used to acquire topographic images in air at room temperature. The surface composition of the polymer brush was determined by a Surface Science Instruments SSX-100 spectrometer with an operating pressure $< 2 \times 10^{-9}$ Torr using monochromatic AlKα x rays at 1486.6 eV. Photoelectrons were collected at an angle of 55-degrees from the surface normal using a hemispherical analyer with pass energies of 150 V acquired at 1 eV/step (survey scan) and 50 V acquired at 0.065 eV/step (high resolution scan). The C—C 1s peak was corrected to a binding energy of 285 eV.

Direct Patterning of Polymer Brushes. Patterning of the polymer brushes was done at the Cornell Nanoscale Facility using the JEOL 9300 electron beam

lithography system. In order to get an estimate on the patterning conditions needed, contrast curves were generated from 10 μm x 1 μm areas exposed to the electron beam with linearly increasing electron dosage. A 0.5 nA beam current, 100 kV accelerating voltage, and 5 nm pixel size was used for the generation of the contrast curves and for higher resolution patterning. Doses ranging from 65 to 689 μC/cm^2 were used for the PMMA, PHEMA and PNPMA brushes. The PIBMA brushes were patterned at doses ranging from 130 to 1378 μC/cm^2. PTFEMA brushes were patterned at e-beam doses ranging from 5 to 150 μC/cm^2. After e-beam exposure, the polymer brushes were developed in an appropriate solvent, thoroughly rinsed in deionized water and then dried under a stream of nitrogen.

Metrology. Optical microscopy imaging was performed using the Nikon Digital Sight DS-5M-L1 optical microscope. The patterned brush surface was analyzed using a Veeco Dimension 3100 scanning probe microscope. Olympus tapping mode etched silicon probes were used to acquire topographic images in air at room temperature.

Semi-empirical Calculations. High quality quantitative predictions for the methacrylic systems were performed using *ab initio* methods. Density functional theory (DFT) were carried at the B3LYP/6-31G(d) level using the *Gaussian 03* package.[46]

Results and Discussion

Preparation and Characterization of Polymer Brushes

Synthesis and Characterization of Initiators on Silicon Substrates. The silane ATRP initiator, 3-(chlorodimethylsilyl)propyl 2-bromo-2-methylpropionate, was synthesized in one step using a literature procedure. The disappearance of the alkene protons in the ^{1}H NMR spectra of the hydrosilylated product confirmed the

completion of the reaction after 24 h. The covalent attachment of the silane initiator on to the silicon substrate was carried out in a single step. The formation of a monolayer of initiator was confirmed by ellipsometry and AFM. The dry ellipsometric thickness of the covalently attached monolayer was measured to be 1.6 ± 0.3 nm (the error is due to uncertainties present during the calculation of the film thickness from the optical data). This value is in good agreement with the theoretical height of the initiator containing SAM. The surface topography and roughness was measured by AFM. The root mean square (RMS) roughness of the initiator coated silicon substrate was 0.2 nm in a 0.5 x 0.5 μm^2 scanning area. This is similar to the RMS roughness measured for clean bare silicon pieces.

Preparation and Characterization of Polymer Brushes. PMMA and PHEMA brushes were prepared using a literature procedure.[45] Jones and Huck reported the controlled surface initiated polymerization of MMA and HEMA to grow thick polymer brushes using aqueous atom transfer radical polymerizations at room temperature. This strategy resulted in controlled brush growth without the addition of sacrificial initiator. Polymerization in aqueous media allows rapid increase in rate of polymerization to grow brushes without losing control over the reaction. The same concept was applied to grow poly(isobutyl methacrylate) (PIBMA) and poly(neopentyl methacrylate) (PNPMA) brushes. To date there is no report of surface initiated polymerization of isobutyl methacrylate (IBMA) and neopentyl methacrylate (NPMA) to grow PIBMA and PNPMA brushes. Both monomers were polymerized via ATRP in isopropanol and water mixture at 32 ºC. The formation of PIBMA and PNPMA brushes is fast in this solvent mixture. Chen and co-workers have reported the surface initiated polymerization of TFEMA on silicon substrates.[47] They showed that the ATRP reaction of TFEMA is better controlled in a fluorinated solvent such as α,α,α–trifluorotoluene. The use of dNnbpy as the ligand gave a more linear kinetic

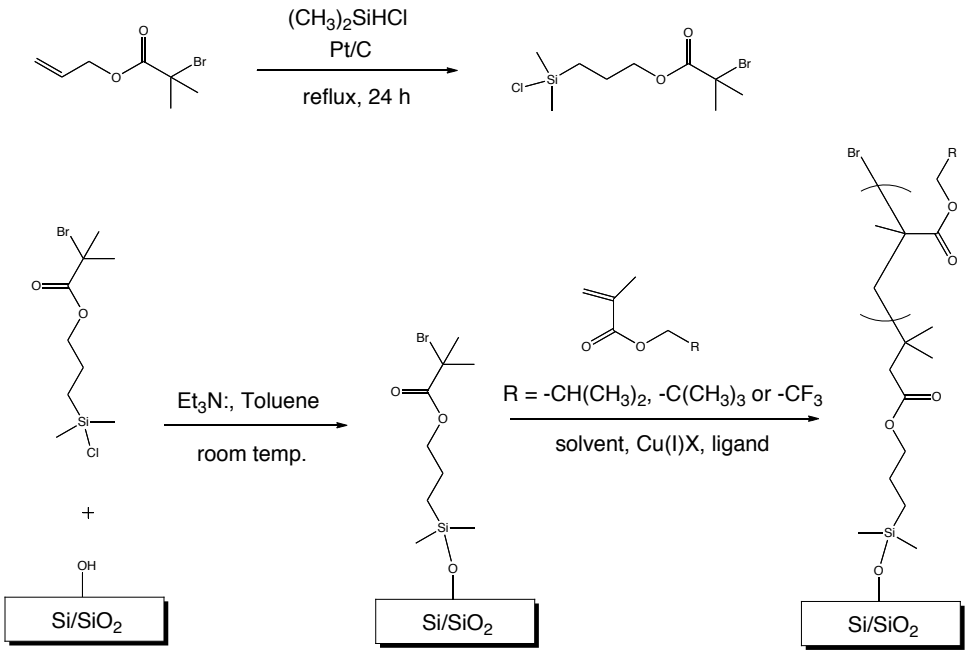

Scheme 3.1. Synthesis of the polymer brushes: synthesis of the ATRP silane initiator, immobilization of the initiator on the silicon substrate and surface initiated polymerization of the methacrylate monomer.

plot of monomer conversion with polymerization reaction time. The reaction for the synthesis of the ATRP silane initiator and preparation of polymer brushes is shown in Scheme 3.1. No sacrificial initiator was added to the solvent mixture and the polymerization was surface initiated and surface confined. This prevents the formation of undesirable polymer in solution, resulting in easy retrieval of the delicate polymer brush surfaces. Clean polymer brush surfaces were obtained simply by washing the polymer brushes with water, acetone and ethanol.

For this study, polymer brushes with thicknesses less than 100 nm were required. The reaction time was determined by measuring the dry ellipsometric thicknesses of the polymer brushes prepared at various polymerization reaction times. The polymerization reactions appeared to be well controlled. It has been reported elsewhere that the thickness of the PTFEMA brushes increases linearly with respect to reaction time up to approximately 24 h.[48] Figure 3.2 shows the plot of ellipsometric thickness versus polymerization reaction time for the PIBMA and PNPMA brushes. The formation of these brushes is fast and thick polymer brushes were obtained within 2 h at 32 ºC. NPMA polymerized at a relatively faster rate than IBMA. PNPMA brushes as thick as 120 nm were obtained in an hour. About 100 nm thick PIBMA brushes were obtained after 2 h. The addition of water to the ATRP reaction speeds up the reaction considerably. At longer reaction times, the increase in brush thickness seems to slow down. This is attributed to the loss of active chain ends or to the increase in deactivator concentration that slows down the activation/deactivation cycles, which in turn slows down the polymer brush growth.

The polymer brushes were characterized by ellipsometry, tapping-mode AFM, water contact angle goniometry and XPS. The dry thicknesses of the polymer brushes were measured by ellipsometry at a 70º incident angle. The value of n=1.50 was used

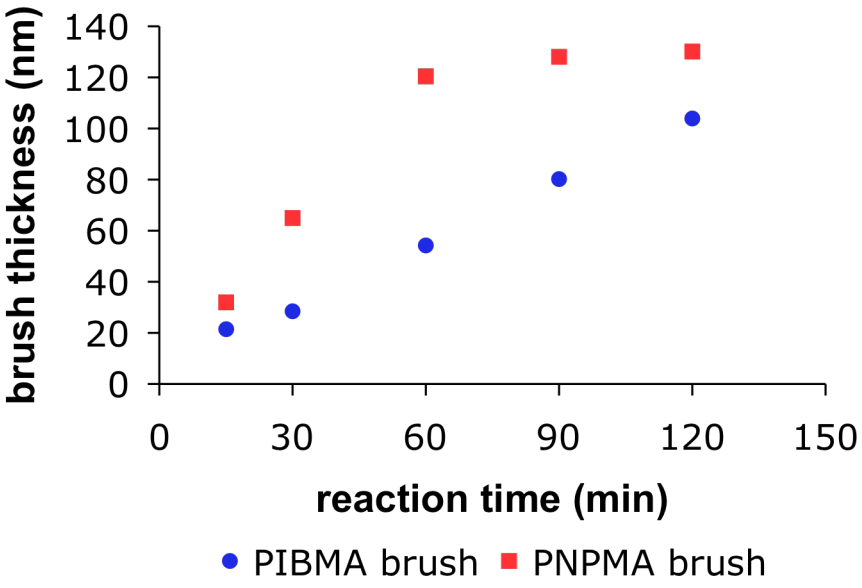

Figure 3.2. Dry ellipsometric thickness of the PIBMA and PNPMA brushes as a function of polymerization reaction time. A linear increase in brush thickness over times suggests that the brush growth is controlled. NPMA polymerizes at a faster rate than IBMA.

as the refractive index to determine the thickness of PMMA, PHEMA, PIBMA and PNPMA brushes. Value of n=1.437 was used as the refractive index for PTFEMA brushes. Tapping mode AFM images of all polymer brushes showed a RMS roughness between 0.32 nm to 0.46 nm, indicating that the polymer brushes were homogeneous throughout the silicon substrate. At room temperature, in ambient air, the advancing and receding water contact angles for the PIBMA brushes were 93±1° and 72±2°, respectively. The advancing and receding contact angles for PNPMA brushes were 113±2° and 55±2° and those for the PTFEMA brushes were 94±2° and 70±1°, respectively. The PIBMA brushes were rinsed with acetone and dichloromethane, THF or isopropanol and dried at room temperature in a vacuum oven before measuring the water contact angles. As expected, the PIBMA, PNPMA and PTFEMA brushes caused the surface to be much more hydrophobic than bare silicon. The surface composition of the polymer brushes was determined using X-ray photoelectron spectroscopy (Figure 3.3). The C 1s (285 eV), O 1s (533 eV) and F 1s (687 eV) peaks were clearly observed in the XPS spectrum. The relative areas of these peaks are in good agreement with the known composition of PIBMA, PNPMA and PTFEMA. The atomic percentages from the XPS spectra were C (81.5 %), O (18.5%) for PIBMA brushes, C (83.4%), O (16.6%) for PNPMA brushes and C (53.4%), O (17.2%), F (29.41%) for PTFEMA brushes.

Direct Patterning of Polymer Brushes Using E-beam Lithography. The fabrication of nanopatterned polymer brush architectures on surfaces is of paramount importance in many areas of modern science and technology as these surfaces are much more robust compared to traditional polymer films. Generation of patterned polymer brushes is traditionally achieved by optical lithography. Some of the conventional approaches involve the immobilization of initiators on surfaces patterned

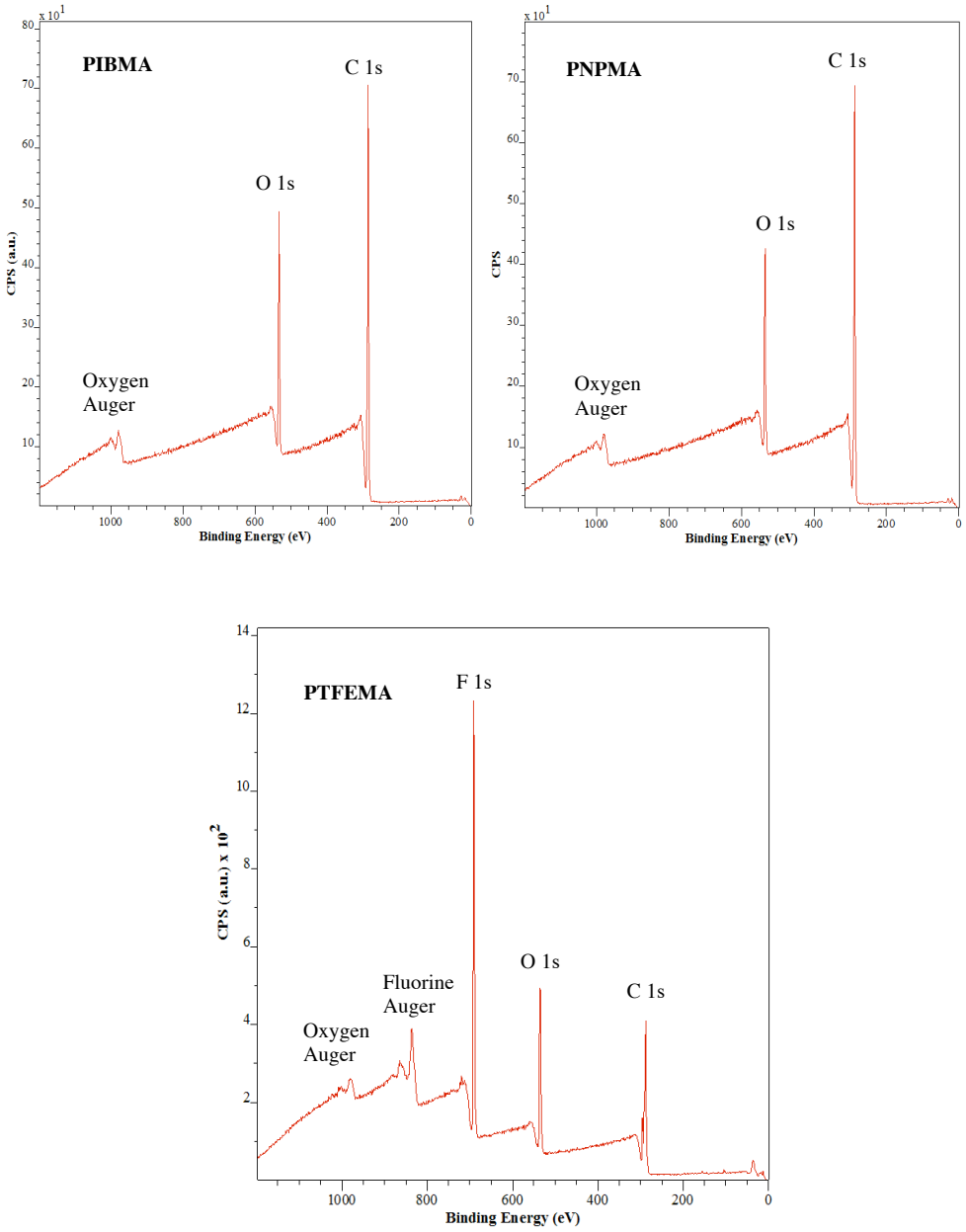

Figure 3.3. X-ray photoelectron spectroscopy survey spectra of PIBMA, PNPMA and PTFEMA brushes. The XPS spectra suggest atomic compositions as expected from the structure of each polymer.

using photolithography. In another approach, an initiator containing self-assembled monolayer is patterned to form a patterned initiator layer. Surface initiated polymerization of a suitable monomer on these surfaces gives rise to patterned polymer brushes. These methods are quite complex and require multistep lithographic schemes that can increase the chances of surface contamination. Whitesides and co-workers introduced the concept of microcontact printing for the preparation of patterned SAMs on planar and curved surfaces.[49] This method offers advantages in applications where photolithography is ineffective. However, it does not enable the fabrication of nanometer-scale patterns and requires a minimum of three steps to obtain the patterned brush surfaces. Moreover, Patra and Linse used computational simulations to show that the growth of brushes from patterned initiator layers lead to lower resolution features when the polymer brush height is comparable in length to the pattern width due to chain relaxation in the voided regions during growth.[50] Andruzzi et al. reported the micro-patterning of polymer brushes using a photolithographic process involving the chemical vapor deposition of parylene.[34] Though successful, this method can damage the delicate brush surface and the functionalities on the surface during the parylene peel-off step.

In an attempt to prepare nano-patterened polymer brushes in a single step, we investigated the direct patterning of methacrylic polymer brushes using electron beam lithography. Electron-beam lithography enables the fabrication of nanometer-scale patterns as small as 20 nm. The primary advantage of e-beam lithography over photolithography is that the e-beam process uses electrons of wavelength less than 0.1 nm and is not diffraction limited. Besides high lateral resolution, e-beam lithography makes it possible to write complex patterns by adjusting the irradiation dose. Electron beam processing has been used to boost properties by creating controlled degradation or chain scission of certain polymers. Electron beams have been used to break down

polymeric materials to create micro-powders used in inks, coatings and lubricants. Doses ranging from 65 to 689 μC/cm^2 were used for the PMMA, PHEMA and PNPMA brushes. The PIBMA brushes were pattered at doses ranging from 130 to 1378 μC/cm^2. PTFEMA brushes were patterned at e-beam doses ranging from 5 to 150 μC/cm^2 with a beam current of 0.5 nA. After electron beam exposure, followed by development in a suitable organic solvent, a contrast curve was generated in which the normalized thickness was plotted as a function of the log of the exposure (Figure 4). Using the appropriate dose ascertained from the contrast curve, higher resolution lines of patterned PIBMA, PNPMA and PTFEMA brushes, were imaged. Factors such as the electron beam diameter, beam current and dose were optimized to improve the resolution of the patterned brushes.

Sensitivity of Polymer Brushes Towards E-beam Patterning. Different positive tone methacrylate polymers were chosen that lead to scission reactions on the polymer backbone on exposure to electron beams. The scission reaction leads to the degradation of polymers by rupture of covalent bonds. This reaction causes a decrease in molecular weight and intrinsic viscosity. The exposed PIBMA and PNPMA brushes were developed in isopropanol (IPA) for 90 s at room temperature. Tetrahydrofuran (THF) (90 s at room temperature) was used as the developer for the PTFEMA brushes. The degraded polymer fragments showed good solubility in the two solvents leaving the covalently attached polymer brushes on the surface unaffected. Polymer brushes were successfully patterned in a single step on exposure to an electron beam and characterized and imaged by tapping mode AFM. The contrast curve of the different methacrylate brushes is shown in Figure 3.4. The contrast curves indicate that PNPMA brushes are the most sensitive to e-beam lithography while PMMA brushes are the least sensitive. The increasing order of polymer brush sensitivity towards direct

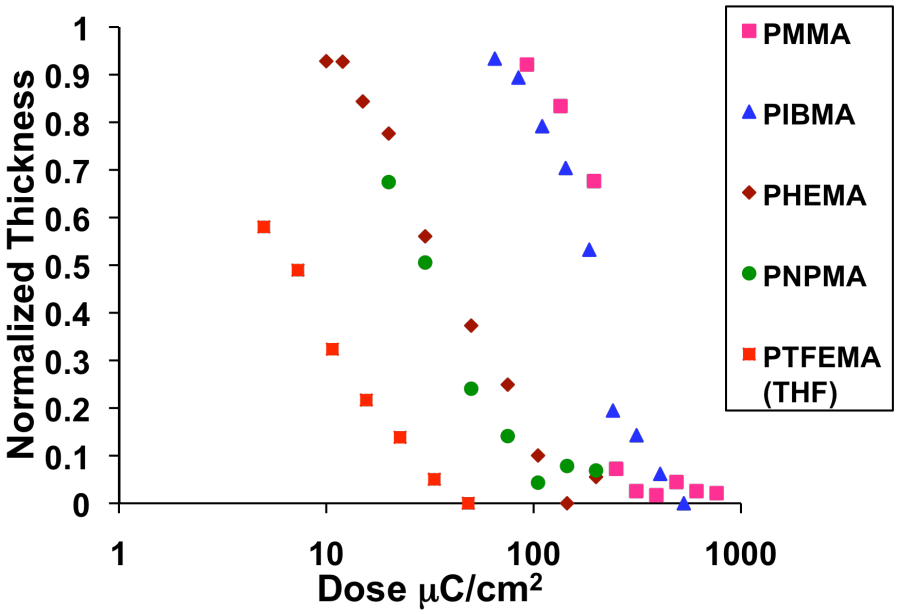

Figure 3.4. Normalized thickness versus electron beam exposure dose of the PMMA, PHEMA, PIBMA, PNPMA and PTFEMA brushes.

patterning via e-beam lithography is PMMA < PIBMA < PHEMA ≈ PNPMA < PTFEMA.

Figure 3.5 (a) is an AFM image of 50 nm lines of a patterned PIBMA brush with a pitch size of 100 nm that was patterned by e-beam lithography with an exposure dose of 1060.8 $\mu C/cm^2$ and developed in IPA solvent for 90 s at room temperature. Figure 3.5 (b) is an AFM image of 80 nm lines of a patterned PTFEMA brush with a pitch size of 160 nm obtained using similar lithographic and development conditions. Figure 3.5 (c) and 3.4 (d) are AFM images of 100 nm lines/200 nm pitch and 200 nm lines/400 nm pitch of patterned PNPMA brushes, respectively that were patterned by e-beam lithography with an exposure dose of 185.9 $\mu C/cm^2$ and developed in IPA solvent for 90 s at room temperature.

With the development of patterned PNPMA brushes in IPA, we observed line broadening of the PNPMA brushes. This is because in the IPA solvent, the PNPMA polymer chains tend to relax or collapse in the patterned silicon regions. This lateral relaxation in the voided regions makes it possible to vary the resolution of the lines formed from the PNPMA brushes. Such strategies have recently gained much interest. Chang and co-workers recently reported the ability to control the resolution of lines and dots formed from PMMA brushes by immersion of the brushes in water or THF.[51] However, they report the patterning of PMMA brushes using an elaborate, labor-intensive lithographic scheme. One could control the width of the patterned features by varying polymerization time and annealing temperature. THF is a good solvent for PTFEMA and was used to develop the exposed regions of the PTFEMA brushes. Figures 3.6 (a) and Figure 3.6 (b) show 50 nm lines of isolated PTFEMA brush regions with a pitch size of 2 μm and 100 nm lines of patterned PTFEMA brushes with pitch size of 400 nm, respectively. These patterns were obtained by e-beam

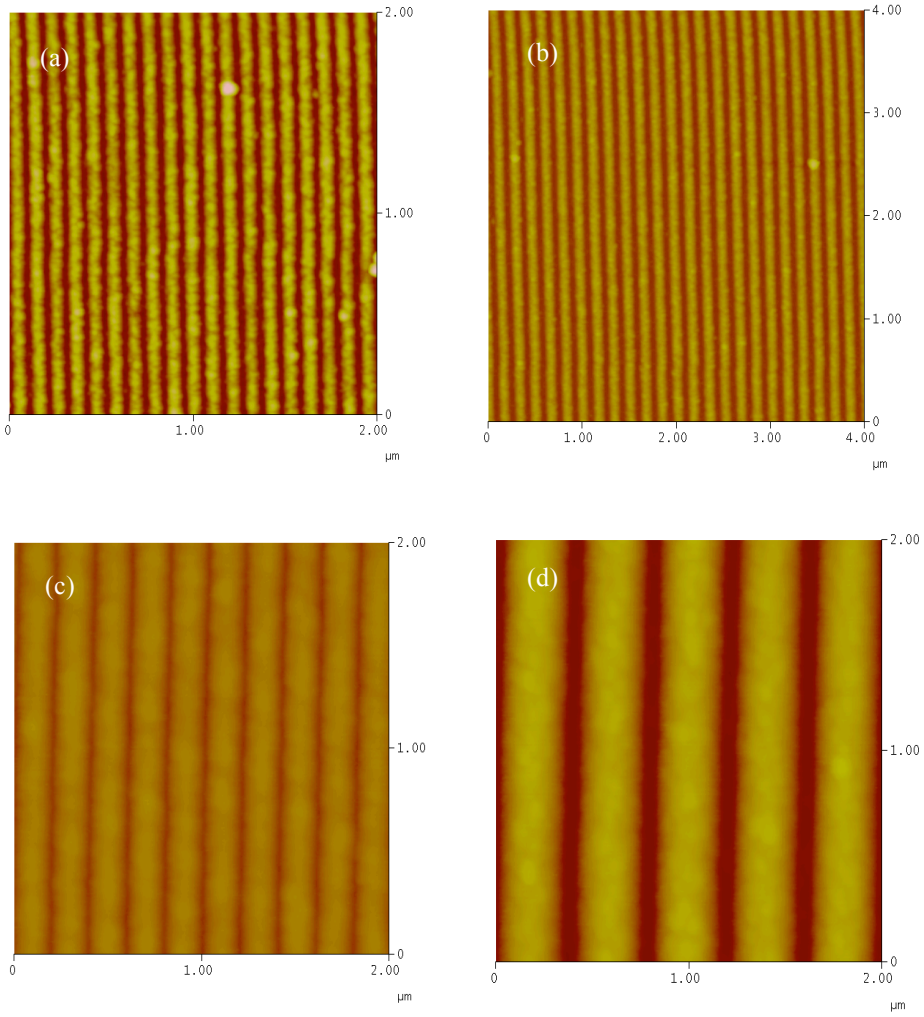

Figure 3.5 Tapping- mode AFM height images of patterned PIBMA and PNPMA brushes. (a) 50 nm lines/100 nm pitch size and (b) 80 nm lines/160 nm pitch size of a patterned PIBMA brush, patterned by e-beam lithography with an exposure dose of 1060.8 μC/cm^2 and developed in IPA for 90 s at room temperature in air. (c) 100 nm lines/200 nm pitch size and (d) 200 nm lines/400 nm pitch size of patterned PNPMA brushes, patterned by e-beam lithography with an exposure dose of 185.9 μC/cm^2 and developed in IPA for 90 s at room temperature in air.

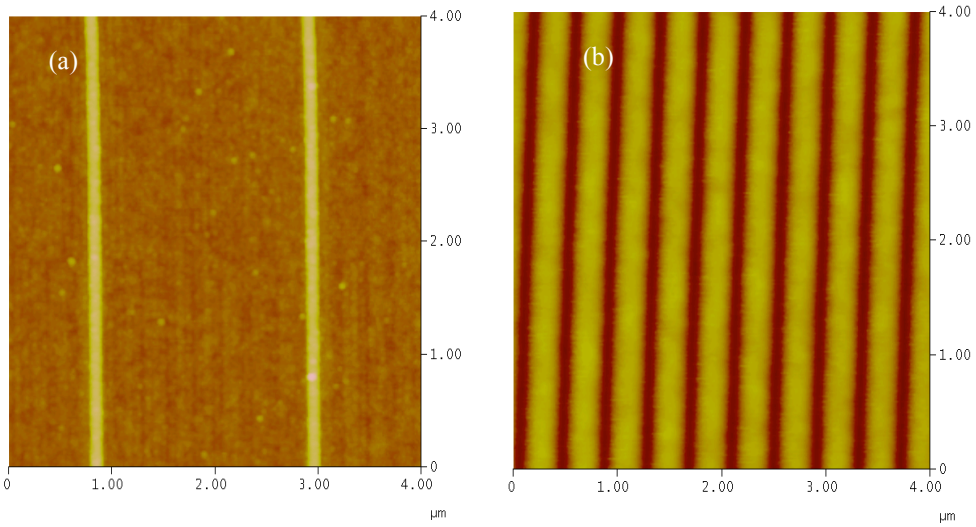

Figure 3.6 Tapping- mode AFM height images of patterned PTFEMA brushes. (a) 50 nm lines of isolated PTFEMA brush regions. Here the pattern size is 1950 nm with a pitch size of 2 μm. Figure 6 (b) 100 nm lines/400 nm pitch size of patterned PTFEMA brushes. These patterns were obtained by e-beam lithography with an exposure dose of 48.4 μC/cm^2, followed by development in THF for 90 s at room temperature.

lithography with an exposure dose of 48.4 μC/cm^2, followed by development in THF for 90 s at room temperature.

The observed polymer brush sensitivity towards direct patterning using e-beam lithography was explained on the basis of the stability of radicals formed on e-beam exposure. Bakhru and co-workers reported the degradation of PMMA by electron beam irradiation.[52] Noda *et al*. performed an electron spin resonance study of the free-radical formation of plasma irradiated poly(methacrylic acid) and its esters.[53] Both these studies suggest the degradation of methacrylate polymers to occur as shown in Scheme 3.2. One would expect that the degradability of the other methacrylate systems to be quite similar to the degradation of PMMA. Based on this mechanism, it may be hypothesized that the polymer that degrades to form a more stable radical on e-beam irradiation should be the most sensitive as a more stable product would drive the forward reaction. The molecular free energy values for the main chain radicals, formed by scissioning of the polymer backbone was evaluated using computational methods. In addition, the stability of $\bullet CH_3$ (from PMMA), $\bullet CH_2CH(CH_3)_2$ (from PIBMA), $\bullet CH_2CH_2OH$ (from PHEMA), $\bullet CH_2C(CH_3)_3$ (from PNPMA) and $\bullet CH_2CF_2$ (from PTFEMA) radicals that are formed later in the degradation process by decarboxylation was compared.

Computational chemistry has been used extensively to simulate chemical structures and reactions numerically. Electronic structure methods such as *ab initio* methods (implemented in the *Gaussian* package) are used to compute the free energy of a particular molecular structure. This method was used to quantitative predict the energies of the methacrylic systems. Density functional theory (DFT) calculations were carried at the B3LYP/6-31G(d) level corresponding to the Becke-style 3-Parameter Density Functional Theory approximation method using the *Gaussian 03*

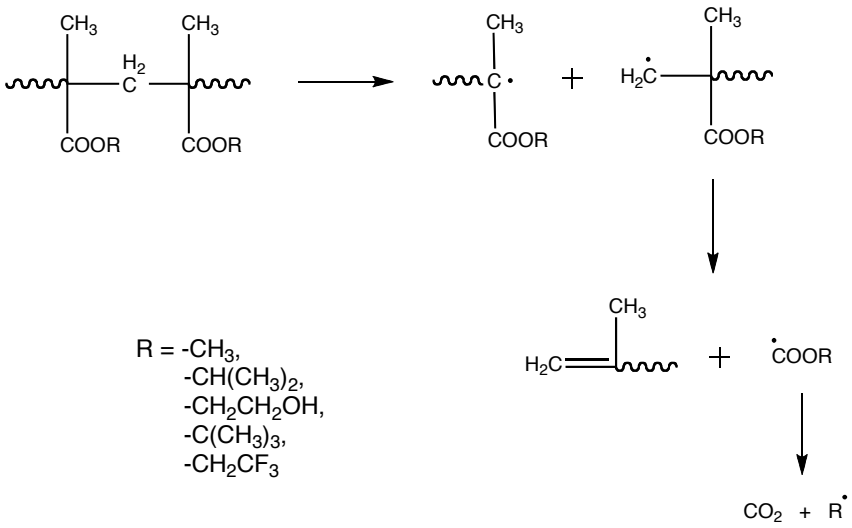

Scheme 3.2 Schematic representation of the degradation of methacrylate polymers on exposure to electron beams.

package.[46] The optimized low molecular energy conformation of each main chain radical is shown in Figure 3.7.

Based on the DFT calculations we report the molecular free energy values for the optimized low energy conformation for the different main chain radicals. We expect the methacrylate main chain radical with the lowest molecular free energy to be the most sensitive to e-beam exposure. The molecular free energy value of the PTFEMA main chain radical was calculated to be -722.57 E_h. It has the lowest molecular free energy amongst the other methacrylates which explains the high sensitivity of PTFEMA brushes. Molecular free energy calculated for PMMA was -385.53 E_h. The low sensitivity of PMMA brushes was attributed to the high energy value. The computationally obtained molecular energy values for main chain radicals of PNPMA, PHEMA and PIBMA were -542.69 E_h and -500.02 E_h and -503.4 E_h, respectively. The molecular energy values for the main chain radicals and the $R^{\bullet}$ radicals are summarized in Table 1. The stability of the $R^{\bullet}$ radicals can also be explained on the basis of the 1,3-hydride shift. The methyl radical is the least stable as it is not stabilized. The $\bullet CH_2C(CH_3)_3$ and $\bullet CH_2C(CH_3)_3$ radicals are stabilized by a 1,3-hydride shift. $\bullet CH_2CH_2OH$ is stabilized by hyperconjugation. Based on these arguments, we see that the order of sensitivity of the polymer brush systems is similar to the order of radical stability. It can be concluded that the e-beam degradable methacrylate polymer brush system forming a more stabilized radical on e-beam exposure is more sensitive to e-beam irradiation. This direct patterning method makes it possible to obtain nano-patterned polymer brushes in a single step.

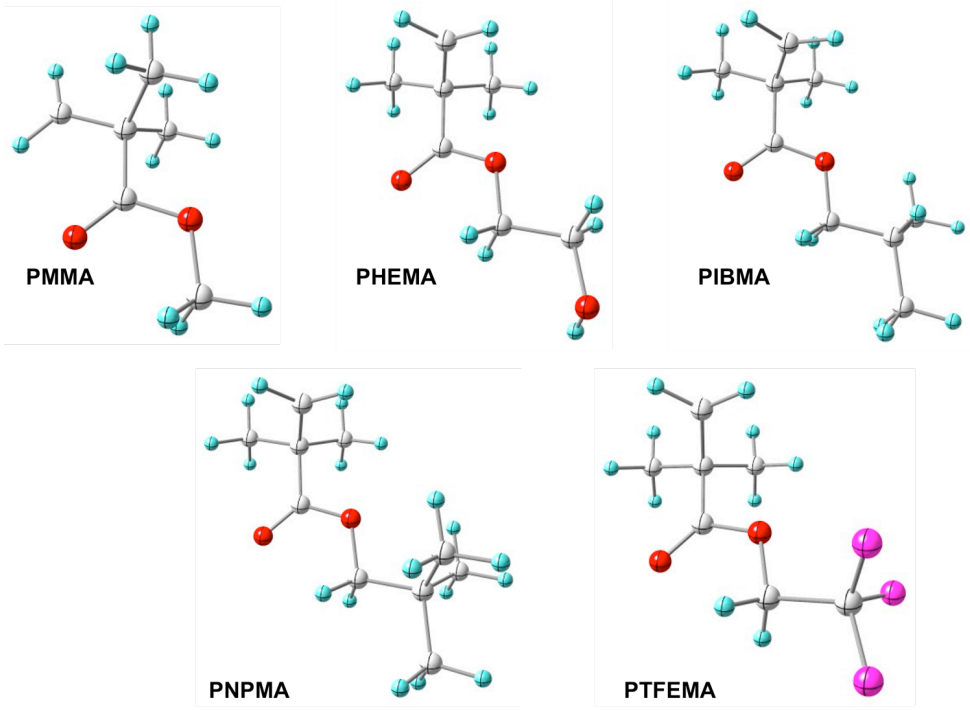

Figure 3.7. Optimized low molecular free energy conformations of the different main chain radicals formed on e-beam irradiation of polymer brushes.

Table 3.1. Density functional theory (DFT) calculations on optimized low molecular energy conformation of each main chain radical and each R• radical. The calculations were carried at the B3LYP/6-31G(d) level corresponding to the Becke-style 3-Parameter Density Functional Theory approximation method using the *Gaussian 03* package.

Methacrylate	Molecular free energy (E_h) *(DFT calculations)*	
	Main Chain Radical	R•
PTFEMA	-722.57	-376.87 [•CH_2CF_3]
PNPMA	-542.69	-196.98 [•$CH_2C(CH_3)_3$]
PHEMA	-500.02	-154.32[•CH_2CH_2OH]
PIBMA	-503.40	-157.70[•$CH_2CH(CH_3)_2$]
PMMA	-385.53	-39.83[•CH_3]

Conclusions

In conclusion, a single step approach to form patterned polymer brushes on oxide surfaces by electron beam lithography has been demonstrated. PIBMA, PNPMA and PTFEMA brushes were grown on silicon substrates via ATRP. The chemical structure of the different brushes was confirmed by XPS and the physical properties were characterized by ellipsometry, water contact angle measurements. AFM confirmed the successful nano-patterning of the polymer brushes. Using e-beam lithography, polymer brush patterns as small as 50 nm were obtained. The contrast curves for PIBMA, PNPMA and PTFEMA brushes were obtained and compared to PMMA and PHEMA brushes. The increasing order of polymer brush sensitivity towards e-beam patterning is PMMA < PIBMA < PHEMA ≈ PNPMA < PTFEMA. These studies indicate the e-beam degradable methacylate polymer brush system that degrades to form a more stable main chain radical and R˙ radical tends be more e-beam sensitive. Hence one can tailor-make polymer brushes to be highly sensitive for direct patterning using e-beam lithography by chemical modifications at the β-position to the carbonyl group. This direct method of patterning brush is much less complicated compared to conventional lithographic methods. The direct patterning of brushes is an efficient method to fabricate patterned macromolecular architectures with nanoscale precision.

Acknowledgments

This work was supported by the National Science Foundation under agreement No. DMR-0518785. The Cornell NanoScale Science and Technology Facility (CNF) and the Cornell Center for Materials Research (CCMR) are acknowledged for use of their facilities. AR thanks Lekha Gupta (Cornell University) for help with the computational analysis of the methacrylate systems.

REFERENCES

1. Milner, S. T., *Science* **1991,** 251, 905.

2. Zhao, B.; Brittain, W. J., *Prog. Polym. Sci.* **2000,** 25, 677.

3. Advincula, R. C.; Brittain, W. J.; Caster, K. C.; Ruhe, J., *Polymer Brushes: Synthesis, Characterization, Applications*. Wiley-VCH: Weinheim, Germany, 2004.

4. Prucker, O.; Ruhe, J., *Langmuir* **1998,** 14, 6893.

5. de Boer, B.; Simon, H. K.; Werts, M. P. L.; van der Vegte, E. W.; Hadziioannou, I., *Macromolecules* **2000,** 33, 349.

6. Weck, M.; Jackiw, J. J.; Rossi, R. R.; Weiss, P. S.; Grubbs, R. H., *J. Am. Chem. Soc.* **1999,** 121, 4088.

7. Zhao, B.; Brittain, W. J., *Macromolecules* **2000,** 33, 342.

8. Jordan, R.; Ulman, A.; Kang, J. F.; Rafailovich, M. H.; Sokolov, J., *J. Am. Chem. Soc.* **1999,** 121, 1016.

9. Husseman, M.; Malmstrom, E. E.; McNamara, M.; Mate, M.; Mecerreyes, O.; Benoit, D. G.; Hedrick, J. L.; Mansky, P.; Huang, E.; Russell, T. P.; Hawker, C. J., *Macromolecules* **1999,** 32, 1424.

10. Li, C.; Benicewicz, B. C., *Macromolecules* **2005,** 38, (14), 5929.

11. Matyjaszewski, K.; Miller, P. J.; Shukla, N.; Immaraporn, B.; Gelman, A.; Luokala, B. B.; Siclovan, T. M.; Lickelbick, G.; Vallant, T.; Hoffmann, H.; Pakula, T., *Macromolecules* **1999,** 32, 8716.

12. Geissler, M.; Xia, Y., *Advanced Materials* **2004,** 16, (15), 1249.

13. Nie, Z.; Kumacheva, E., *Nat. Mater.* **2008,** 7, 277.

14. Senaratne, W.; Andruzzi, L.; K., O. C., *Biomacromolecules* **2005,** 6, 2427.

15. Dong, R.; Krishnan, S.; Baird, B. A.; Lindau, M.; Ober, C. K., *Biomacromolecules* **2007,** 8, 3082.

16. Slim, C.; Tran, Y.; Chehimi, M. M.; Garraud, N.; Roger, J.; Combellas, C.; Kanoufi, F., *Chem. Mater.* **2008,** 20, 6677.

17. Ahn, S. J.; Kaholek, M.; Lee, W.; LaMattina, B.; LaBean, T. H.; Zauscher, S., *Adv. Mater.* **2004,** 16, (23-24), 2141.

18. Khire, V. S.; Harant, A. W.; Watkins, A. W.; Anseth, K. S.; Bowman, C. N., *Macromolecules* **2006,** 39, 5081.

19. Konradi, R.; Ruhe, J., *Langmuir* **2006,** 22, 8571.

20. Chen, T.; Zhang, J.; Chang, D. P.; Garcia, A.; Zauscher, S., *Adv. Mater.* **2009,** 21, 1.

21. Jones, D. M.; Smith, J. R.; Huck, W. T. S., *Adv. Mater.* **2002,** 14, 1130.

22. Choi, H. G.; Amara, J. P.; Swager, T. M.; Jensen, K. F., *Langmuir* **2007,** 23, 2483.

23. Edmondson, S.; Vo, C. D.; Armes, S. P.; Unali, G. F., *Macromolecules* **2007,** 40, 5271.

24. Ma, H.; Li, D.; Sheng, X.; Zhao, B.; Chilkoti, A., *Langmuir* **2006,** 22, 3571.

25. Azzaroni, O.; Brown, A. A.; Cheng, N.; Wei, A.; Jonasc, A. M.; Huck, W. T. S., *J. Mater. Chem.* **2007,** 17, 3433.

26. Bhat, R. R.; Tomlinson, M. R.; Wu, Y.; Genzer, J., *J. Adv. Polym. Sci.* **2006,** 198, 51.

27. von Werne, T. A.; Germack, D. S.; Hagberg, E. C.; Sheares, V. V.; Hawker, C. J.; Carter, K. R., *J. Am. Chem. Soc.* **2003,** 125, 3831.

28. Kaholek, M.; Lee, W.; LaMattina, B.; Caster, K. C.; Zauscher, S., *Nano Lett.* **2004,** 4, 373.

29. Steenackers, M.; Kuller, A.; Stoycheva, S.; Grunze, M.; Jordan, R., *Langmuir* **2009,** 25, 2225.

30. He, Q.; Kuller, A.; Grunze, M.; Li, J., *Langmuir* **2007,** 23, 3981.

31. Ahn, S. J.; Kaholek, M.; Lee, W. K.; LaMattina, B.; LaBean, T. H.; Zauscher, S., *Adv. Mater.* **2004,** 16, 2141.

32. Xu, F. J.; Song, Y.; Cheng, Z. P.; Zhu, X. L.; Zhu, C. X.; Kang, E. T.; Neoh, K. G., *Macromolecules* **2005,** 38, 6254.

33. Zhou, F.; Jiang, L.; Liu, W. M.; Xue, Q., *Macromol. Rapid. Commun.* **2004,** 25, 1979.

34. Andruzzi, L.; Senaratne, W.; Hexemer, A.; Sheets, E. D.; Ilic, B.; Kramer, E. J.; Baird, B. A.; Ober, C. K., *Langmuir* **2005,** 21, 2495.

35. Liu, Y.; Klep, V.; Luzinov, I., *J. Am. Chem. Soc.* **2006,** 128, 8106.

36. Slim, C.; Tran, Y.; Chehimi, M. M.; Garraud, N.; Roger, J. P.; Combellas, C.; Kanoufi, F., *Chem. Mater.* **2008,** 20, 6677.

37. Christman, K. L.; Enriquez-Rios, V. D.; Maynard, H. D., *Soft Matter* **2006,** 2, 928.

38. Jhaveri, S. B.; Beinhoff, M.; Hawker, C. J.; Carter, K. R.; Sogah, D. Y., *ACS Nano* **2008,** 2, 719.

39. Martinez, R. V.; Losilla, N. S.; Martinez, J.; Huttel, Y.; Garcia, R., *Nano Letters* **2007,** 7, 1846.

40. Hou, S.; Li, Q.; Liu, Z., *Appl. Surf. Sci.* **2004,** 222, 338.

41. Liu, G.; Amro, N. A., *Proc. Natl. Acad. Sci. USA* **2002,** 99, 5165.

42. Slimani, K.; Moine, L.; Aymes-Chodur, C.; Laurent, A.; Labarre, D.; Yagoubi, N., *Polymer Degradation and Stability* **2009,** 94, 584.

43. Paik, M.; Rastogi, A.; Tanaka, M.; Ober, C. K., *PMSE Preprints* **2008,** 99, 541.

44. Ramakrishnan, A.; Dhamodharan, R.; Ruhe, J., *J. Macromol. Rapid Commun.* **2002,** 23, 612.

45. Jones, D. M.; Huck, W. T. S., *Adv. Mater.* **2001,** 13, 1256.

46. Frisch, M. J. e. a. *Gaussian 03, revision B.04*, Gaussian, Inc.: Wallingford, CT, 2004.

47. Chen, R.; Feng, W.; Zhu, S.; Botton, G.; Ong, B.; Wu, Y., *Journal of Polymer Science: Part A: Polymer Chemistry* **2006,** 44, 1252.

48. Rastogi, A.; Y., P. M.; Ober, C. K., *ACS Appl. Mater. Interfaces* **submitted**.

49. Xia, Y.; Whitesides, G. M., *Angew. Chem.* **1998,** 110, 568.

50. Patra, M.; Linse, P., *Nano Letters* **2006,** 6, (1), 133.

51. Chen, J. K.; Hsieh, C. Y.; Huang, C. F.; Li, P. M.; Kuo, S. W.; Chang, F. C., *Macromolecules* **2008,** 41, 8729.

52. Choi, J. O.; Moore, J. A.; Corelli, J. C.; Silverman, J. P.; Bakhru, H., *J. Vac. Sci. Technol. B* **1988,** 6, (6), 2286.

53. Kuyuza, M.; Noguchi, A.; Ishikawa, M.; Koide, A.; Sawada, K.; Ito, A.; Noda, N., *J. Phys. Chem.* **1991,** 95, 2398.

CHAPTER FOUR

DEVELOPMENT OF A DIRECTLY PATTERNED LOW SURFACE ENERGY POLYMER BRUSH IN SUPERCRITICAL CARBON DIOXIDE[*]

Abstract

Carbon dioxide is a sustainable solvent as CO_2 is non-flammable, exhibits a relatively low toxicity and is naturally abundant. As a selective, non-polar solvent, supercritical carbon dioxide ($scCO_2$) is an ideal fit for developing low surface energy polymers. This chapter describes the development of directly patterned poly(2,2,2-trifluoroethyl methacrylate) (PTFEMA) brushes in $scCO_2$. PTFEMA was particularly selected over other fluorinated polymers because of its very high e-beam sensitivity. PTFEMA brushes were grown on silicon substrates via controlled surface-initiated atom transfer radical polymerization of TFEMA. Surface analysis techniques including ellipsometry, contact angle goniometry, atomic force microscopy (AFM) and X-ray photoelectron spectroscopy (XPS) were used to characterize the thickness, hydrophilicity, roughness and chemical composition of the polymer brushes. PTFEMA brushes were directly patterned in a single step using electron beam lithography and were processed in an environmentally benign $scCO_2$ solvent. Tapping-mode AFM imaging confirmed the successful electron beam patterning and development of these brushes. The sensitivity of PTFEMA brushes towards direct patterning with e-beam, followed by $scCO_2$ development was studied and compared to development in THF solvent. Using this direct patterning method, followed by dry

[*]This work was done in collaboration with Marvin Y. Paik (Department of Materials Science & Engineering, Cornell University).

development in $scCO_2$, highly resolved nano-structured polymer brush lines down to 78 nm could be prepared. This method can be generalized to prepare fluorinated low surface energy polymer brush surfaces in a single step for various applications.

Introduction

Carbon dioxide has continued to emerge as an environmentally benign solvent in the area of polymer synthesis and processing. Carbon dioxide is nontoxic, nonflammable, unreactive under most conditions, leaves no liquid waste and is one of the most promising candidates for a more environmentally friendly replacement for organic and aqueous solvents in many applications. Supercritical fluid technology has been widely used as a processing tool in polymer synthesis, coatings, biomaterials and microelectronics.[1, 2] A supercritical fluid is a substance at a temperature and pressure above its thermodynamic critical point. Supercritical carbon dioxide ($scCO_2$) has the advantage of having an easily accessible critical point (T_c = 31.1°C, P_c = 72.8 atm). Under these conditions, CO_2 exhibit properties such as high gas-like diffusivity, zero surface tension, ease of solvent removal by depressurization, the ability to be recycled and can be tuned to achieve the desired density and solvent properties.[3] These unique properties associated with supercritical CO_2 offer a range of possibilities in polymer chemistry.[4-6] One area where $scCO_2$ has been studied in detail is as a development solvent for photoresist patterning.[7-10]

Surface modification using end-tethered polymer brushes[11] is an attractive, versatile and effective method of tailoring the surface properties of a material to specific needs. Polymer brushes have been utilized to prepare "smart" or responsive surfaces for a variety of applications in the area of microelectronics and biotechnology.[12, 13] Generally, end-tethered polymer brushes, with covalent attachment of polymers on the substrate surface are assembled by either the "grafting to" or the

"grafting from" approach. In the "grafting to" approach, pre-formed polymers are made to react with the reactive sites on the surface.[14] For kinetic and thermodynamic reasons[12, 13] the "grafting-to" approach is limited to formation of polymer brushes of relatively low thickness. The "grafting from" method, often referred to as surface-initiated polymerization has become the method of choice mainly because it offers a way to assemble polymer brushes with tunable grafting density and high polymer brush thickness in a controllable fashion. Surface-initiated polymerization involves polymerizing a monomer from an immobilized monolayer of surface initiators. Surface-initiated polymer brushes have been grown using conventional radical polymerization,[15] iniferter,[16] ring-opening,[17] cationic,[18] anionic,[19] aminoxyl mediated,[20] radical addition fragmentation chain transfer (RAFT)[21] and atom transfer radical polymerization (ATRP) reactions.[22]

The fabrication of patterned polymer brushes has attracted great interest in recent years and is typically a complex, multistep process. Nano-patterned polymer arrays with controlled chemical functionality, shape and feature dimensions have a wide range of potential applications in microelectromechanical systems, development of biosensors, biochips, combinatorial arrays, study of cell-surface interactions and in micro/nanofluidic devices.[23, 24] Conventionally, patterned polymer brushes are produced from the initiator monolayer immobilized on patterned surfaces.[23, 25, 26] Patterned brushes have also been grown from self-assembled monolayers (SAMs) patterned by microcontact printing,[27-31] two-dimensional gradients,[32] scanning probe microscopy[33] or chemical lithography with electron irradiation and subsequent surface initiated polymerization of a desired monomer.[34, 35] New patterning methods such as nanografting, dip-pen nanolithography, contact lithography and atomic force microscopy lithography have produced surface motifs with resolution down to tens of nanometers.[36-38] More recently, the direct patterning of poly(methyl methacrylate) and

poly(2-hydroxyethyl methacrylate) brushes using e-beam lithography has been demonstrated. Using this single step patterning approach, high resolution polymer brush patterns down to 50 nm lines were obtained.[39]

Fluorinated polymers have been extensively utilized in optical devices, biomaterials and high quality coatings due to special properties of these materials such as high thermal and chemical stability, low refractive index, low surface energy and high hydrophobicity.[40] Recently, fluorinated polymer brushes have been prepared by surface initiated "living" polymerization to prepare low surface energy surfaces. Brantley et al. used the "grafting to" approach to prepare poly(2-hydroxyethyl methacrylate) brushes on gold substrates. The hydroxyl groups were then fluorinated to obtain fluorinated brushes.[41] Andruzzi et al. have grown styrene based homopolymer and copolymer brushes bearing semifluorinated alkyl side groups by surface initiated aminoxyl mediated polymerization.[42] Granville et al. reported the synthesis of stimuli-responsive semifluorinated polymer brushes prepared by ATRP.[43-45]

2,2,2-Trifluoroethyl methacrylate (TFEMA) has features of typical methacrylate monomers and a fluorine containing monomer. Poly(2,2,2-trifluoroethyl methacrylate) (PTFEMA) is a transparent, amorphous polymer with excellent water repellency and stain resistance. PTFEMA has been used in various coating applications because of its heat and chemical resistance, low refractive index, weatherability, water and oil repellency and electric insulating properties. Recently, Chen *et al*. reported the grafting of PTFEMA from silicon wafer surfaces by surface initiated ATRP.[24] However, there is no report of direct patterning of PTFEMA brushes to obtain nano-patterned polymer brush surfaces.

Previously, the e-beam patterning of hot-filament fluorocarbon films prepared by chemical vapor deposition, using $scCO_2$ as the developer has been reported.[46, 47] The

development of spun-coat fluorinated polymeric photoresists in $scCO_2$ has also been demonstrated.[10] This chapter described the development of directly patterned low surface energy PTFEMA brushes in $scCO_2$. PTFEMA was particularly selected over other fluorinated polymers because of its very high e-beam sensitivity. PTFEMA degrades into smaller fragments under e-beam exposure and this happens at a practically low e-beam dose. Figure 4.1 shows a schematic representation of the direct patterning process to obtain nano-patterned PTFEMA brushes. PTFEMA brushes were prepared via controlled ATRP. The brushes were characterized by ellipsometry, water contact angle goniometry, atomic force microscopy (AFM) and X-ray photoelectron spectroscopy (XPS). The sensitivity of the brushes towards e-beam lithography, after development in the supercritical solvent was studied and compared to the development in THF solvent. The use of $scCO_2$ as a processing solvent has no negative effect on the polymer contrast and pattern fidelity of the nanosized features. Using this direct patterning approach, followed by $scCO_2$ development, patterns on the order of 78 nm have been demonstrated. High resolution, sub-100 nm features showed line broadening due to lateral relaxation of the polymer brushes in the voided regions. The 50 nm isolated lines showed 56 % line broadening in $scCO_2$. The same 50 nm isolated lines showed increased line broadening of 88 % in THF. This direct method of patterning combined with development in an environmentally benign solvent is a desirable method to prepare patterned low surface energy polymer brush surfaces in a single step using e-beam degradable polymers.

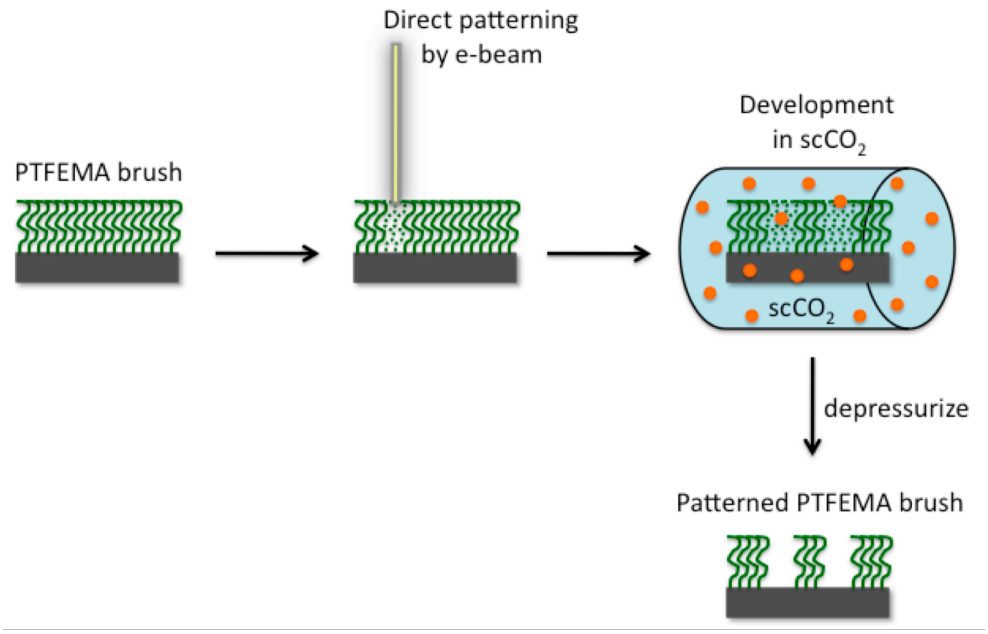

Figure 4.1. Schematic representation of the direct patterning process. PTFEMA brushes were directly patterned using e-beam lithography and then developed in $scCO_2$ to obtain patterned brush surfaces.

Experimental Section

Materials. Allyl-2-bromo-2-methylpropionate, chlorodimethyl- hydrosilane, Pt on activated carbon (10 wt %), triethylamine, copper (I) chloride (99.999%), copper (II) dibromide, 4,4′-dinonyl-2,2′-dipyridyl (dNnbpy), α,α,α-trifluorotoluene and inhibitor remover packing material were purchased from Sigma Aldrich and used without purification. The monomer, 2,2,2-trifluoroethyl methacrylate (TFEMA) (inhibited with 50 ppm MEHQ) was purchased from Scientific Polymer Products, Inc. TFEMA was further purified before use by passing through a short column of MEHQ and HQ inhibitor remover packing material. Deionized water with a resistivity of 18.2 MΩ•cm at 25 °C was obtained from Millipore's Milli-Q® Synthesis A10 system. Tetrahyrofuran was purchased from Fisher Scientific. Carbon dioxide (99.999 %) and argon gas was obtained from Airgas Inc. Doped silicon wafers were obtained from Montco Silicon Technologies, Inc.

Synthesis and Immobilization of the Surface Initiator. Hydrosilylation of allyl 2-bromo-2-methylpropionate was carried out using a literature procedure to obtain the ATRP silane initiator, 3-(chlorodimethylsilyl)propyl 2-bromo-2-methylpropionate.[48] Silicon wafers were diced into 3 cm x 1 cm pieces and cleaned by rinsing with acetone and dried under a nitrogen stream. To remove any organic residues on the surface, the substrates were further cleaned in Piranha solution (3:1 conc. H_2SO_4/30% H_2O_2 soln) for 30 minutes. (*Caution*: piranha solution reacts violently with organic materials and should be handled carefully). After rinsing with copius amounts of deionized water, the substrates were washed with dichloromethane and then dried in a vacuum oven for 10 min at 120 °C. The clean Si wafer pieces were immersed in a toluene solution of the silane initiator (2 mM) and triethyamine (0.05 mM) for 24 h. The wafers were then removed from the solution and washed with dichloromethane and left to stand in dichloromethane for 18 h. The initiator covered

wafers were either used immediately or stored under standard conditions. No loss of activity was observed on storage for couple of weeks.

Preparation of Poly(2,2,2-trifluoroethyl methacrylate) (PTFEMA) Brushes. In a typical reaction, two initiator coated silicon substrates (3 cm x 1cm) were placed in a 25 mL Schlenk flask under an argon atmosphere. The flask was evacuated and back filled with argon three times. CuCl (32 mg, 0.324 mmol), $CuBr_2$ (8mg, 0.0324 mmol) and dNnbpy (285.6 mg, 0.712mmol) were taken in another 25 mL Schlenk flask equipped with a magnetic stir bar. The air in the flask was evacuated and replaced with argon three times. The solvent (α,α,α-trifluorotoluene, 13 mL) and purified TFEMA (8 mL, 56 mmol) were purged separately with argon for about an hour and cannulated into the flask containing the ligand and copper salts. The reaction mixture was stirred at room temperature for 10 min to ensure the dissolution of the monomer and the copper-ligand complex in the solvent. This solution was then transferred into the flask containing the silicon wafer pieces. Polymerization was carried out for a set reaction time at 90 °C. After polymerization, the substrates were removed from the flask and washed with THF and gently sonicated in THF for 5 min and dried under a stream of nitrogen.

Characterization of PTFEMA Brushes. Polymer brushes were characterized by ellipsometry, water contact angle goniometry and atomic force microscopy (AFM) and X-ray Photoelectron Spectroscopy (XPS). Thicknesses of the polymer brushes were measured using a Woollam variable angle spectroscopic ellipsometer at a 70° angle of incidence. A Cauchy model (Cauchy layer/silicon substrate) was used to fit the data, in which the Cauchy layer was representative of the PTFEMA polymer brush. Water contact angles were measured using a VCA optima XE goniometer. Dynamic water contact angle measurements were performed by addition and retraction of a drop of water on the surface. At least three sample spots were taken on each surface.

Surface topography was analyzed and the root-mean-square (RMS) roughness was measured using a Veeco Dimension 3100 scanning probe microscope. Olympus tapping mode etched silicon probes were used to acquire topographic images in air at room temperature. The surface composition of the polymer brush was determined by XPS using a Surface Science Instruments SSX-100 spectrometer with an operating pressure < 2 x 10^{-9} Torr using monochromatic AlKα x rays at 1486.6 eV. Photoelectrons were collected at an angle of 55° from the surface normal using a hemispherical analyzer with a pass energy of 150 V acquired at 1 eV/step for the survey scan. The C—C 1s peak was corrected to a binding energy of 285 eV.

Direct Patterning of PTFEMA Brushes. Patterning of the PTFEMA brushes was done at the Cornell Nanoscale Facility using the JEOL 9300 electron beam lithography system. In order to get an estimate on the patterning conditions needed, contrast curves were generated from 10 μm x 1 μm areas exposed to the electron beam with linearly increasing electron dosage. A 0.5 nA beam current, 100 kV accelerating voltage, and 5 nm pixel size was used for the generation of the contrast curves and for higher resolution patterning. Doses ranging from 5 to 150 μC/cm^2 were used in this study. After e-beam exposure, the PTFEMA brushes were developed in $scCO_2$ (50 °C, 5000 psi) for 5 min and dried under a stream of nitrogen. Exposed PTFEMA brushes were also developed in THF for 60 s followed by thorough rinsing in deionized water and then dried under a stream of nitrogen.

Development of Patterned PTFEMA Brushes in $scCO_2$. Patterned PTFEMA brushes were developed in $scCO_2$ using a dissolution-rate monitor apparatus.[49] The patterned PTFEMA brush was placed into a 25 mL observation vessel. CO_2 was introduced into this vessel and kept for 5 min at the desired temperature and pressure (50 °C, 5000 psi) to develop the patterned into $scCO_2$. After $scCO_2$ development, the vessel was flushed with fresh $scCO_2$ for 2 min to wash out any of the dissolving

polymer residue. The PTFEMA brushes were then removed from the dissolution-rate monitor apparatus and cleaned under a stream of nitrogen for a couple of seconds.

Metrology. Optical microscopy imaging was performed using the Nikon Digital Sight DS-5M-L1 optical microscope. Imaging and depth measurements of the patterned surfaces was done with the Veeco Dimension 3100 scanning probe microscope using a Veeco Dimension 3100 scanning probe microscope. Olympus tapping mode etched silicon probes were used to acquire topographic images in air at room temperature.

Results and Discussion

Preparation of Polymer Brushes:

Synthesis and Characterization of Initiators on Silicon Substrates. The silane ATRP initiator, 3-(chlorodimethylsilyl)propyl 2-bromo-2-methylpropionate was synthesized in one step using a literature procedure. The disappearance of the alkene protons in the ^{1}H NMR spectra of the hydrosilylated product confirmed the completion of the reaction after 24 h. The covalent attachment of the silane initiator onto the silicon substrate was carried out in a single step. The formation of a monolayer of initiator was confirmed by ellipsometry and AFM. The dry ellipsometric thickness of the covalently attached monolayer was measured to be 1.6 ± 0.3 nm (the error is due to uncertainties present during the calculation of the film thickness from the optical data). This value is in good agreement with the theoretical height of the initiator containing SAM. The surface topography and roughness was measured by AFM. The root mean square roughness of the initiator coated silicon substrate was 0.2 nm in a 0.5 x 0.5 μm^2 scanning area. This is similar to the rms roughness measured for clean bare silicon pieces.

Preparation and Characterization of Polymer Brushes. PTFEMA brushes were synthesized via ATRP using a variation of the procedure described by Chen and co-workers[24] in α,α,α-trifluorotoluene at 90 ºC for a set polymerization time using a various. Haddleton and co-workers reported the solution ATRP of TFEMA in toluene with pyridine imine as the ligand.[50] Chen and co-workers showed that the ATRP reaction of TFEMA is better controlled in a fluorinated solvent such as trifluorotoluene.[24] They also showed that the use of 4,4′-dinonyl-2,2′-dipyridyl (dNnbpy) as the ligand, gave a more linear kinetic plot of monomer conversion with polymerization reaction time. The reaction for the synthesis of the ATRP silane initiator and preparation of polymer brushes is shown in Scheme 4.1. No sacrificial initiator was added to the solvent mixture and the polymerization was surface initiated and surface confined. This prevents the formation of undesirable polymer in solution and clean polymer brush covered surfaces were obtained simply by washing the polymer brushes with water, acetone and ethanol.

This study was done usng polymer brushes with thicknesses close to or less than 100 nm. The reaction time was determined by measuring the dry ellipsometric thicknesses of the PTFEMA brushes prepared at various polymerization reaction times. The polymerization reaction was controlled as indicated by a linear increase in thickness of the brushes with respect to reaction time[51-55] up to approximately 24 h. Figure 4.2 shows the plot of ellipsometric thickness versus polymerization reaction time. At longer reaction times, the increase in brush thickness seems to slow down. This is attributed to the loss of active chain ends or to the increase in deactivator concentration that slows down the activation/deactivation cycles, which in turn slows down the polymer brush growth.

The homopolymer brushes were characterized by ellipsometry, tapping-mode AFM, water contact angle goniometry and XPS. The dry thicknesses of the PTFEMA

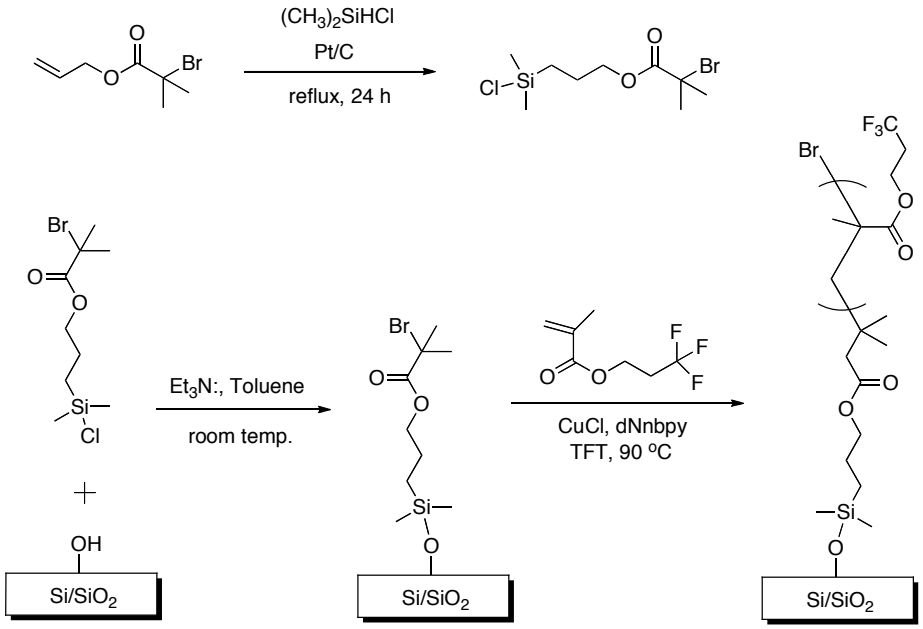

Scheme 4.1. Synthesis of the ATRP silane initiator, immobilization of the initiator on the silicon substrate, followed by surface initiated polymerization of TFEMA.

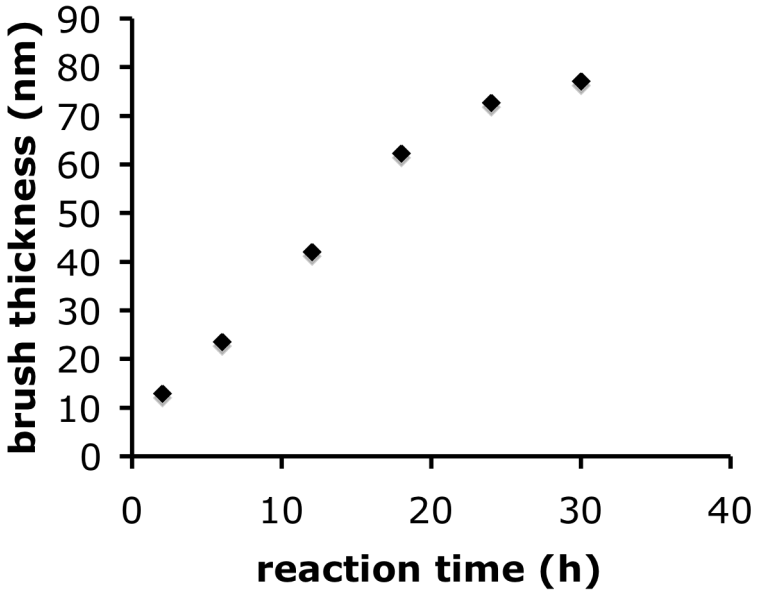

Figure 4.2. Dry ellipsometric thickness of the PTFEMA brushes as a function of polymerization reaction time. A linear increase in brush thickness over time suggests that the brush growth is controlled.

brushes were measured by ellipsometry at a 70 º incident angle. The value of n=1.437 was used as the refractive index to determine the thickness. Tapping mode AFM of the PTFEMA brushes showed the root-mean-square roughness to be 0.42 nm, indicating that the polymer brushes were homogeneous throughout the silicon substrate. At room temperature, in ambient air, the advancing and receding water contact angles for the PTFEMA brushes were 94°±1° and 70±2 °, respectively. The polymer brushes were rinsed with acetone and THF and dried at room temperature in a vacuum oven before measuring the water contact angles. Thus, as expected the fluorinated polymer brush caused the surface to be much more hydrophobic than bare silicon. After polymerization, the surface composition of the PTFEMA brush was characterized using X-ray photoelectron spectroscopy (Figure 4.3). The C 1s (285 eV), O 1s (533 eV) and F 1s (687 eV) peaks were clearly observed in the XPS spectrum. The relative areas of these peaks are in good agreement with the known composition of PTFEMA. The atomic percentages of carbon, oxygen and fluorine were 53.4%, 17. 2% and 29.41%, respectively.

Preparation of Patterned PTFEMA Brushes:

Direct Patterning of PTFEMA Polymer Brushes Using E-beam Lithography. In recent years, the preparation of patterned polymer brushes has emerged as a robust method for creating surfaces due to the stability of polymer brushes against solvents or harsh conditions. Patterned brush surfaces are routinely produced from an initiator monolayer on a patterned surface. While successful, this method requires complicated lithographic schemes. The inclusion of extra steps leads to additional opportunities for contamination. The compatibility of the photoresist is important since the patterned photoresist if soluble in the initiator solution, will restrict the formation of patterned initiators. To address these challenges, Whitesides and co-

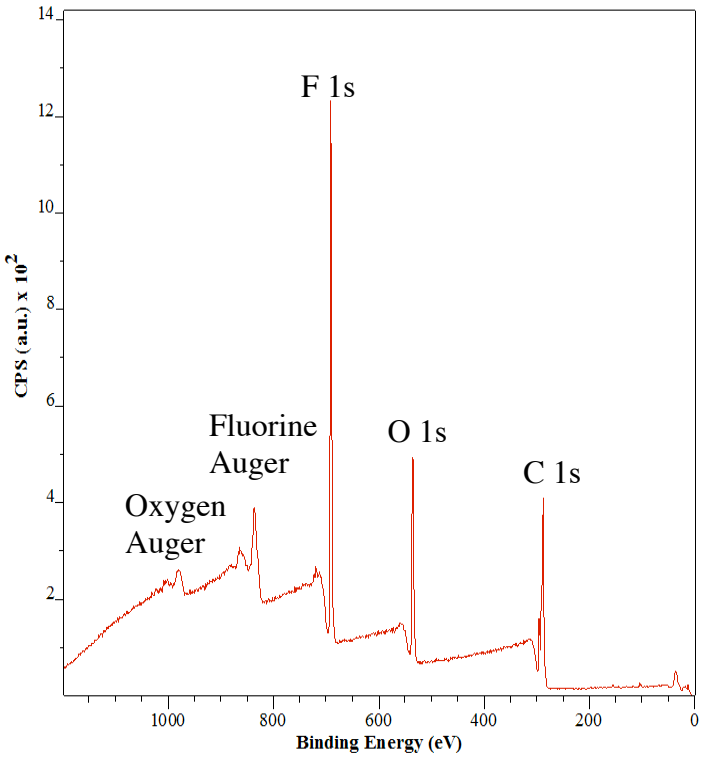

Figure 4.3. X-ray photoelectron spectroscopy survey spectrum of a 50 nm PTFEMA brush grown off a silicon substrate. The XPS spectrum suggests an atomic composition of carbon (53.4%), oxygen (17.2 %) and fluorine (29.41%) as expected from the structure of the polymer.

workers developed microcontact printing for the preparation of patterned SAMs on both planar and curved surfaces.[56] These replication methods such as microtransfer molding (μTM) offer advantages in applications where photolithography is ineffective. However, this method requires at least three steps to complete. In addition, as we go down to sub-50 nm features the impact at contact can cause structure deformation. In addition, there can be clogging from contaminants collected at contacts. Recently, we demonstrated a single step approach to achieve patterned polymer brushes. In this method, polymer brushes were prepared via ATRP and directly patterned using e-beam lithography to achieve 50 nm patterned PMMA brush surfaces.[38]

Electron beam processing has been used to boost properties by creating controlled degradation or chain scission of certain polymers. Electron beams have been used to break down polymeric materials to create micro-powders used in inks, coatings and lubricants. Upon e-beam exposure, scission reactions occur on the polymer backbone. The scission reaction leads to the degradation of polymers by rupture of covalent bonds. This causes a decrease in molecular weight and intrinsic viscosity.[57] The primary advantage of e-beam lithography over photolithography is that the e-beam process uses electrons of wavelength less than 0.1 nm and is not diffraction limited.

PTFEMA is a highly sensitive positive tone e-beam resist that degrades into smaller fragments on e-beam irradiation. PTFEMA brushes (ellipsometric thickness of 50 nm) were patterned at e-beam doses ranging from 5 to 150 $\mu C/cm^2$ with a beam current of 0.5 nA. After electron beam exposure, followed by a $scCO_2$ or THF development step, a contrast curve was generated in which the normalized thickness was plotted as a function of the log of the exposure dose as shown in Figure 4. Using the appropriate dose ascertained from the contrast curve, higher resolution lines of

patterned PTFEMA brushes were imaged. Factors such as the electron beam diameter, beam current and dose were optimized to improve the resolution of the patterned brushes.

Dry Development of Patterned PTFEMA Brushes in $scCO_2$. PTFEMA homopolymers and copolymers have been used as cladding materials in optical fibers, protectives for marble statues.[58] Fluorinated polymers have many unique characteristics, among which the oleophobic-hydrophobic nature of fluorinated polymer surfaces and their remarkable thermal and chemical resistance stand out. The properties arise due to the low intermolecular forces present in highly fluorinated organic compounds. The presence of non-polar $-CF_3$ groups at the surface of PTFEMA brushes lowers the surface energy of a surface. The non-polar nature of fluorinated polymers confers a range of properties, including water repellence and solubility in $scCO_2$. Patterned low surface energy polymer brush surfaces have the potential to be used in the preparation of superhydrophobic surfaces and in the patterning of hydrophilic inks.

The exposed PTFEMA polymer brushes were developed in $scCO_2$ and in THF. The degraded polymer chains showed good solubility in the two solvents leaving the covalently attached polymer brushes on the surface unaffected. PTFEMA brushes were successfully patterned in a single step on exposure to an electron beam and characterized and imaged by tapping mode AFM. The contrast curves of the PTFEMA brushes, developed in THF (shown in blue) and in $scCO_2$ (shown in red) are shown in Figure 4.4. The contrast was not as sharp as expected in the environmentally benign $scCO_2$ solvent, however PTFEMA brushes are highly sensitive to e-beam patterning. Also, the development of patterned PTFEMA brushes in $scCO_2$ does not have a negative effect on the contrast and sensitivity of PTFEMA brushes.

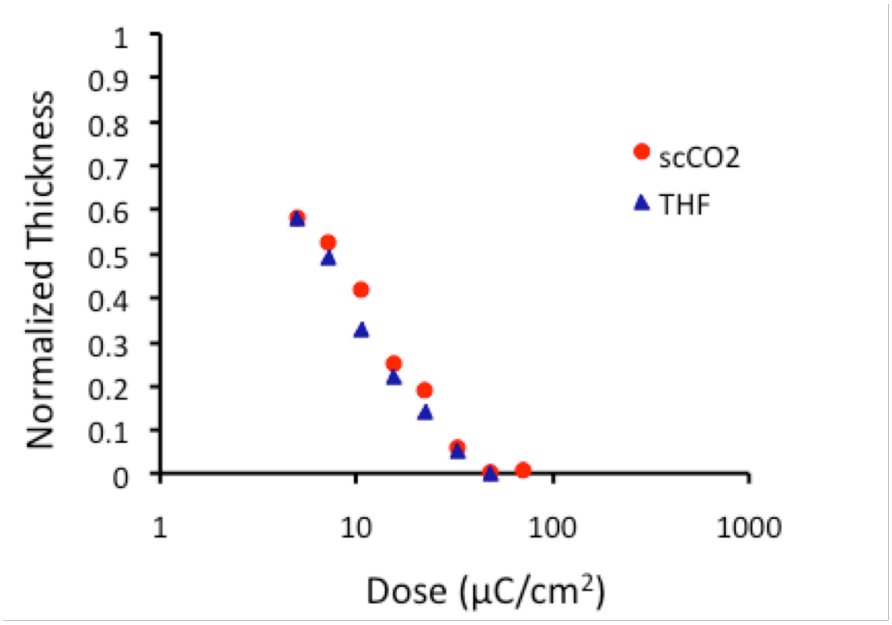

Figure 4.4. Contrast curves of the PTFEMA brushes developed in $scCO_2$ at 50 °C, 5000 psi for 5 min (shown in red), or developed in tetrahydrofuran (THF) solvent at room temperature for 90 s (shown in blue).

Figure 4.5 (a) is an AFM image of 200 nm lines of a patterned PTFEMA brush with a pitch size of 2 μm that was patterned by e-beam lithography with an exposure dose of 48.4 μC/cm^2 and developed in $scCO_2$ solvent for 5 min at 50 °C and 5000 psi. Figure 4.5 (b) is an AFM image of 150 nm lines of a patterned PTFEMA brush with a pitch size of 400 nm obtained using similar lithographic and development conditions. The $scCO_2$ development step was compared to development in an organic solvent. THF is a good solvent for PTFEMA and was used to dissolve the exposed regions of the PTFEMA brushes. Figures 4.6 (a) and 4.6 (b) show AFM images of 200 nm lines of patterned PTFEMA brushes with pitch sizes of 2 μm and 400 nm, respectively. These patterns were obtained by e-beam lithography with an exposure dose of 48.4 μC/cm^2 followed by development in THF for 90 s at room temperature.

For sub-100 nm features reduced line broadening was observed with $scCO_2$ development when compared to the development in organic (THF) solvent. Figures 4.7 (a) and 4.7 (b) show AFM images of 50 nm isolated lines of patterned PTFEMA brushes with pitch sizes of 2 μm that were developed in $scCO_2$ and THF, respectively. The 50 nm patterns exhibited line broadening due to the lateral relaxation/collapse of the extended polymer chains in the voided patterned regions. After $scCO_2$ development, the 50 nm patterns broadened to 78 nm. This is a 56 % increase in pattern size. The same features developed in THF showed 88 % line broadening resulting in 94 nm patterned lines as measured by AFM. This difference in behavior is attributed to the fact that THF is a very good solvent for PTFEMA, which makes the pattern edges much more susceptible to polymer chain relaxation. Because of the increased line broadening with the THF developer, we label THF as a poorer developer compared to $scCO_2$. Residual polymer fragments are not a concern as THF is such a good solvent it can wash away all the fragments easily. Usually, a good solvent cannot be used as a developer for traditionally spun coat polymer resists as not

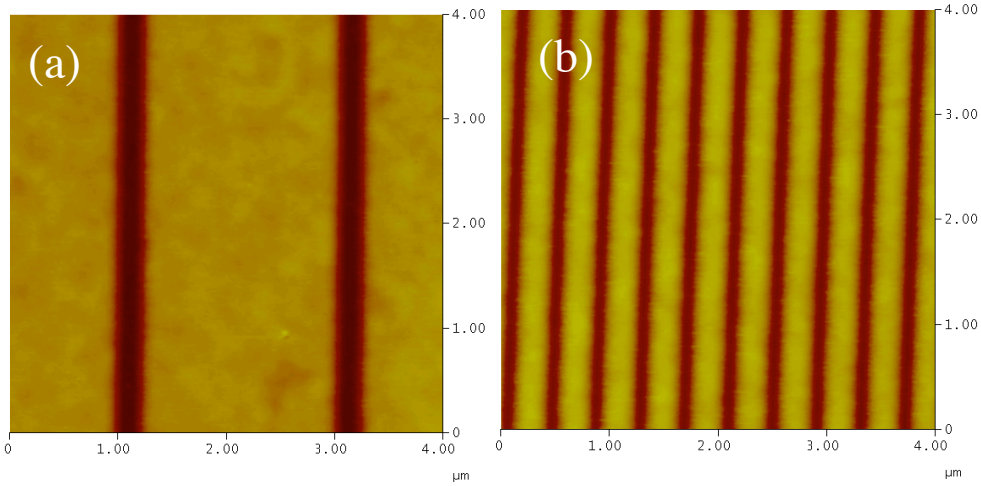

Figure 4.5. Tapping-mode AFM height images of patterned PTFEMA brushes, developed in $scCO_2$ at 50 °C, 5000 psi for 5 min and imaged at room temperature in air. (a) 200 nm lines/2 μm pitch size (b) 150 nm lines/400 nm pitch size of patterned PTFEMA brushes.

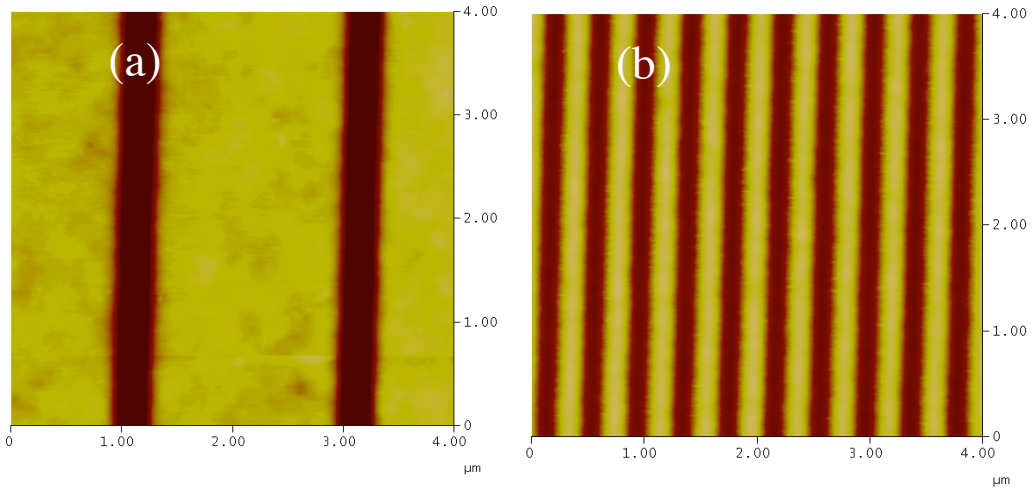

Figure 4.6. Tapping-mode AFM height images of patterned PTFEMA brushes, developed in THF at room temperature for 90 s and imaged at room temperature in air. (a) 200 nm lines/2 µm pitch size and (b) 200 nm lines/400 nm pitch size of patterned PTFEMA brushes.

only would the patterned fragments be washed away, but the polymer film as well. However that is not the case for polymer brushes, as the chains are tethered to the surface.

In contrast to the use of THF as a development solvent, processing of patterned PTFEMA brushes in $scCO_2$ has several advantages. The high diffusivity and low viscosity of $scCO_2$ allows for its efficient removal via depressurization, which allows easy separation from the polymer brushes. Since, the solvating power of a supercritical fluid is directly related to its density, a large variation in solubility can be achieved with relatively small changes in operating conditions. Direct patterning by e-beam lithography involves the dissolution of relatively small polymer fragments. Since CO_2 can dissolve small molecules and low surface energy polymers such as fluoropolymers, $scCO_2$ could replace a sizeable fraction of the solvents used in the processing of low surface energy patterned surfaces. In addition, $scCO_2$ serves as an ecological and economical alternative processing solvent that eliminates the use of toxic and flammable organic solvents.

Conclusions

Highly e-beam sensitive PTFEMA brushes were directly patterned in a single step to prepare nano-patterned PTFEMA brush surfaces. The exposed brushes were successfully developed in an environmentally benign, supercritical CO_2 solvent at 50 °C and 5000 psi for 5 min. The contrast and sensitivity of PTFEMA brushes was determined and compared to the development of the exposed brushes in THF. The contrast curve for PTFEMA brushes is not very sharp. However, these brushes are very sensitive to e-beam exposure. Using e-beam lithography, followed by development in $scCO_2$, polymer brush patterns as small as 78 nm could be obtained. The 50 nm isolated line patterns showed increased line broadening with both THF and

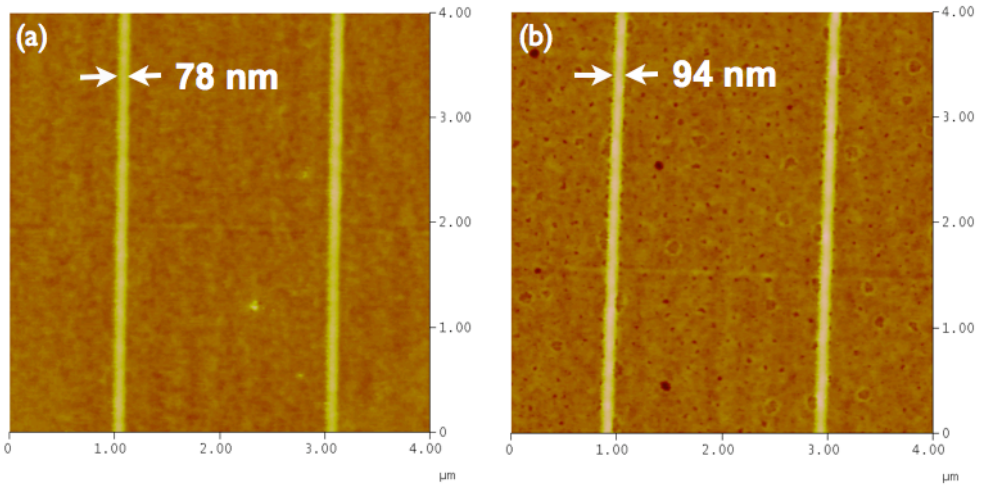

Figure 4.7. Tapping-mode AFM height images of 50 nm isolated lines of patterned PTFEMA brushes imaged at room temperature in air. (a) developed in $scCO_2$ at 50 °C, 5000 psi for 5 min (b) developed in THF at room temperature for 90 s.

$scCO_2$ development. Line broadening up to 88 % was observed in THF developer. This line broadening was reduced to 56 % in $scCO_2$ suggesting that scCO2 is a better developer for sub-100 nm features. A limitation of this method is that it requires a relatively higher pressure and a longer development time as compared to the traditional organic development. Also, the polymer used to prepare the polymer brush surfaces must be degradable under e-beam irradiation. This direct method of obtaining patterned brushes is a shorter and cleaner way to prepare patterned brush surfaces. The use of $scCO_2$ as a development solvent eliminates the generation of organic solvent waste and is an environmentally friendly patterning process.

Acknowledgments

This work was supported by the National Science Foundation under agreement No. DMR-0518785. Cornell NanoScale Science and Technology Facility (CNF) and the Cornell Center for Materials Research (CCMR) is also acknowledged for use of their facilities.

REFERENCES

1. Weibel, G. L.; Ober, C. K., *Microelectronic Engineering* **2003,** 65, 145.
2. McCluskey, G. E.; Lee, J. K.; Sha, J.; Ober, C. K.; Watkins, S. E.; Holmes, A. B., *MRS Bulletin* **2009,** 34, 108.
3. Kirby, C. F.; McHugh, M. A., *Chem. Rev.* **1999,** 99, 565.
4. Kendall, J. L.; Canelas, D. A.; Young, J. L.; DeSimone, J. M., *Chem. Rev.* **1999,** 99, 543.
5. Cooper, A. I., *J. Mater. Chem.* **2000,** 10, 207.
6. Beckman, E. J., *J. Supercrit. Fluids* **2004,** 25, 121.
7. Tanaka, M.; Rastogi, A.; Toepperwein, G. N.; Riggleman, R. A.; de Pablo, J. J.; Ober, C. K., *Chem. Mater.* **accepted**.
8. Felix, N.; Ober, C. K., *Chem. Mater.* **2008,** 20, 2932.
9. Zhou, X.; Ober, C. K.; Oberdorf, S. K.; Allen, R. D., *Chem. Mater.* **2000,** 12, 41.
10. Sha, J.; Ober, C. K., *Polymer International* **2009,** 58, (3), 302.
11. Milner, S. T., *Science* **1991,** 251, 905.
12. Zhao, B.; Brittain, W. J., *Prog. Polym. Sci.* **2000,** 25, 677.
13. Advincula, R. C.; Brittain, W. J.; Caster, K. C.; Ruhe, J., *Polymer Brushes: Synthesis, Characterization, Applications*. Wiley-VCH: Weinheim, Germany, 2004.
14. Murthy, R.; Shell, C. E.; Grunlan, M. A., *Biomaterials* **2009,** 30, 2433.
15. Prucker, O.; Ruhe, J., *Langmuir* **1998,** 14, 6893.
16. de Boer, B.; Simon, H. K.; Werts, M. P. L.; van der Vegte, E. W.; Hadziioannou, I., *Macromolecules* **2000,** 33, 349.
17. Weck, M.; Jackiw, J. J.; Rossi, R. R.; Weiss, P. S.; Grubbs, R. H., *J. Am. Chem. Soc.* **1999,** 121, 4088.

18. Zhao, B.; Brittain, W. J., *Macromolecules* **2000,** 33, 342.

19. Jordan, R.; Ulman, A.; Kang, J. F.; Rafailovich, M. H.; Sokolov, J., *J. Am. Chem. Soc.* **1999,** 121, 1016.

20. Husseman, M.; Malmstrom, E. E.; McNamara, M.; Mate, M.; Mecerreyes, O.; Benoit, D. G.; Hedrick, J. L.; Mansky, P.; Huang, E.; Russell, T. P.; Hawker, C. J., *Macromolecules* **1999,** 32, 1424.

21. Li, C.; Benicewicz, B. C., *Macromolecules* **2005,** 38, (14), 5929.

22. Matyjaszewski, K.; Miller, P. J.; Shukla, N.; Immaraporn, B.; Gelman, A.; Luokala, B. B.; Siclovan, T. M.; Lickelbick, G.; Vallant, T.; Hoffmann, H.; Pakula, T., *Macromolecules* **1999,** 32, 8716.

23. Dong, R.; Krishnan, S.; Baird, B. A.; Lindau, M.; Ober, C. K., *Biomacromolecules* **2007,** 8, 3082.

24. Chen, R.; Feng, W.; Zhu, S.; Botton, G.; Ong, B.; Wu, Y., *Journal of Polymer Science: Part A: Polymer Chemistry* **2006,** 44, 1252.

25. Slim, C.; Tran, Y.; Chehimi, M. M.; Garraud, N.; Roger, J.; Combellas, C.; Kanoufi, F., *Chem. Mater.* **2008,** 20, 6677.

26. Ahn, S. J.; Kaholek, M.; Lee, W.; LaMattina, B.; LaBean, T. H.; Zauscher, S., *Adv. Mater.* **2004,** 16, (23-24), 2141.

27. Jones, D. M.; Huck, W. T. S., *Adv. Mater.* **2001,** 13, 1256.

28. Chen, T.; Zhang, J.; Chang, D. P.; Garcia, A.; Zauscher, S., *Adv. Mater.* **2009,** 21, 1.

29. Zhou, F.; Zheng, Z.; Yu, B.; Liu, W.; Huck, W. T. S., *J. Am. Chem. Soc.* **2006,** 128, 16253.

30. Husemann, M.; Mecerreyes, D.; Hawker, C. J.; Hedrick, J. L.; Shah, R.; Abbott, N. L., *Angew. Chem. Int. Ed.* **1999,** 38, 647.

31. Jones, D. M.; Smith, J. R.; Huck, W. T. S., *Adv. Mater.* **2002,** 14, 1130.

32. Bhat, R. R.; Tomlinson, M. R.; Wu, Y.; Genzer, J., *J. Adv. Polym. Sci.* **2006,** 198, 51.

33. Kaholek, M.; Lee, W.; LaMattina, B.; Caster, K. C.; Zauscher, S., *Nano Lett.* **2004,** 4, 373.

34. He, Q.; Kuller, A.; Grunze, M.; Li, J., *Langmuir* **2007,** 23, 3981.

35. Steenackers, M.; Kuller, A.; Stoycheva, S.; Grunze, M.; Jordan, R., *Langmuir* **2009,** 25, 2225.

36. Christman, K. L.; Enriquez-Rios, V. D.; Maynard, H. D., *Soft Matter* **2006,** 2, 928.

37. Jhaveri, S. B.; Beinhoff, M.; Hawker, C. J.; Carter, K. R.; Sogah, D. Y., *ACS Nano* **2008,** 2, 719.

38. Martinez, R. V.; Losilla, N. S.; Martinez, J.; Huttel, Y.; Garcia, R., *Nano Lett.* **2007,** 7, 1846.

39. Paik, M.; Rastogi, A.; Tanaka, M.; Ober, C. K., *PMSE Preprints* **2008,** 99, 541.

40. Ciardelli, F.; Agleitto, M.; Montagnini, M. L.; Passaglia, E.; Giancristoforo, S.; Castelvetro, V.; Ruggeri, G., *Prog. Org. Coat.* **1997,** 32, 43.

41. Brantley, E. L.; Jennings, G. K., *Macromolecules* **2004,** 37, 1476.

42. Andruzzi, L.; Hexemer, A.; Li, X. F.; Ober, C. K.; Kramer, E. J.; Galli, G.; Chiellini, E.; Fischer, D. A., *Langmuir* **2004,** 20, 10498.

43. Granville, A. M.; Boyes, S. G.; Akgun, B.; Foster, M. D.; Brittain, W. J., *Macromolecules* **2005,** 38, (8), 3263.

44. Granville, A. M.; Brittain, W. J., *Macromol. Rapid Commun.* **2004,** 25, 1298.

45. Granville, A. M.; Boyes, S. G.; Akgun, B.; Foster, M. D.; Brittain, W. J., *Macromolecules* **2004,** 37, (8), 2790.

46. Mao, Y.; Felix, N. M.; Nguyen, P. T.; Ober, C. K.; Gleason, K. K., *Chem. Vap. Deposition* **2006,** 12, 259.

47. Pryce Lewis, H. G.; Weibel, G. L.; Ober, C. K.; Gleason, K. K., *Chem. Vap. Deposition* **2001,** 7, (5), 195.

48. Ramakrishnan, A.; Dhamodharan, R.; Ruhe, J., *J. Macromol. Rapid Commun.* **2002,** 23, 612.

49. Pham, V. Q.; Rao, N.; Ober, C. K., *J. Supercrit. Fluids* **2004,** 31, 323.

50. Perrier, S.; Jackson, S. G.; Haddleton, D. M., *Macromolecules* **2003,** 36, (24), 9042.

51. Brown, A. A.; Khan, N. S.; Steinbock, L.; Huck, W. T. S., *Eur. Polym. J.* **2005,** 41, 1757.

52. Jones, D. M.; Brown, A. A.; Huck, W. T. S., *Langmuir* **2002,** 18, (4), 1265.

53. Li, J.; Chen, X.; Chang, Y. C., *Langmuir* **2005,** 21, 9562.

54. Zhang, K.; Li, H.; Zhao, S.; Wang, W.; Wang, S.; Xu, Y.; Yu, W.; Wang, J., *Polymer Bulletin* **2006,** 57, 253.

55. Wang, Y. P.; Pei, X. W.; He, X. Y.; Lei, Z. Q., *Eur. Polym. J.* **2005,** 41, (4), 737.

56. Xia, Y.; Whitesides, G. M., *Angew. Chem.* **1998,** 110, 568.

57. Slimani, K.; Moine, L.; Aymes-Chodur, C.; Laurent, A.; Labarre, D.; Yagoubi, N., *Polymer Degradation and Stability* **2009,** 94, 584.

58. Kwon, S.; Bae, W.; Lee, W.; Byun, H.; Kim, H., *J. Chem. Eng. Data* **2007,** 52, 89.

CHAPTER 5

PREVENTING NON-SPECIFIC ADSORPTION ON POLYMER BRUSH COVERED GOLD ELECTRODES USING A MODIFIED ATRP INITIATOR*

Abstract

Biological systems have a tendency to adsorb non-specifically onto a solid substrate, thus reducing the efficacy of the interface being used in biorecognition. This non-specific adsorption is a common problem in the development of biosensors as it typically reduces the efficacy of the sensor platform. This chapter describes the synthesis of an oligo(ethylene glycol) (OEG) containing ATRP (atom transfer radical polymerization) thiol initiator and demonstrate the role of this initiator in preventing non-specific adsorption of IgG antibodies on chemically functionalized gold electrode surfaces using cyclic voltammetry. A new synthetic route for the synthesis of the new ATRP thiol initiator in high yields has been reported. Surface initiated poly(acrylic acid) brushes grown off the gold surface with modified OEG containing and conventional ATRP thiol initiators were chemically modified with 2,4-dinitrophenyl (DNP) groups. Amperometric studies were carried out on gold electrodes modified with DNP-PAA brushes using DNP-specific and non-specific IgG antibodies. The cyclic voltammograms of an osmium redox mediator recorded over time suggest that the chemical modification of the gold electrodes with DNP-PAA brushes using the

* This work was done in collaboration with Dr. Manabu Tanaka (Department of Materials Science & Engineering, Cornell University), Dr. Nicolas Da Mota, Michele Tague, Prof. Barbara A. Baird and Prof. Hector D. Abruna (Department of Chemistry & Chemical Biology, Cornell University).

OEG-containing ATRP initiator is much more effective in preventing non-specific adsorption of antibodies than polymer brushes grown from the conventional initiator. Finally, these results were confirmed with the quartz crystal microbalance (QCM) technique by quantitatively evaluating the adsorption of non-specific IgG antibodies on DNP-PAA functionalized QCM surfaces. The use of this modified ATRP thiol initiator to chemically functionalize macro/micro electrode surfaces will help develop reproducible, reliable and robust electrochemical biosensors with minimized non-specific adsorption.

Introduction

Preventing non-specific adsorption of biological molecules on solid surfaces is crucial for the production of biomedical devices, implants, biosensors and diagnostic arrays where a layer of biomolecules is designed as a functional coating. Most biological systems have the capability to recognize specific ligands through intricate receptor-recognition interactions. However, many biological molecules also have a tendency to physically adsorb onto a solid substrate without specific receptor-recognition interactions. This type of contamination is known as non-specific adsorption.[1, 2] This creates a problem, common to biosensors, that typically reduces the efficacy of an interface otherwise engineered for specific biorecognition. This can result, for example, in high background noise or "false positives". Another manifestation of random adsorption is denatured proteins that show loss of bioactivity and leaves behind inaccessible biomolecules and unreacted surface sites. The problem of non-specific adsorption can be avoided by pre-coating the surface with a material that is resistant to protein adsorption. Polymers such as poly(vinyl alcohol), poly(acrylamide), dextran and poly(ethylene glycol) (PEG) have been used as coating materials to prevent non-specific adsorption.[3-7]

The elimination or minimization of non-specific binding itself may not be enough for certain applications. The development of biosensors for biomedical diagnostics requires controlled immobilization of bioactive species so that the specific recognition ligands are bound to the sensor surface in a favorable orientation.

Quantitative immunological methods have long been essential to many clinical, pharmaceutical and basic scientific investigations since late 1960s.[8] An immunosensor uses, for example, antibodies, antibody fragments or antigens as the specific recognition component. Antibodies, generated naturally as part of the adaptive immune response, are early markers for many infectious diseases. In general, antibodies can be generated to recognize a vast range of antigenic groups with exquisite specificity. Thus, sensitive and selective antibody detection is a fundamental requirement for diagnosing infections. The capacity to measure low concentrations of antibodies in complex media, while minimizing false positives, is a clear goal of most immunoassays. Amperometric electrochemical sensors represent the most rapidly growing class of sensors due to their miniaturization potential, design simplicity, low cost and low detection limits, in addition to the capability of direct readout of transduction signals.[9, 10] However, such direct electrochemical detection can often be limited by the poor selectivity, low sensitivity, interference via other species and high susceptibility to electrode fouling.[11-13] Thus, the deliberate tailoring of surface chemistry by synthetic tools is of utmost importance for the production of surfaces with biospecific binding properties and minimized background interferences.

Ethylene glycol containing self-assembled monolayers (SAMs) have been used extensively in biological applications to construct protein resistant surfaces with well oriented bioactive species on the transducer surface.[1] PEG is nontoxic and nonimmunogenic, making it an attractive candidate for use in biological research. SAMs of alkane thiols, terminated in short oligomers of ethylene glycol groups

(OEG_nalkane thiols with n = 2-17) were the primary SAMs developed to resist the adsorption of proteins on gold surfaces. Prime and Whitesides showed that densely packed self-assembled monolayers of oligo(ethylene glycol) (OEG) with only a few ethylene oxide units per molecule were resistant to protein adsorption on gold.[14] Zhu et al. showed that the adhesion of cells to gold surfaces was sensitive to the length of the OEG chains with longer chains being more effective than shorter ones in preventing non-specific adsorption.[15] More recently, Senaratne et al. functionalized silicon substrates with PEG by modifying amine functionalized SiOx with active succinimidyl carbonate functionalized PEG to create molecular templates with highly mitigated nonspecific adsorption.[16]

Polymer brushes[17] have recently attracted considerable interest for the generation of surfaces for applications in nanotechnology, molecular biology and biomedical sciences.[18] Generally, diagnostic devices comprise of covalently bound enzymes that exhibit enhanced stability over that of free enzymes.[19] However, the activity of the immobilized species is often reduced upon immobilization.[20] Thus, in order to compensate for this low activity, the density of immobilized biomolecules is often increased by the use of polymer brushes. Recently, the modification of electrode surfaces with polymer brushes has gained a lot of interest.[21-23] Using this method, electrodes with switchable and tunable redox activity have been prepared.[24, 25] Polymer brushes have the added advantage of providing 3-D coatings with higher binding capacities (moles of biomolecules per unit area), which can yield lower detection limits in biosensors. Polymer brushes bearing OEG moities resist non-specific protein adsorption and provide surfaces with improved long term stability due to the robust structure and high density of OEG groups. Andruzzi et al. used styrenic monomers containing OEG moities to study the biocompatibility of polymer brushes tethered to silicon oxide surfaces.[26] The results showed that brushes with short OEG

side chains suppressed protein adsorption significantly more than polystyrene brushes alone. Chilkoti et al. prepared "non-fouling" surfaces by growing OEG containing methyl methacrylate polymer brushes on gold substrate.[27] These functionalized surfaces showed reduced protein and cell adsorption. Zhou et al. prepared effective polymer brushes for specific bioattachment with distinguishably reduced non-specific adsorption.[28] In another study, binary (oligoethylene glycol) methacrylate brushes were prepared by a combination of microcontact printing and surface initiated atom transfer radical polymerization[29] (ATRP). More recently, Dong et al. grew poly(acrylic acid) (PAA) brushes via surface initiated polymerization of sodium acrylate in aqueous media to generate carboxylic acid groups on a silicon surface.[30] The use of sodium acrylate enables a direct and efficient formation of PAA brushes in contrast to prior methods that involve hydrolysis of poly(tert-butyl acrylate) brushes using acidic conditions in undesirable organic solvents.[31-33] These PAA brushes provide a high density of carboxylic acid groups for protein immobilization via esterification, amidation and nitrilotriacetate(NTA)-Cu^{2+} complexation reactions.[32]

Surface initiated polymerization on gold substrates is widely carried out using ω-mercaptoundecyl bromoisobutyrate as an ATRP thiol initiator.[31, 34-36] We refer to this initiator as the "conventional initiator". This initiator has been shown to be highly efficient for surface initiated polymerizations from gold surfaces. However, the efficacy and reliability of bio-analytical interfacial systems is highly limited by non-specific adsorption of biomolecules on polymer brush coated electrode surfaces grown from this conventional initiator. Electrochemical signals from chemically modified electrodes in amperometric devices are highly sensitive to changes in current due to non-specific adsorption. In fact, most immunosensors are relatively short-lived due to electrode fouling. Thus to improve upon the reliability and stability of electrochemical

sensors, there is a need to create surfaces that are more effective in preventing surface fouling.

In this chapter, a new synthetic route for the synthesis of an OEG containing ATRP thiol initiator in high yield is reported. The role of this initiator in preventing non-specific adsorption of IgG antibodies on polymer brush covered gold electrodes has been demonstrated. The chemical structures of the conventional and modified ATRP thiol initiators are shown in Figure 5.1. Each of the two initiators was immobilized on gold coated silicon wafers, gold electrodes and gold deposited QCM electrodes, respectively. The ease of polymerization of sodium acrylate in water and straightforward chemistry of functionalization of PAA encouraged us to chemically modify the gold electrode and QCM surfaces with a model, 2,4-dinitrophenyl (DNP) antigenic group using PAA brushes. The PAA brushes were characterized by ellipsometry, water contact angle goniometry, atomic force microscopy (AFM), FTIR and X-ray photoelectron spectroscopy (XPS). The PAA brush covered gold surfaces were functionalized with DNP groups as a model antigen. In immunosensor research, DNP groups are often used as model antigens due to their known immunogenic behavior, easy accessibility and availability of DNP reagents and anti-DNP antibodies.[37-40] In addition, cyclic voltammetry is easily used to determine surface coverage of DNP groups because nitro groups in DNP have well defined redox activity. The DNP functionalized PAA (DNP-PAA) brushes were analyzed both qualitatively and quantitatively. A qualitative analysis was done using fluorescently labeled anti-DNP IgE antibodies. Quantitative analysis of these DNP functionalized brushes was performed using cyclic voltammetry.

To date, no direct comparison has been made between polymer brush covered electrode surfaces that are modified with the conventionally used ATRP thiol initiator and the modified ATRP thiol initiator. The role of the OEG containing ATRP initiator

in preventing non-specific adsorption of antibodies on polymer brush covered electrodes was demonstrated using amperometric methods. Cyclic voltammetric measurements were carried out on DNP-PAA modified gold electrodes, grown from the OEG containing and conventional initiators. The functionalized electrodes were tested with DNP-specific and non-specific antibodies. The cyclic voltammetric response of an osmium redox mediator was recorded before and after immersion in a solution of non-specific IgG antibodies. These results suggest that the chemical modification of the gold electrode surfaces with DNP-PAA brushes using our modified ATRP thiol initiator is much more effective in preventing non-specific adsorption of IgG antibodies than polymer brushes grown from the conventional initiator. Finally, the adsorption of non-specific IgG antibodies on DNP-PAA modified quartz crystal microbalance (QCM) electrodes, prepared using the two initiators, was quantified and compared. QCM studies confirmed that the modification of surfaces using the OEG modified ATRP initiator show significant diminution of non-specific adsorption of antibodies on the gold substrate compared to the conventional ATRP initiator.

Experimental Section

Chemical Reagents and Materials. 11-bromo-1-undecene, tetra(ethylene glycol), sodium hydroxide solution, thioacetic acid, azobisisobutyronitrile (AIBN), 2-bromo-isobutylryl bromide, pyridine, methylene chloride, ethyl acetate, sodium acrylate, copper (I) bromide (99.999%), copper (II) dibromide, 2,2'-bipyridine, 2-(2-aminoethoxy)ethanol, DNP-*e*-amino-*n*-caproic acid, *N*,*N*'-diisopropyl carbodiimide (DIPC), dimethyl formamide (DMF), sulfuric acid (99.999% content), absolute anhydrous ethanol, cystamine, phosphate buffered saline (PBS, pH=7.4) and insulin from bovine pancreas were purchased from Aldrich and used without further

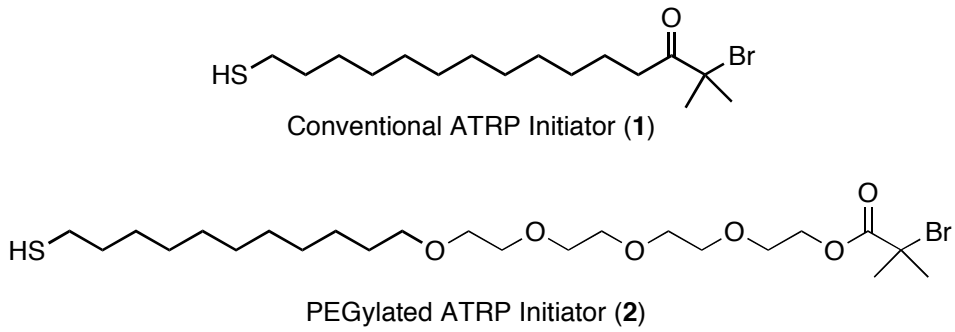

Figure 5.1. Chemical structures of the conventional **(1)** and OEG-containing ATRP thiol **(2)** initiators.

purification. Deionized water with a resistance of 18.2 MΩ•cm at 25 °C was obtained from Millipore's Milli-Q® Synthesis A10 system. 4-(dimethylamino)pyridinium 4-toluene sulfonate (DPTS) was prepared from dimethyl amino pyridine and sodium p-toluene sulfonate following a literature procedure.[41] 1,10-phenanthroline (phen) and 1,10-phenanthroline-5,6-dione (phendione) and ammonium hexafluorophosphate were purchased from Sigma Aldrich and used without further purification. The electron-transfer mediator, [Os(1,10-phenanthroline-5,6-dione)(1,10-phenanthroline)$_2$](PF_6)$_2$ complex was synthesized using a previously published procedure.[42] Anti-DNP IgG antibodies were purchased from ZYMED® Laboratories (now Invitrogen™). AlexaFluor 488 labeled IgE antibodies were obtained from Molecular Probes. AT-cut quartz crystals (5 MHz) of 24.5 mm diameter with Au electrodes deposited on a Ti adhesion layer were obtained from MaxTek Inc. (currently Inficon Technologies).

Synthesis of the Conventional ATRP Initiator. The conventional non-PEGylated initiator, *w*-mercaptoundecyl bromoisobutyrate (**1**), was synthesized from 11-mercapto-1-undecanol based on a literature procedure.[35] ^{1}H NMR (300 MHz, $CDCl_3$): d = 4.15 (t, J = 5.1 Hz, 2H, -C$\underline{H}_2$-COO-), 2.50 (q, J = 5.4 Hz, 2H, HS-C$\underline{H}_2$-), 1.91 (s, 6H, -C$\underline{H}_3$), 1.68-1.55 (m, 4H, HS-CH_2-C$\underline{H}_2$-, -C$\underline{H}_2$-CH_2-COO-), 1.35-1.26 (m, 15H, -C$\underline{H}_2$-, -S$\underline{H}$).

Synthesis of the Modified PEG Containing ATRP Initiator. The PEG containing modified thiol headed ATRP initiator (**2**) was synthesized in four steps.

3,6,9,12-tetraoxatricos-22-en-1-ol (3). 11-Bromo-1-undecene (10 g, 42.9 mmol) was reacted with 10 equivalents of tetra(ethylene glycol) (83.3 g, 429 mmol) in 10 M NaOH aqueous solution for 24 h at 100 °C. The reaction mixture was allowed to cool to room temperature. The product was extracted with 100 mL hexane five times and purified by column chromatography (eluent: ethyl acetate, R_f = 0.24) to obtain colorless viscous liquid (yield: 69.7 %); ^{1}H NMR (300 MHz, $CDCl_3$): d = 5.73

(m, 1H, CH_2=C<u>H</u>-), 4.87 (m, 2H, C<u>H</u>$_2$=CH-), 3.66-3.55 (m, 16H, -O-C<u>H</u>$_2$-C<u>H</u>$_2$-O-), 3.37 (t, *J* = 5.1 Hz, 2H, -CH_2--CH_2-C<u>H</u>$_2$-O-), 3.20 (s, 1H, -OH), 2.95 (m, 2H, CH_2=CH-C<u>H</u>$_2$-), 1.50 (m, 2H, -CH_2-C<u>H</u>$_2$-CH_2-O-), 1.31-1.15 (m, 12H, -CH_2-).

S-1-hydroxy-3,6,9,12-tetraoxatricosan-23-yl ethanethioate (4). To a methanol solution (65 mL) of **3** (8.16 g, 23.5 mmol), thioacetic acid (7.17 g, 94.2 mmol) and AIBN (19.6mg, 0.12 mmol) were added. The mixture was stirred for 6 h at room temperature under UV irradiation using a high intensity UVEXS 110 series spot curing system (10 W/cm^2). The solvent and excess of thioacetic acid were removed under vacuum. The product was purified by column chromatography (eluent: ethyl acetate, R_f = 0.15) to obtain pale yellow viscous liquid (yield: 93.5 %); ^{1}H NMR (300 MHz, $CDCl_3$): *d* = 4.05 (q, *J* = 7.2 Hz, 2H, -C<u>H</u>$_2$-OH), 3.67-3.51 (m, 15H, -O-C<u>H</u>$_2$-C<u>H</u>$_2$-O-, -O<u>H</u>), 3.38 (t, *J* = 6.9 Hz, 2H, -CH_2-CH_2-C<u>H</u>$_2$-O-), 2.79 (t, *J* = 7.5 Hz, 2H, -S-C<u>H</u>$_2$-), 2.25 (s, 3H, -C<u>H</u>$_3$), 1.55-1.44 (m, 4H, -S-CH_2-C<u>H</u>$_2$-, -CH_2-C<u>H</u>$_2$-CH_2-O-), 1.27-1.16 (m, 14H, -C<u>H</u>$_2$-).

25-oxo-3,6,9,12-tetraoxa-24-thiahexacosyl 2-bromo-2-methylpropanoate (5). 2-Bromo-isobutyryl bromide (1.97 g, 8.61 mmol) was reacted with **4** (4.0 g, 9.47 mmol) in 35 mL of dichloromethane in the presence of pyridine (0.681 g, 8.61 mmol). The mixture was stirred for 1h at 0 °C and followed 16 h at room temperature under argon atmosphere. The solvent was removed and the product was purified by column chromatography (eluent: ethyl acetate, R_f = 0.46) to obtain pale yellow viscous liquid (yield: 55.7 %); ^{1}H NMR (500 MHz, $CDCl_3$): *d* = 4.29 (t, *J* = 6.5 Hz, 2H, -C<u>H</u>$_2$-OOO-), 3.72-3.54 (m, 14H, -O-C<u>H</u>$_2$-C<u>H</u>$_2$-O-), 3.40 (t, *J* = 8.5 Hz, 2H, -CH_2-CH_2-C<u>H</u>$_2$-O-), 2.82 (t, *J* = 9.5 Hz, 2H, -S-C<u>H</u>$_2$-), 2.29 (s, 3H, -C<u>H</u>$_3$), 2.01 (s, 6H, -C<u>H</u>$_3$), 1.60-1.47 (m, 4H, -S-CH_2-C<u>H</u>$_2$-, -CH_2-C<u>H</u>$_2$-CH_2-O-), 1.26-1.20 (m, 14H, -C<u>H</u>$_2$-).

23-mercapto-3,6,9,12-tetraoxatricosyl 2-bromo-2-methylpropanoate (2). To a 2 mL solution of **5** (1.0 g, 1.75 mmol) in dichloromethane, cystamine (0.134 g, 1.75 mmol) was added to selectively deprotect the acetyl group from thioacetate. After stirring the reaction mixture for 24 h at room temperature, the product was purified by column chromatography (eluent: ethyl acetate, $R_f = 0.33$) to obtain pale yellow viscous liquid (yield: 82 %); ^{1}H NMR (500 MHz, $CDCl_3$): d = 4.29 (t, J = 6.0 Hz, 2H, -C$\underline{H}_2$-OOO-), 3.72-3.53 (m, 14H, -O-C$\underline{H}_2$-C$\underline{H}_2$-O-), 3.41 (t, J = 8.5 Hz, 2H, -CH_2-CH_2-C$\underline{H}_2$-O-), 2.49 (q, J = 9.0 Hz, 2H, -S-C$\underline{H}_2$-), 2.01 (s, 3H, -S$\underline{H}$), 1.91 (s, 6H, -C$\underline{H}_3$), 1.57-1.52 (m, 4H, -S-CH_2-C$\underline{H}_2$-, -CH_2-C$\underline{H}_2$-CH_2-O-), 1.32-1.21 (m, 14H, -C$\underline{H}_2$-).

Immobilization of Initiators on Gold Surfaces. The gold coated silicon wafers (200 nm Au deposited on a 50 nm Ti adhesion layer) and QCM electrodes were plasma cleaned for 5 min to remove any adsorbed organic layer on the surface. Prior to use, all electrodes were polished to a mirror finish using increasing grades of sand paper on a polishing wheel and with 1 μm diamond paste (Buehler Ltd., MetaDi®) and rinsed thoroughly with water and acetone. The gold and platinum electrodes were dipped in 0.1 M sulfuric acid and further cleaned electrochemically. The gold electrodes were cleaned until the cyclic voltammetric response of a clean polycrystalline gold electrode was obtained. The initiators were immobilized on clean gold-deposited silicon wafers, gold working electrodes, and QCM electrodes by immersing the wafers and electrodes in a 2 mM ethanol solution of initiator for 24 h at room temperature. Samples were finally rinsed with anhydrous ethanol and dried under a dry nitrogen atmosphere. The initiator was immobilized on the gold working electrode and QCM surfaces similarly using custom designed glassware.

Preparation of Poly(acrylic acid) (PAA) Brushes. PAA brushes were grown on initiator coated gold substrates using a modified literature procedure.[30] A typical reaction is described using gold coated silicon wafers as an example. In a typical

reaction, two gold coated silicon substrate pieces (2 cm x 1cm) were placed in a 25 mL Schlenk flask under an argon atmosphere. The flask was evacuated and back filled with argon three times. Sodium acrylate (2.16 g, 23 mmol), CuBr (103.32 mg, 0.7 mmol), $CuBr_2$ (15.8 mg, 0.07 mmol), bipyridine (247.32 mg, 1.58 mmol) were taken in another 50 mL Schenk flask equipped with a magnetic stir bar. The air in the flask was evacuated and replaced with argon three times. Water (12 mL) was purged with argon for about an hour and cannulated into the flask containing the mononer, ligand and copper salts. The reaction mixture was stirred at room temperature for 20 min to ensure the dissolution of the monomer and the copper-ligand complex in water. This solution was then transferred into the flask containing the gold coated wafer pieces. Polymerization was carried out for 2 h at 32 °C. After polymerization, the substrates were washed with water, sonicated in water for a minute and then dipped into ethylenediaminetetra EDTA solution to remove the catalyst. The brushes were finally immersed in pH 5 aqueous solution to protonate the carboxylic acids. Polymerization reaction on gold working electrodes and QCM surfaces was carried out using a similar procedure in custom designed glassware.

Preparation of DNP-Functionalized Poly(acrylic acid) (DNP-PAA) Brushes. PAA brushes were functionalized with DNP groups in two steps. PAA brush coated gold substrates were placed in a 25 mL Schlenk flask under argon atmosphere. The flask was evacuated and back filled with argon three times. A solution of 2-(2-aminoethoxy)ethanol (250 μL, 2.5 mmol), DIPC (125 μL, 0.8 mmol), and DPTS (187.5 mg, 0.63 mmol) in anhydrous DMF (10 mL) was cannulated into the flask. The mixture was allowed to stir for a minute and then transferred into the flask containing the wafers. The reaction continued for 24 h at 32 °C. Next, the substrates were washed with DMF and water. DNP groups were introduced into the activated carboxylic groups of the polymer brushes using DNP-*e*-amino-n-caproic acid. The modified

substrates were functionalized with DNP groups using a similar procedure as described above. A solution of DNP-*e*-amino-*n*-caproic acid (37.5 mg, 1.12 mmol), DIPC (125 μL, 0.8 mmol), and DPTS (187.5 mg, 0.63 mmol) in anhydrous DMF (10 mL) was cannulated into the flask containing the substrates. After reacting for 24 h at 32 °C, the substrates were washed with DMF, water and anhydrous ethanol.

Qualititative Analysis of DNP-PAA Brushes. Fluorescently labeled IgE antibodies were diluted with PBS. The DNP-PAA brush modified gold substrates were immersed in a 10 μg mL^{-1} solution of AlexaFluor 488 labeled IgE antibodies in the dark at room temperature for 90 min. The samples were removed from the IgE solution and washed with PBS. PAA brushes without DNP functionalization were used as control samples. DNP-PAA brushes incubated only in PBS served as a control for background fluorescence. Fluorescent images were taken using an Olympus BX51 upright fluorescence microscope, equipped with a Roper Cool Snap hx CCD camera. Alexa488 was observed with a 450-490 nm excitation and 520 nm emission filter set.

Quantification of DNP Groups on DNP-PAA Brushes. Electrochemical experiments were carried out at 25 ºC with a BAS CV-27 potentiostat. Au electrodes (0.001 cm^2) functionalized with PAA-DNP were used as working electrode. A large area platinum wire coil and a saturated Ag/AgCl electrode were used as counter and reference electrodes, respectively. All potentials were referenced to the satd. Ag/AgCl electrode without regard for the liquid junction potential. Cyclic voltammogram was recorded using sulfuric acid solution (0.10 M) as the supporting electrolyte at 25 °C at a scan rate of 50 mV/s. Standard three compartment electrochemical cells were used. All solutions were purged with nitrogen for at least 5 min before use. Surface coverage of DNP groups was calculated from the anodic and cathodic peak areas of the redox active DNP groups. The electrochemical measurements were also performed with a

CV-27 potentiostat made by BioAnalytical Systems, Inc. Data were recorded using a custom interface made with the LabWindows program.

Adsorption Studies of DNP Functionalized Gold Electrodes Using Cyclic Voltammetry

Cyclic voltammetric experiments were carried out on DNP-PAA brush modified gold electrodes, grown from both initiators. The modified electrodes were dipped in a 0.2 mM solution of [Os(1,10-phenanthroline-5,6-dione)(1,10-phenanthroline)$_2$]$(PF_6)_2$ complex in 0.1 M in PBS buffer (pH = 7). The cyclic voltammogram of the osmium complex was observed over time before and after immersion in a solution of either non-DNP-specific or DNP-specific IgG antibodies for a known period of time.

Quantitative Adsorption Studies on DNP-functionalized QCM Surfaces.

Measurements were carried out using an AT-cut quartz crystal (5 MHz) of 1 inch diameter with Au electrodes, modified with DNP-PAA. The crystal was set in a water tight probe (TPS-550, MaxTek Inc.) made of Teflon® leaving only the larger front side electrode (1.37 cm^2) exposed. The probe included the oscillator circuit and was held vertically in a water jacketed, one compartment electrochemical cell. The QCM probe was immersed in a phosphate buffer saline (PBS) solution (pH = 7.4) and stabilized for at 25.0±0.1 °C until a constant frequency was reached. The frequency was monitored with a PM-740 (MaxTek Inc.) plating monitor, which was, in turn, connected to a computer via a 9-pin serial port. The anti-DNP IgG antibodies (6.7×10^{-10} mol) were added to the PBS solution with the immersed QCM electrode and the frequency was constantly monitored until a new stable frequency was reached.

Characterization. ^{1}H NMR spectra were recorded on a Mercury-300 (300 MHz) or INOVA-500 (500 MHz) spectrometer at room temperature, using the chemical shift of a residual protic solvent (chloroform at δ 7.24 ppm) as an internal

reference. All shifts are quoted in parts per million (ppm) relative to chloroform or acetonitrile, and coupling constants *J* are measured in hertz. The multiplicity of the signal is indicated as follows: s (singlet), d (doublet), t (triplet), q (quartet), and m (multiplet). Polymer brushes were characterized by ellipsometry, water contact angle goniometry, atomic force microscopy (AFM), FTIR and X-ray photoelectron spectroscopy (XPS). Thicknesses of the polymer brushes were measured by a Woollam variable angle spectroscopic ellipsometer at a 70° angle of incidence. A Cauchy model (Cauchy layer/Au substrate) was used to fit the data, in which the Cauchy layer was representative of the PAA brush. Water contact angles were measured using a VCA optima XE goniometer. Dynamic water contact angles measurements were performed by addition and retraction of a drop of water on the surface. Surface topography and roughness were measured using a Veeco Dimension 3100 scanning probe microscope. Olympus tapping mode etched silicon probes were used to acquire topographic images in air at room temperature. The surface composition of the PAA and PAA-DNP brushes was characterized by FTIR using a Bruker Optics Vertex80v spectrometer. The XPS spectrum was obtained using a Surface Science Instruments SSX-100 spectrometer with an operating pressure < 2 $\times 10^{-9}$ Torr using monochromatic AlKα x rays at 1486.6 eV. Photoelectrons were collected at an angle of 55-degrees from the surface normal using a hemispherical analyer with pass energies of 150 V acquired at 1 eV/step (survey scan) and 50 V acquired at 0.065 eV (high resolution scan). The system was calibrated to Au $4f_{7/2}$ at 84 eV. The C—C 1s peak was corrected to a binding energy of 285 eV.

Results and Discussion

OEG Containing ATRP Initiator. From an analytic point of view, it is very important to generate biocompatible surfaces that preclude non-specific adsorption of

bioactive species on the sensor surface. Our initiator is based on the findings of Prime and Whitesides, who prepared OEGn alkane thiol self-assemblies of different chain lengths on gold and characterized these films for protein adsorption.[14] The modified tetra(ethylene glycol) containing ATRP initiator consists of a thiol head and a hydrocarbon segment with $n > 10$. This last feature is important for the enhancement of molecular organization and surface packing of the initiator molecules. The tetra(ethylene glycol) units assist in mitigating non-specific adsorption and the α-bromoester tail, initiates the surface initiated ATRP. We synthesized the precursor of the OEG containing initiator, namely 24-mercapto-4,7,10,13-tetraoxatetracosan-l-ol, using the procedure described by Prime and Whitesides. This precursor, when reacted with 2-bromo-isobutylryl bromide, in the presence of pyridine gave the desired initiator albeit in very low yield. This synthetic route was abandoned after poor yields in the final step. A new synthetic route was designed wherein S-1-hydroxy-3,6,9,12-tetraoxatricosan-23-yl ethanethioate **(4)** was reacted with 2-bromo-isobutyryl bromide to form 25-oxo-3,6,9,12-tetraoxa-24-thiahexacosyl 2-bromo-2-methylpropanoate **(5)**. The OEG containing ATRP initiator was obtained in higher yields by selectively deprotection of the thiol ester with cystamine. Cystamine is used extensively in protein purification technique called Intein purification where it assists in similar reactions.[43] The synthetic scheme of the OEG containing ATRP initiator is shown in Scheme 5.1. The OEG containing ATRP initiator formed well-ordered SAMs on the gold surface. The ellipsometric thicknesses of the OEG-containing and conventional initiator monolayers were 3.4 nm and 1.8 nm, respectively. The advancing and receding water contact angles of the OEG initiator surface were $\theta_{AW} = 58.7°$ and $\theta_{RW} = 37.9°$, respectively. Laibinis and coworkers have reported an advancing contact angle of 63°±2° for water on gold surfaces modified with methoxy-terminated tri(ethylene glycol).[44] These contact angles are lower than that for the conventional initiator

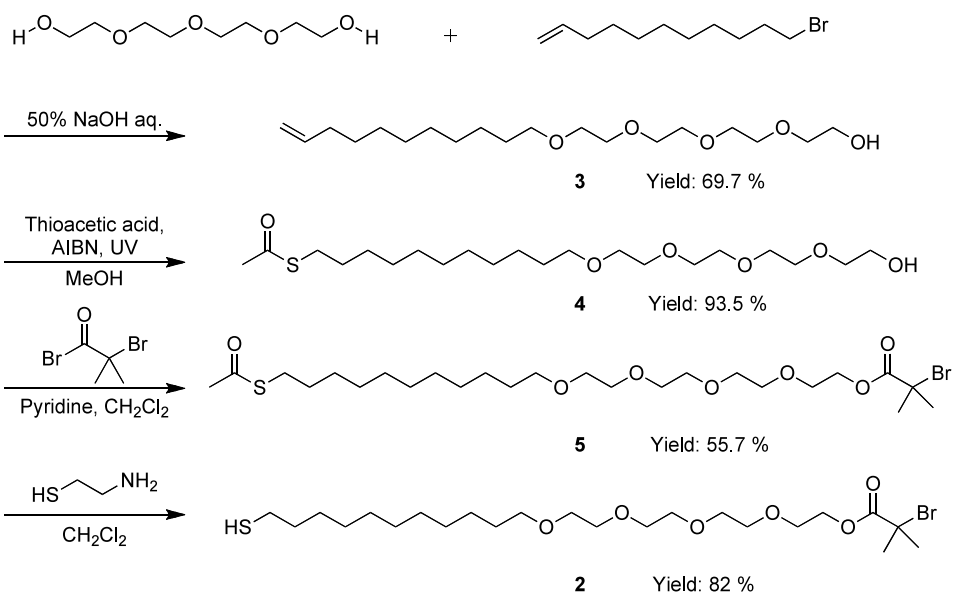

Scheme 5.1. Synthesis of the oligo(ethylene glycol) containing ATRP thiol initiator.

surface (θ_{AW} = 74.5° and θ_{RW} = 42.3°). These lower values for water contact angles are as expected since the oligo(ethylene glycol) units make the surface more hydrophilic.

DNP-Functionalized PAA Brushes. Poly(acrylic acid) brushes grown via ATRP of sodium acrylate were utilized as platforms to immobilize the DNP groups. This polymerization was in an aqueous medium at room temperature (Scheme 5.2 (a)). The poly(sodium acrylate) brushes were washed with EDTA solution to remove any traces of copper salt and then immersed in dilute acid solution (pH=5) to protonate the carboxylate groups. The advancing and receding contact angles of the PAA brush were q_{AW} = 44.8° and q_{RW} = 13.6°, respectively (Table 5.1). The dry ellipsometric thickness of the PAA brushes was 18 nm. The root-mean-square roughness measured using AFM was 0.7 nm (Figure 5.2). The surface composition of the PAA brush was characterized using X-ray photoelectron spectroscopy (Figure 5.3). The composition ratio of carbon and oxygen in the PAA brush was calculated to be 63.9:36.1, which is similar to the theoretical values (3:2). The narrow scan of C_{1s} showed two peaks at 284.9 and 288.9 eV corresponding to C-C/C-H and C-O/C=O, respectively. The compositions of C-C/C-H and C-O/C=O were 71.4 and 28.9%, respectively, which is very close to the theoretical values (71.4 and 28.6%). The FTIR spectra showed the strong characteristic C=O stretch for a carboxylic acid at 1732 cm^{-1} and the broad –OH stretch from 3100-3400 cm^{-1}. These PAA brushes were functionalized with DNP groups in two steps (Scheme 5.2 (b)). In the first step, the PAA brushes were reacted with an excess of 2-(2-aminoethoxy)ethanol to quench most of the carboxylic acid groups. The amine end of 2-(2-aminoethoxy)ethanol has a more active lone pair and is much more basic and more nucleophilic than the hydroxyl end. Thus the carboxylic acid groups are quantitatively quenched via an amide linkage. This was confirmed by FTIR spectra which showed the C=O stretch at 1615 cm^{-1} for an amide bond. The

(a)

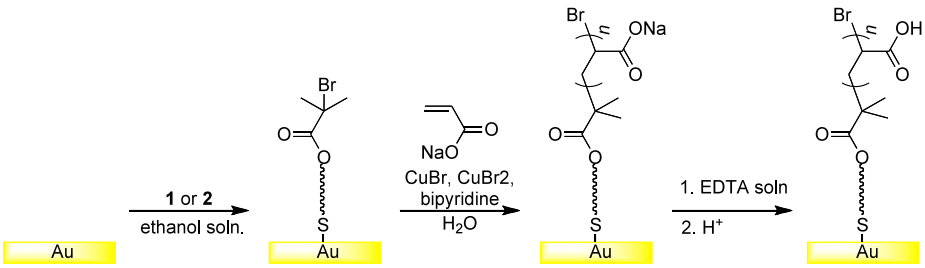

(b)

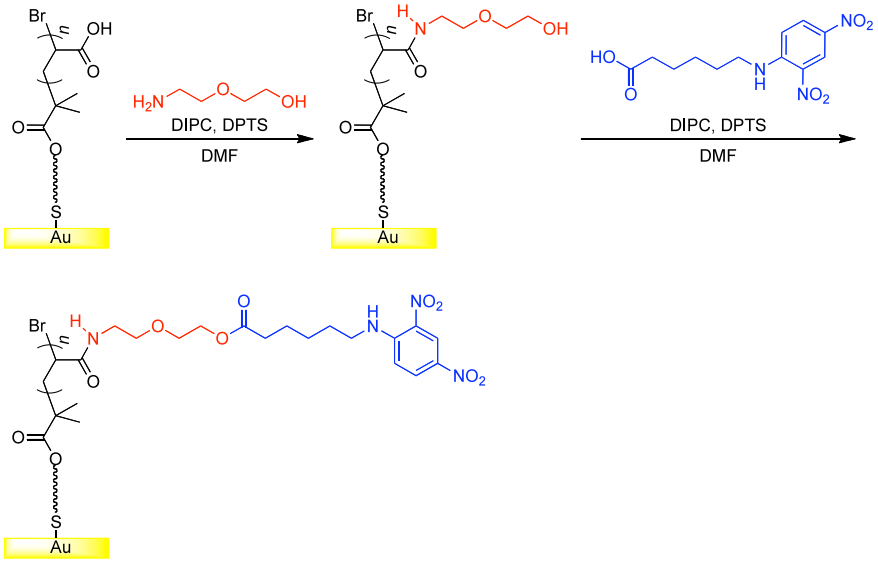

Scheme 5.2. (a) Preparation PAA on gold substrates grown via ATRP of sodium acrylate. (b) Functionalization of PAA brushes with DNP model antigenic groups.

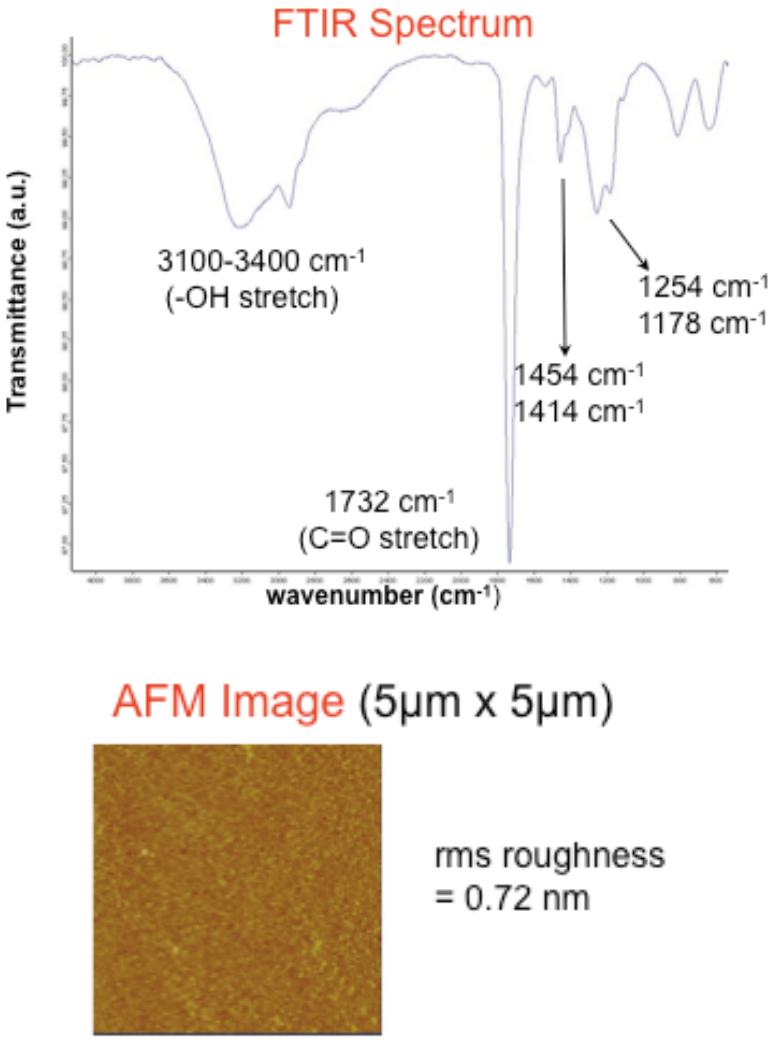

Figure 5.2 FTIR spectrum and an AFM image of a 18 nm thick PAA brush.

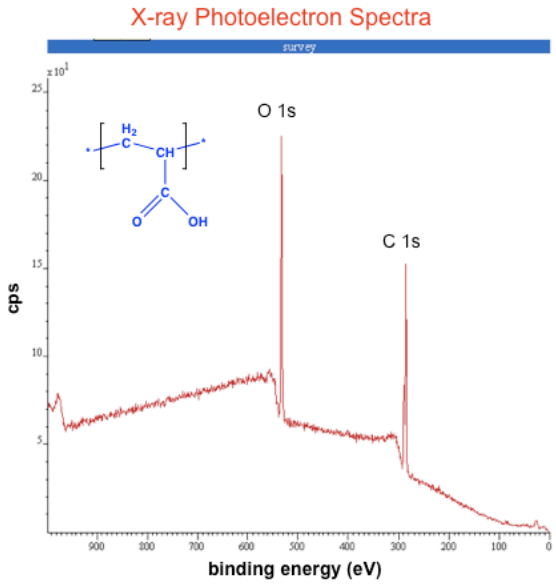

Element	BE (eV)	atomic %
C (1s)	285.0	63.89
O (1s)	532.7	36.11

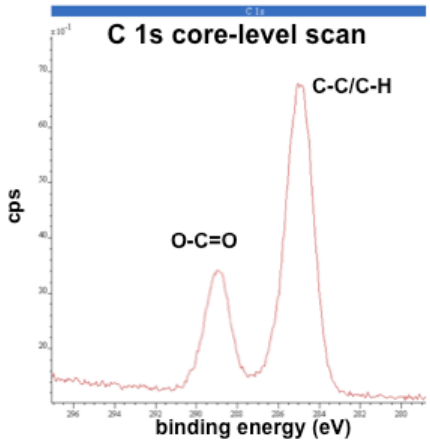

Element	BE (eV)	atomic %
C-C, C-H	285.0	71.43
O-C=O	289.0	28.57

Figure 5.3. The chemical composition on the surface of a PAA brush determined by XPS spectrum.

Table 5.1. Advancing and receding water contact angle measurements for non-PEGylated initiator SAM, PEGylated iniator SAM, PAA brush, PAA-DNP brush

	Water θ_A	Water θ_R
PAA-DNP brush	21.5°	9.5°
PAA brush	44.8°	13.6°
PEG Initiator SAM	58.7°	37.9°
Initiator SAM	74.6°	42.3°

second step involved the reaction with DNP-caproic acid to obtain DNP terminated PAA brushes. These advancing and receding water contact angle measurements for the DNP-PAA brushes were q_{AW} = 21.5° and q_{RW} = 9.5°, respectively (Table 5.1). The % composition of carbon, oxygen and nitrogen on the DNP-PAA brush surface was calculated to be 66.2 %, 23.98 % and 9.82 %, respectively. This ratio is quite close to the theoretical composition ratio.

Qualitative Analysis of DNP Functionalized PAA Brushes. The selectivity of binding of DNP-specific IgE antibodies to DNP groups was evaluated by immersing DNP-PAA brushes in a dilute solution of AlexaFluor 488 labeled antibodies in PBS buffer, in the dark at room temperature for 90 min. PAA brushes with no DNP functionalization were used as control samples. Both, DNP-PAA and PAA polymer brush samples were prepared using the OEG containing ATRP thiol initiator (Figure 1.1, structure (2)) to suppress non-specific adsorption of the antibodies. The DNP-PAA coated gold substrates exhibited green fluorescent images which were color analyzed using a customized version of a previously reported Matlab program.[44] The bright region shows fluorescently labeled anti-DNP IgE antibodies that are immobilized via binding to the DNP modified brush. No fluorescence was observed with the PAA brushes indicating that little or no DNP-specific IgE was immobilized on the surface.

Fluorescence micrographs for the DNP-PAA brush and the PAA brush are shown in Figure 5.4 (a) and 5.4 (b), respectively. The surface density contour plot of the immobilized fluorescently labeled DNP-specific IgE antibodies on the DNP-terminated polymer brush with initiator **(2)** shows a uniform coverage of the labeled antibody molecules, with very small spots of high fluorescence which are attributed to dust contamination (Figure 5.4 (c)).

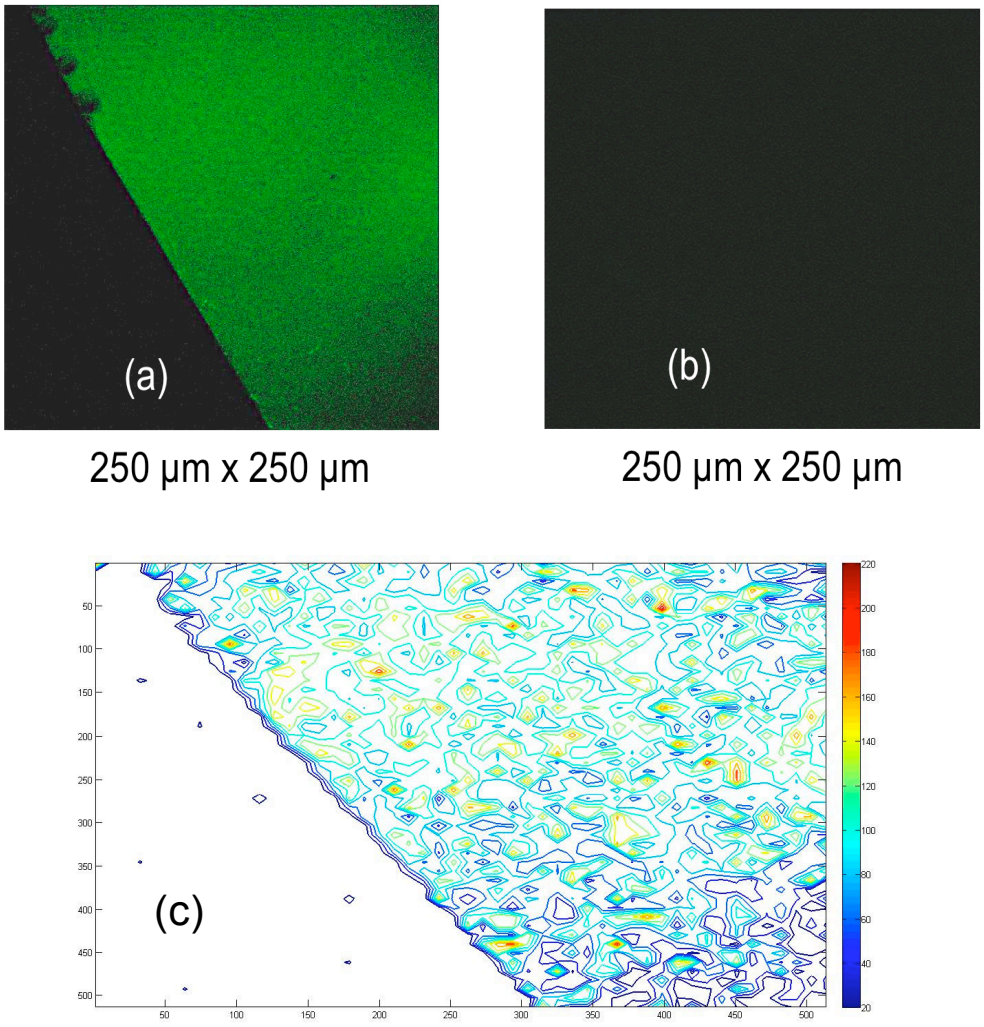

Figure 5.4 (a) Binding of AlexaFluor 488 labeled anti-DNP IgE to DNP functionalized PAA brushes. Background subtracted fluorescence micrograph. Brushes with DNP on the surface show green fluorescence. (b) No fluorescence is observed on surfaces with PAA brushes without DNP. functionalization. (c) Surface density contour plot of immobilized fluorescently labeled anti-DNP IgE antibodies on DNP functionalized PAA brushes.

Quantitative Analysis of DNP Functionalized PAA Brushes. The DNP functionalized polymer brush modified gold electrode surfaces were characterized by cyclic voltammetry. Figure 5.5 shows a typical cyclic voltammogram at 50 $mV \bullet s^{-1}$ in 0.5 M sulfuric acid for a DNP functionalized PAA brush on a gold electrode surface. The DNP-PAA modified gold electrode and a large area coiled platinum wire served as the working and counter electrodes, respectively. The first cathodic scan exhibited an irreversible reduction wave at about -0.27 V vs Ag/AgCl reference electrode which has been previously attributed to reduction of the DNP group to hydroxylamine.[45]

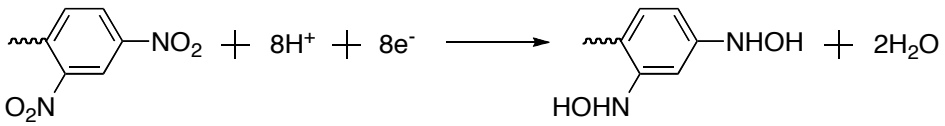

The subsequent anodic scan showed an anodic peak at +0.38 V and its cathodic counterpart at +0.35 V. This reversible signal has been attributed to a two-electron, two-proton redox reaction (per site) of the hydroxylamine group to the nitroso group.

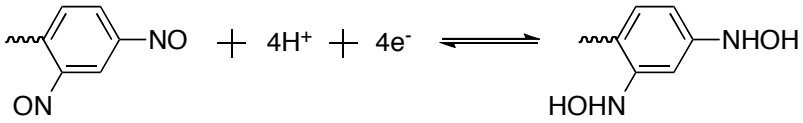

This reaction was used to determine the number of DNP groups present on the electrode surface that are accessible electrochemically. By integration of the area under the voltammetric wave, the coverage was found to be 2.7 x 10^{-10} mol per cm^2. Surface immobilization of DNP-specific IgG on DNP coated surfaces was studied using quartz crystal microbalance. Our experiments yielded a 1:10 binding of IgG to the number of DNP groups present.

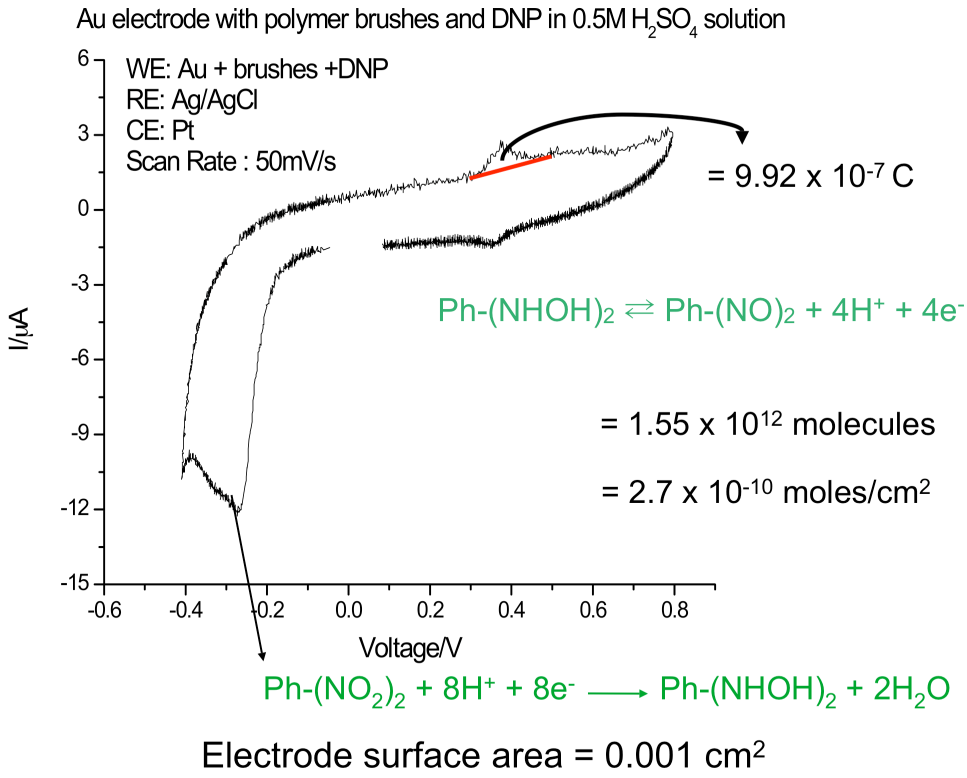

Figure 5.5 Cyclic voltammogram showing the electrochemical characterization of 2,4-dinitrophenol end groups on polymer brush modified gold electrodes. Surface coverage of DNP groups was calculated using the anodic peak area.

Antibody Adsorption Studies on DNP Functionalized Gold Electrodes

Cyclic voltammetric experiments were carried out on DNP-PAA brush modified gold electrodes, grown from the OEG containing and conventional initiators. The modified electrodes were immersed in a 0.2 mM solution of [Os(1,10-phenanthroline-5,6-dione)(1,10-phenanthroline)$_2$](PF_6)$_2$ complex in 0.1 M in PBS buffer (pH = 7). The quinone moiety was used (formal potential, E° = -0.004V vs Ag/AgCl) within the 1,10-phenanthroline-5,6-dione ligand of the transition metal complex as an electron-transfer mediator in solution. Abruña *et al.* have demonstrated the utility of these complexes as diffusional mediators between the active site of the immobilized enzyme and electrode surface in the development of an H_2O_2 biosensor.[47] The cyclic voltammogram of the osmium complex was observed over time in the presence of DNP-specific and non-specific IgG antibodies. In Figure 5.6 (a), the black curve shows the cyclic voltammetry of the osmium complex as observed at a DNP-PAA modified gold electrode (using the conventional initiator (1)) before treatment with polyclonal DNP-non-specific IgG antibodies. Immersion of this modified electrode in a solution of non-specific IgG for 1.5 h resulted in an observable increase of the peak currents, as indicated by the red curve. The effect was ascribed to non-specific adsorption of these antibodies on the electrode surface. These adsorbed antibodies cause the partitioning of the osmium complex near the electrode surface and in solution due to possible electrostatic and/or specific interactions. The resulting higher concentration of the osmium redox active molecule near the electrode surface causes an increase in the peak current.

To confirm this hypothesis, a fresh gold electrode coated with DNP-PAA brushes with initiator **(1)** was immersed in a solution of non-specific antibodies for 1.5 h. The electrode was removed and thoroughly rinsed with 0.1 M phosphate buffer (pH=7.0). When a cyclic voltammogram was performed using this electrode in fresh

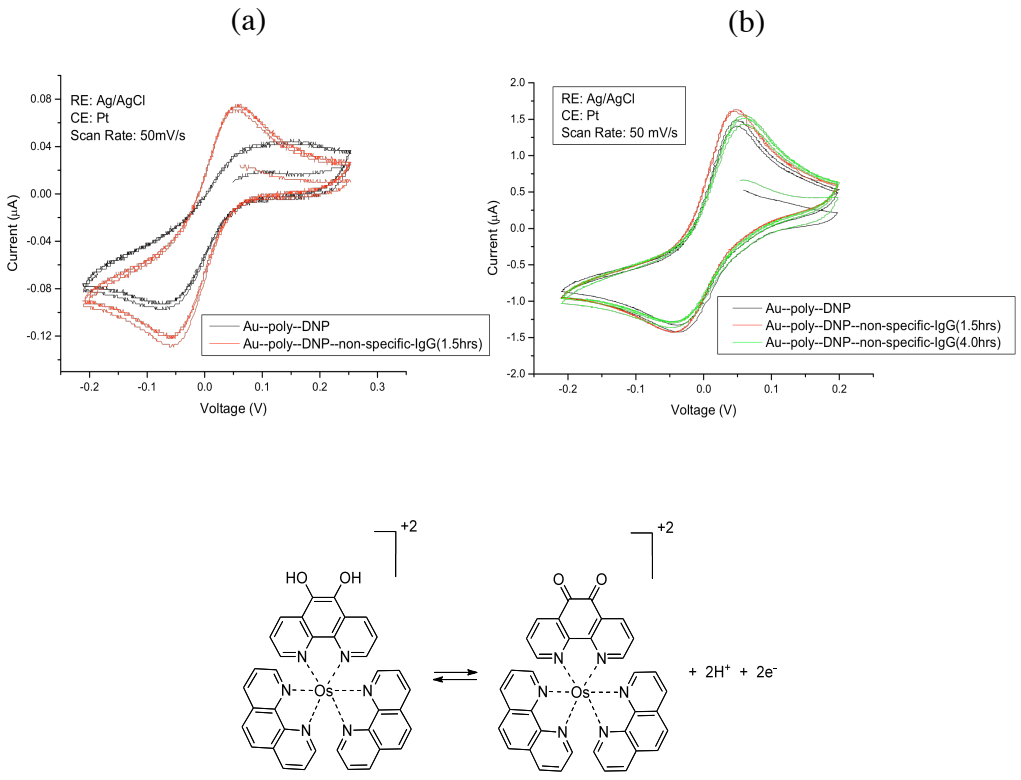

Figure 5.6 Cyclic voltammograms of a fresh gold electrode functionalized with DNP-PAA brushes using initiator (1) used to investigate a solution of 0.2 mM osmium complex in 0.1 M pH 7 phosphate buffer (a) before (black curve) and after (red curve) treatment with polyclonal non-DNP-specific IgG antibodies. Immersion of this modified electrode in a solution of non-DNP-specific IgG for 1.5 h results in an observable increase in peak current. (b) Before (black curve) and after 1.5 h (red curve) and 4 h (green curve) treatment with polyclonal non-DNP-specific IgG antibodies. Immersion of this modified electrode in a solution of non-DNP-specific IgG results in no observable increase in peak current. Note: the difference in current (Y-axis) in the two plots corresponds to the relative size of the gold electrodes used.

buffer solution with no osmium complex, the voltammetric response of the adsorbed osmium complex was observed confirming our assertion that the complex is partitioned into the film and that it retains its redox activity.

In order to mitigate this undesirable effect due to non-specific adsorption, the OEG containing ATRP initiator **(2)** was used to modify the gold electrodes with DNP-PAA brushes. Gold electrodes modified using initiator **(2)** did not display a significant change in electrochemical current upon treatment with non-specific IgG antibodies (Figure 5.6 (b)) indicating that there was no partitioning of the osmium complex into the film and that non-specific adsorption had been largely eliminated. Similarly, cyclic voltammograms of the osmium complex before and after treatment of the modified electrodes using initiators **(1)** and **(2)**, with DNP-specific monoclonal IgG antibodies, showed no change in the peak currents. This further confirms that it is the antibodies that interact with the surface via non-specific interactions that cause this change in electrochemical signal. These results indicate that the chemical modification of the gold electrode surfaces with DNP-PAA brushes using the modified (OEG containing) ATRP thiol initiator is much more effective in preventing non-specific adsorption of antibodies when compared to polymer brushes grown using the conventional initiator.

Quantitative Adsorption Studies on DNP-functionalized QCM Surfaces

Our electrochemical results were confirmed by quantitative micro gravimetric characterization using a QCM. A QCM can be used to determine the changes in the mass adsorbed onto a surface by measuring the change in frequency of a quartz crystal resonator. The change in frequency can be correlated to a mass change using the Sauerbrey equation.[48]

$$\Delta m = - C_f \Delta F \qquad (5.1)$$

where Δm is the change in mass (ng cm^{-2}), ΔF is the change in frequency and C_f (17.7 ng Hz^{-1} cm^{-2}) is the proportionality constant for a 5 MHz crystal.

Studies were carried out with IgG antibodies that are commonly used in biosensor applications. Non-specific IgG antibodies (150 kDa) are proteins that do not bind to DNP via specific interactions. Any adsorption on the DNP modified surfaces would be due to non-sepcific adsorption. A schematic representation of the quantification of non-specific IgG antibodies on a DNP functionalized PAA brush modified QCM electrode is shown in Figure 5.7. As expected, the bare (unmodified) gold QCM surfaces exhibited high protein adsorption (29.5 pmol/cm^2 for non-specific IgG antibodies) in a 0.67 nM protein solution. QCM surface functionalized with the conventional initiator **(1)** showed some resistance to protein adsorption. However the amount of protein adsorbed was still quite significant. QCM surfaces covered with SAMs of the OEG containing initiator **(2)** exhibited greatly improved resistance to non-specific adsorption. For the non-specific IgG antibodies, when the substrates covered with SAMs of initiators (**1**) and (**2**) (without polymer brushes) are compared, there is a 20% decrease in surface concentration of non-specific IgG antibodies, to further support that initiator **(2)** decreases non-specific adsorption. The incorporation of short chain length, protein resistant OEG units in the modified ATRP initiator helps lower the adsorption of biomolecules to some extent. Surface-tethered polymer brushes grown from the two initiators performed better in inhibiting protein adsorption than the initiator covered surfaces. As the QCM electrodes are modified with PAA-DNP and the contrasting initiators are implemented, a significant decrease in surface mass change is observed with both initiators. This higher protein resistance of the brushes over SAMs is attributed to a thicker film and better surface coverage of the polymer brushes. However as the brush thickness decreases, the effect of the initiator becomes significant. Similar to the electrochemical experiments, it is observed that DNP functionalized PAA brushes grown using initiator **(2)** inhibit non-specific surface adsorption of proteins on the gold QCM surface. When the DNP-functionalized

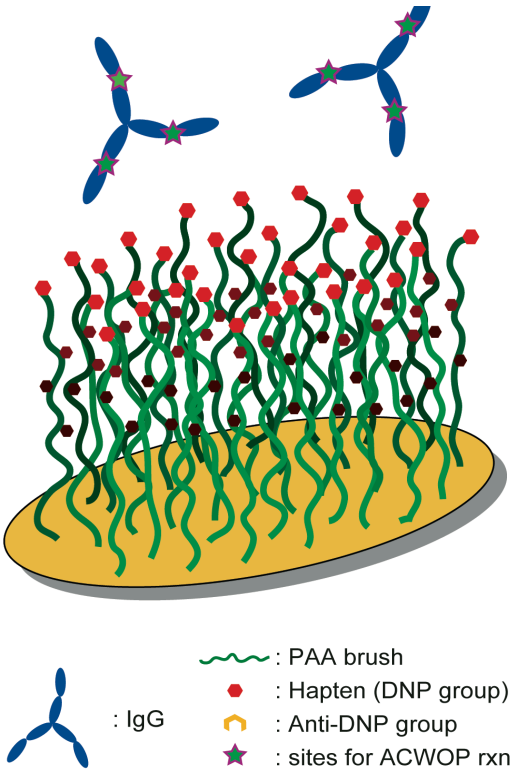

Figure 5.7 Schematic representation of the quantification of non-specific IgG antibodies on DNP functionalized PAA brush modified QCM electrode.

Table 5.2. Frequency change and calculated adsorption of non-specific IgG antibodies on modified QCM surfaces.

	ΔF (Hz)	Δm (ng/cm²)	pmol/cm²
Bare Gold	-250	4429	29.5
SAM of Initiator (1)	-224	3965	26.4
SAM of Initiator (2)	-179	3168	21.1
Initiator (1)-PAA-DNP	-15	266	1.77
Intiator (2)-PAA-DNP	-7.5	133	0.89
Protein solution concentration = 0.67 nM. Molecular mass of non-specific IgG antibodies = 150,000 Da.			

polymer brush covered surfaces grown using initiators (**1**) and intiator (**2**) were compared using non-specific IgG antibodies, a 50% decrease in surface concentration of non-specific IgG on polymer brush surfaces grown from the OEG containing initiator **(2)** was observed. The frequency change and calculated adsorption of non-specific IgG on modified QCM surfaces is tabulated in Table 5.2.

Conclusion

An OEG containing ATRP thiol initiator was synthesized in high yields using a new synthetic route. The ability of this OEG containing initiator to prevent non-specific adsorption of non-specific IgG antibodies was compared to that of a widely used conventional initiator. Gold wafers, electrodes and QCM surfaces were chemically modified with DNP-PAA brushes. Both, cyclic voltammetry and gravimetric methods were carried out on DNP-PAA brush functionalized gold electrode and QCM surfaces, respectively. These studies indicate that surfaces covered with brushes grown off the OEG containing ATRP initiator are more resistant to non-specific adsorption. The use of this initiator is important for the development of a reliable amperometric biosensor where it is crucial to eliminate any interference in electrical signals due to non-specific adsorption.

Acknowledgments

This work was supported by the Nanobiotechnology Center (NBTC), an STC Program of the National Science Foundation under Agreement No. ECS-9876771. Cornell NanoScale Science and Technology Facility (CNF) and Cornell Center for Materials Research (CCMR) are acknowledged for use of their facilities. Norah Smith (Cornell), Dr. Zeki Naal and Dr. Rose Naal (Universidade de São Paulo) are also thanked for their invaluable suggestions during our technical discussions.

REFERENCES

1. Senaratne, W.; Andruzzi, L.; Ober, C. K., *Biomacromolecules* **2005,** 6, (5), 2427.

2. Mrksich, M., *Cell. Mol. Life. Sci.* **1998,** 54, 653.

3. Amanda, A.; Mallapragada, S. K., *Biotechnol. Prog.* **2001,** 17, 917.

4. Park, S.; Bearinger, J. P.; Lautenschlager, E. P.; Castner, D. G.; Healy, K. E., *J. Biomed. Mater. Res.* **2000,** 53, 568.

5. Holland, N. B.; Qiu, Y.; Ruegsegger, M.; Marchant, R. E., *Nature* **1998,** 392, 799.

6. Harris, J. M., *Poly(ethylene glycol) chemistry: Biotechnical and Biomedical Applications*. Plenum Press: New York, 1992.

7. Masson, J. F.; Battaglia, T. M.; Davidson, M. J.; Kim, Y. C.; Prakash, A. M. C., *Talanta* **2005,** 67, 918.

8. Clark Jr, L. C.; Lyons, C., *Ann. N.Y. Acad. Sci.* **1962,** 102, 29.

9. Grieshaber, D.; MacKenzie, R.; Voros, J.; Reimhult, E., *Sensors* **2008,** 8, 1400.

10. Belluzo, M. S.; Ribone, M. E.; Lagier, C. M., *Sensors* **2008,** 8, 1366.

11. Bokoch, M. P.; Devadoss, A.; Palencsar, M. S.; Burgess, J. D., *Anal. Chim. Acta.* **2004,** 519, 47.

12. Moatti-Sirat, D.; Velho, G.; Reach, G., *Biosens. Bioelectron.* **1992,** 7, 345.

13. Ram, M. K.; Bertoncello, P.; Ding, H.; Paddeu, S.; Nicolini, C., *Biosens. Bioelectron.* **2001,** 16, 849.

14. Prime, K. L.; Whitesides, G. M., *J. Am. Chem. Soc.* **1993,** 115, 10714.

15. Zhu, B.; Eurell, T.; Gunawan, R.; Leckband, D., *J. Biomed. Mater. Res.* **2001,** 56, 406.

16. Senaratne, W.; Sengupta, P.; Harnett, C.; Craighead, H.; Baird, B.; Ober, C. K., *NanoBiotechnology* **2005,** 1, (1), 23.

17. Milner, S. T., *Science* **1991,** 251, 905.

18. Liu, X. S.; Jang, C. H.; Zheng, F.; Jurgensen, A.; Denlinger, J. D.; Dickson, K. A.; Raines, R. T.; Abbott, N. L.; Himpsel, F. J., *Langmuir* **2006,** 22, 7719.

19. Grazu, V.; Abian, O.; Mateo, C.; Batista-Viera, F.; Fernandez-Lafuete, R.; Guisan, J. M., *Biotechnology and Bioengineering* **2005,** 90, 597.

20. Xu, F. J.; Cai, Q. J.; Li, Y. L.; Kang, E. T.; Neoh, K., *Biomacromolecules* **2005,** 6, 1012.

21. Choi, E.; Azzaroni, O.; Cheng, N.; Zhou, F.; Kelby, T.; Huck, W. T. S., *Langmuir* **2007,** 23, 10389.

22. Zhou, F.; Hu, A.; Yu, B.; Osborne, V. L.; Huck, W. T. S.; Liu, W., *Anal. Chem.* **2007,** 79, 176.

23. Schepelina, O.; Zharov, I., *Langmuir* **2008,** 24, 14188.

24. Tam, T. K.; Zhou, J.; Pita, M.; Ornatska, M.; Minko, S.; Katz, E., *J. Am. Chem. Soc.* **2008,** 130, 10888.

25. Tam, T. K.; Ornatska, M.; Pita, M.; Minko, S.; Katz, E., *J. Phys. Chem. C* **2008,** 112, (22), 8438.

26. Andruzzi, L.; Senaratne, W.; Hexemer, A.; Sheets, E. D.; Ilic, B.; Kramer, E. J.; Baird, B. A.; Ober, C. K., *Langmuir* **2005,** 21, 2495.

27. Ma, H.; Hyun, J.; Stiller, P.; Chilkoti, A., *Adv. Mater.* **2004,** 16, (4), 338.

28. Liu, Z.; Khan, N.; Hu, H.; Yu, B.; Liu, J.; Chen, M.; Zhou, F., *Macromol. Rapid Commun.* **2008,** 29, 1937.

29. Matyjaszewski, K.; Xia, J., *Chem. Rev.* **2001,** 101, 2921.

30. Dong, R.; Krishnan, S.; Baird, B.; Lindau, M.; Ober, C. K., *Biomacromolecules* **2007,** 8, 3082.

31. Retsch, M.; Walther, A.; Loos, K.; Muller, A. H. E., *Langmuir* **2008,** 24, 9421.

32. Dai, J. H.; Bao, Z. Y.; Sun, L.; Hong, S. U.; Baker, G. L.; Bruening, M. L., *Langmuir* **2006,** 22, 4274.

33. Cullen, S. P.; Liu, X.; Mandel, I. C.; Himpsel, F. J.; Gopalan, P., *Langmuir* **2008,** 24, 913.

34. Hiromi, K.; Kago, H.; Matsuura, K., *J. Colloidal & Interface Science* **2009,** 331, (2), 343.

35. Jones, D. M.; Brown, A. A.; Huck, W. T. S., *Langmuir* **2002,** 18, 1265.

36. Sanjuan, S.; Tran, Y., *Macromolecules* **2008,** 41, 8721.

37. Taira, H.; Nakano, K.; Maeda, M.; Takagi, M., *Anal. Sci.* **1993,** 9, 199.

38. Blonder, R.; Katz, E.; Cohen, Y.; Itzhak, N.; Riklin, A.; Willner, I., *Anal. Chem.* **1996,** 68, 3151.

39. Blonder, R.; Levi, S.; Tao, G.; Ben-Dov, I.; Willner, I., *J. Am. Chem. Soc.* **1997,** 119, 10467.

40. Blonder, R.; Willner, I.; Buckmann, A. F., *J. Am. Chem. Soc.* **1998,** 120, 9335.

41. Moore, J. S.; Stupp, S. I., *Macromolecules* **1990,** 23, 65.

42. Goss, C. A.; Abruna, H. D., *Inorg. Chem.* **1985,** 24, 4263.

43. Tan, L. P.; Yao, S. Q., *Protein and Peptide Letters* **2005,** 12, 769.

44. Harder, P.; Grunze, M.; Dahint, R.; Whitesides, G. M.; Laibinis, P. E., *J. Phys. Chem. B* **1998,** 102, 426.

45. Jin, J. Cornell University, Ithaca, 2007.

46. Senaratne, W.; Takada, K.; Das, R.; Cohen, Y.; Baird, B.; Abruna, H. D.; Ober, C. K., *Biosens. Bioelectron.* **2006,** 22, 63.

47. Darder, M.; Takada, K.; Pariente, F.; Lorenzo, E.; Abruna, H. D., *Anal. Chem.* **1999,** 71, 5530.

48. Sauerbrey, G. Z., *Physics* **1959,** 155, 206.

CHAPTER 6

ELECTROCHEMICAL DETECTION OF ANTIBODIES BASED ON THEIR INTRINSIC CATALYTIC ACTIVITY*

Abstract

Antibodies produced by the immune system are often the first signs of infectious diseases. Because antibodies recognize a vast repertoire of antigenic groups with exquisite specificity, they also are valuable reagents for medical therapeutics, vaccine development and research. The important need for detection of antibodies in diverse media is currently limited by sensitivity and specificity. This chapter describes a general method for electrochemical detection of antibodies to reach new detection limits, based on an antibody catalyzed water oxidation pathway (ACWOP). A detection system was constructed using a model system of 2,4-dinitrophenyl (DNP) antigen and anti-DNP antibodies. This method of detection is readily adaptable to detection of other antibodies and also to other biosensors on the micro- and nanoscale. Functionalized polymer brushes were used to resist non-specific adsorption and

* This work was done in collaboration with Dr. Manabu Tanaka (Department of Materials Science & Engineering, Cornell University), Suddhasattwa Nad, Michele Tague, Norah Smith, Dr. Nicolas Da Mota, Prof. Héctor D. Abruña, Prof. Barbara A. Baird (Department of Chemistry & Chemical Biology, Cornell University), Yelena Bisharyan, Prof. Theodore Clark (Department of Immunology & Microbiology, Cornell University), Lisa Blum and Prof. Judith Appleton (James A. Baker Institute for Animal Health).

provide a bio- and electronically compatible sensor surface. Simultaneously, gold substrates were successfully modified with Ni-NTA to bind the antigenic peptides from the avian influenza virus (H5N1). The Ni-NTA functionalization was qualitatively analyzed using his-tagged green fluorescent protein (GFP).

Introduction

Antibodies generated naturally as part of the adaptive immune response, are early markers for many infectious diseases. Because it is diagnostic for infection, antibody detection is recognized as an essential tool for monitoring the spread of disease by natural means or in the event of bioterrorism. In general, antibodies can be generated to recognize a vast range of antigenic groups (haptens) with exquisite specificity and they have been developed as powerful research tools and therapeutic agents. Sensitive, selective antibody detection is a fundamental requirement for diagnosing infectious diseases as well as for developing antibodies for research and medical applications. Radioisotopic labeling of antibodies and antigens was extensively used in the last couple of decades in immunoassays.[1] Since then, considerable effort has gone into devising better assays that can detect increasingly lower concentrations in complicated media such as blood serum.

Most current assays and devices for antibody detection are based on variations of the ELISA (enzyme-linked immuno-sorbent assay; a simple scheme is depicted in Figure 6.1 (a)).[2] These assays are typically limited by "false negatives" and "false positives". False negatives occur when the antibody is present but in amounts below the detection limit. False positives occur when the assay registers a contaminant as a signal; this can be caused by cross-reactivity but more often by nonspecific interactions. Other limitations of immunoassays are ease of use, speed (throughput), required sample size, expense and portability if field use is desired.

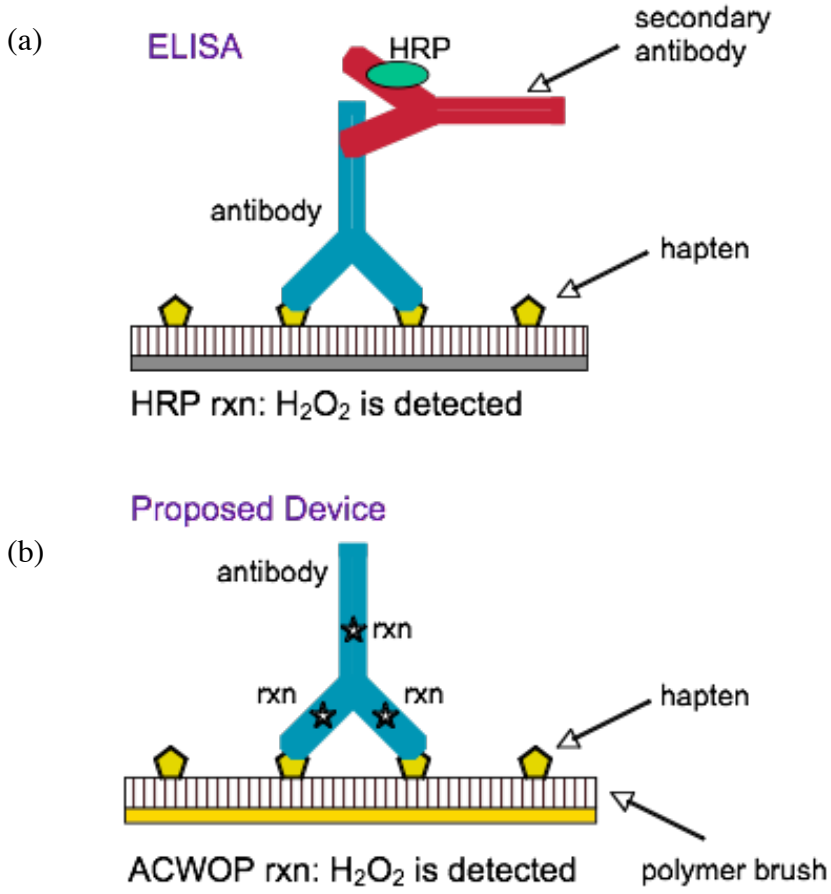

Figure 6.1. Schematic of the (a) Enzyme Linked Immuno-Sorbant Assay (ELISA) and (b) proposed amperometric biosensor based on the antibody catalyzed water oxidation pathway (ACWOP).

In this approach the antigenic hapten is typically presented on a surface and the solution containing the test antibody is applied. After wash steps, a labeled secondary antibody specific for the (sub)class of the primary antibody is allowed to bind, and the substrate is washed again with fresh buffer. The label on the secondary antibody could be fluorescent but more often is a conjugated enzyme (for example, horse radish peroxidase, HRP) that generates a colored product from added substrate (e.g., the Amplex Red colorimetric assay).

Introduction of a catalytic unit in this type of "sandwich" assay substantially enhances sensitivity, but nonspecific binding of the secondary antibody can cause high background noise. Moreover, the assay requires a secondary antibody that is specific for the species and class of the analyte antibody. Sensitivity and specificity for detection of any particular antibody depends on the test medium, the presented antigens, and the detecting reagents available. Consequently, there is no set standard for antibody detection. The most sensitive detection is currently in the range of 10-50 ng/mL.

This chapter describes the develop a method for electrochemical detection of antibodies that eliminates labeled secondary antibodies and associated problems, including special reagents, numerous wash steps (releasing low affinity primary antibodies resulting in false negatives), and nonspecific binding (leading to high background and false positives). It is expected that this detection method, within microscale devices, will be should be more specific and more sensitive than current ELISAs. This new approach takes advantage of the intrinsic catalytic activity of all antibodies (regardless of source or antigenic specificity) i.e. the antibody-catalyzed water oxidation pathway (ACWOP)[3,4] that was recently discovered and characterized in a biological context by Wentworth and colleagues.[5-7] Figure 6.1 (b) shows a schematic for the basic components and chemical reactions in the proposed device.

Previous structural characterization pointed to the interfacial region of the constant and variable domains as the "active site" of ACWOP. Moreover, this reaction has been found in every immunoglobulin fold protein so far tested.[8] A recent study using a simple Amplex Red assay showed that a variety of murine antibodies (0.2 μM amounts in solution) are able to intercept the singlet oxygen ($^1O_2$) generated by photo-oxidation of riboflavin in ambient aerobic conditions to generate hydrogen peroxide (H_2O_2) at a rate of 0.218 to 0.998 μM/min, and this rate is increased ~3-fold in D_2O.[5] Thus, the ACWOP is a universal pathway in all antibodies, wherein antibodies intercept singlet oxygen that can be generated by a photosensitizer in ambient aerobic conditions to produce catalytic amounts of hydrogen peroxide.

As described in the experimental section below, this hydrogen peroxide production will be detected which will confirm the presence of any H_2O_2-producing antibodies that bind to an antigen coated electrode. Selective modification of these detector surfaces was enabled by polymer brushes. This electrochemical/gravimetric detection system was developed and optimized with a model system of 2,4-dinitrophenyl(DNP)-antigen and anti-DNP antibodies.

Simultaneously PAA brushes were derivatized with nitrilotriacetate (NTA)-Ni^{2+} complexes to bind the antigenic peptides from the avian influenza virus (H5N1). NTA forms a tetradentate chelate with the Ni^{2+} ion. NTA occupies four out of the six ligand binding sites in the coordination sphere of the metal ion, leaving two sites free to interact with the electron donor groups on histidine imidazole rings of the His-tag sequence. The binding affinity (K_d) of single-His6 proteins for Ni-NTA modified surfaces have been estimated to be ~ 1 μM by surface Plasmon resonance.[9, 10] The Ni-NTA functionalization on polymer brushes was evaluated with fluorescent labels such as his-tagged GFP and microscopic visualization.

The avian influenza virus, H5N1 subtype has been identified by the Homeland Security Presidential Directive as an "emerging agent" of potential bioterrorism threat and is currently one of the NIAID's (National Institute of Allergy and Infectious Diseases) highest priority targets based on its global pandemic threat. To date, 383 human cases of H5N1 infection and 241 deaths have been reported.[11] These viruses can mutate readily by bioprocesses such as antigenic shift and antigenic drift.[12] This causes low pre-existing immunity amongst humans to the virus, a high mortality rate and resistance of this virus to antiviral drugs. There have been some efforts to develop miniaturized biosensors for avian influenza virus detection.[13-15] The intrinsic catalytic activity (ACWOP) of antibodies involves the production of catalytic amounts of hydrogen peroxide. This hydrogen peroxide reacts with the Amplex Red (present in solution) and oxidizes it to resorufin. The electrochemical detection of resorufin, will allow us to develop a biosensor with higher sensitivity and a lower detection limit. The availability of such a diagnostic test for on-site analysis will be crucial in the control of avian influenza.

Experimental Section

Chemical Reagents and Materials. 1-[3-(dimethylamino)propyl]-3-ethyl-carbodiimide hydrochloride (EDC), N-hydroxysuccinimide (NHS), Nickel(II) chloride, N_{α}, N_{α}-bis(carboxymethyl)-L-lysine hydrate were obtained from Sigma Aldrich. Buffers were prepared using deionized water (Milli-Q, 18.2 MΩ•cm). Absolute alcohol was purchased from Fisher Scientific. His-tagged green fluorescent protein (His-tagged GFP) was provided by Yelena Bisharyan (Department of Microbiology & Immunology, Cornell University). The oligo(ethylene glycol) containing ATRP thiol initiator was synthesized and immobilized on gold substrates (3 cm × 1 cm pieces) as described in chapter 5. Poly(acrylic acid) brushes (PAA)

were prepared and functionalized with 2,4-dinitrophenyl (DNP) groups as described earlier in chapter 5.

Detection of H_2O_2 produced by anti-DNP IgG Antibodies. A 3 cm × 1 cm Si wafer covered with DNP functionalized PAA brushes (prepared using the pegylated initiator) was placed into a 6 mL plastic petri dish with 5 mL of 0.01 M citric acid and 160 mM sodium chloride adjusted to pH 6. A 50 μL aliquot of anti-DNP IgG antibodies was added to the 5 mL solution and the antibodies were left to adsorb for approximately 3.5 hours. In a second petri dish, horseradish peroxidase (HRP) (10 μM), Ampliflu Red (AR) (100 μM), and Tris(2,2'-bipyridyl)dichlororuthenium(II) hexahydrate ($Ru(bpy)_3Cl_2$) (100 μM) were added to 5 mL of the citric acid saline solution. The antibody covered Si wafer was rinsed two times with citric acid saline solution and placed into the second petri dish. Next, the sample was placed into a grounded copper Faraday cage. An Ag/AgCl reference electrode, Pt coiled counter electrode and a carbon fiber ultramicroelectrode (UME – 7 μm diameter) as the working electrode were submerged in the solution above the Si wafer. A potentiostat (Autolab PGSTAT128N) with ECD to measure low currents (pA range), was connected to the electrodes and was computer controlled using Nova 1.4 software. A UV source, UVEXS SCU 110B Fiber Optic (Model #15609, Serial#4672), was clamped approximately 3 cm away from the center of the petri dish.

Cyclic voltammograms were collected from –300mV to 400mV at a scan rate of 10 mV/s. The CVs were collected with UV radiation times over 0 minutes, a few seconds, 10 minutes, 30 minutes, 120 minutes, and 210 minutes. The UV light was turned on for the given amount of time, turned off, and a CV was recorded. Then, the UV light was turned on again and the total time of irradiation was counted accumulatively and the process was repeated. The CVs were plotted and height of the

resorufin reduction peak (about -0.15V) was taken at each UV irradiation time. Thus a graph of peak height was plotted versus total time exposed to UV irradiation.

Preparation of Ni-NTA Functionalized Poly(acrylic acid) Brushes (Ni-NTA-PAA). The derivatization of PAA brushes with Ni-NTA was done in three steps. PAA brush coated gold substrates were placed immersed in a solution of 0.1 M NHS and 0.1 M EDC in deionized water for an hour at room temperature. The substrates were then removed from solution and washed with deionized water and ethanol and dried under a stream of nitrogen. The NHS-modified PAA brushes were immersed in an 0.1 M solution of N_α, N_α-bis(carboxymethyl)-L-lysine hydrate for an hour at room temperature, rinsed with deionized water and dried under a stream of nitrogen. The NTA-Ni^{2+} complex was formed by immersing the substrates in a 50 mM $NiCl_2$ solution for 2 h at room temperature. Finally, the Ni-NTA-PAA substrates were washed with water and ethanol and dried under nitrogen.

Immobilization of His-tagged GFP on Ni-NTA-PAA Brushes. His-tagged GFP was diluted to prepare a 1.5 μM solution of His-tagged GFP in 0.1 M PBS (pH=7.4) buffer. The Ni-NTA functionalized PAA brushes were immersed in the His-tagged GFP solution in the dark at room temperature for 24 h. The films were then rinsed with fresh PBS buffer and ethanol and dried under a stream of nitrogen. Fluorescent images were taken using an Olympus BX51 upright fluorescence microscope, equipped with a Roper Cool Snap hx CCD camera. The immobilized His-tagged GFP was observed with a 450-490 nm excitation and 520 nm emission filter. PAA brushes without any derivatization of the carboxylic acid groups were used as control samples.

Characterization. PAA and DNP-PAA brushes were characterized as described in chapter 5. The surface composition of the Ni-NTA-PAA brushes was characterized by XPS using a Surface Science Instruments SSX-100 spectrometer with

an operating pressure < 2×10^{-9} Torr using monochromatic AlKα x rays at 1486.6 eV. Photoelectrons were collected at an angle of 55-degrees from the surface normal using a hemispherical analyer with pass energies of 150 V at 1eV/step(survey scan) and 50 V at 0.65 eV/step (high resolution scan). The system was calibrated to Au $4f_{7/2}$ at 84 eV. The C—C 1s peak was corrected to a binding energy of 285 eV.

Results and Discussion

Detection of H_2O_2 produced by anti-DNP IgG Antibodies. Detection of low levels of H_2O_2 has been extremely important for the development of amperometric sensors for clinical diagnostics, environmental pollutants and food analysis.[16-22] The use of amperometry as an analytical signal provides a response that is directly proportional to concentration and is highly sensitive and specific. Moreover, amperometry is perfectly adapted to analyze very small solution volumes and can readily be incorporated into microfluidic devices.

The electrochemical detection of antibody-antigen interactions has been investigated by several research groups. Indirect electrochemical detection of antibody-antigen complexes was reported using enzyme labels that produce electroactive species which are sensed by the electrode.[23, 24] The amperometric detection of NADH, phenol, O_2, H_2O_2, or NH_3 generated by the enzymes linked to the antigen or antibody has also been used to probe antigen-antibody interactions.[25] More recently, Gajovic-Eichelmann and Bier reported the use of resorufin (7-hydroxy-3H-phenoxazin-3-one) as a promising candidate for stable and electroactive redox mediator.[26] Since resorufin is the peroxidation product of Amplex Red (N-acetyl-3,7-dihydroxyphenoxazine) in the enzymatic reaction catalyzed by HRP, resorufin was used as the redox mediator. Anti-DNP IgG antibodies were adsorbed on the DNP-PAA functionalized PAA brushes in citric buffer (pH = 6.0) via specific interactions.

The substrate with the adsorbed antibodies was placed in a buffer solution of Ampliflu Red and ($Ru(bpy)_3Cl_2$) (photosensitizer). This sample was then placed in a Faraday cage with Ag/AgCl as the reference electrode, Pt coiled counter electrode and a carbon fiber ultramicroelectrode as the working electrode. Cyclic voltammograms were collected after different UV exposure times from -300 mV to 400 mV at a scan rate of 10 mV/s. The exposure of the antibodies with UV light in the presence of photosensitizer resulted in the formation of catalytic amounts of H_2O_2 due to the ACWOP reaction. This production of H_2O_2 resulted in the chemically irreversible oxidation of Amplex Red to resorufin. Resorufin was subsequently reduced via an electrochemically reversible process to dihydroresorufin. Hence, the current measured herein was quantified as being directly proportional to the initial amount of H_2O_2. The cyclic voltammogram of resorufin at different UV exposure times is shown in Figure 6.2. The intensity of the anodic and cathodic currents was found to increase with increase in UV exposure time. This is attributed to the generation of higher concentrations of H_2O_2 in solution at longer UV exposures. It was also observed that concentration of H_2O_2 increased with time and reached a saturation point after 2 h. This point is shown in Figure 6.3. To make sure that the change in current was due to the generation of H_2O_2 by the anti-DNP IgG antibodies immobilized on the DNP functionalized surface, a control experiment was carried out with PAA brushes without DNP functionalization. The cyclic voltammetry of resorufin with the control sample, showed no increase in current indicating that no H_2O_2 was being generated in solution. This observation in turn suggests that the presence of specifically bound antibodies on the surface is essential for any change in signal.

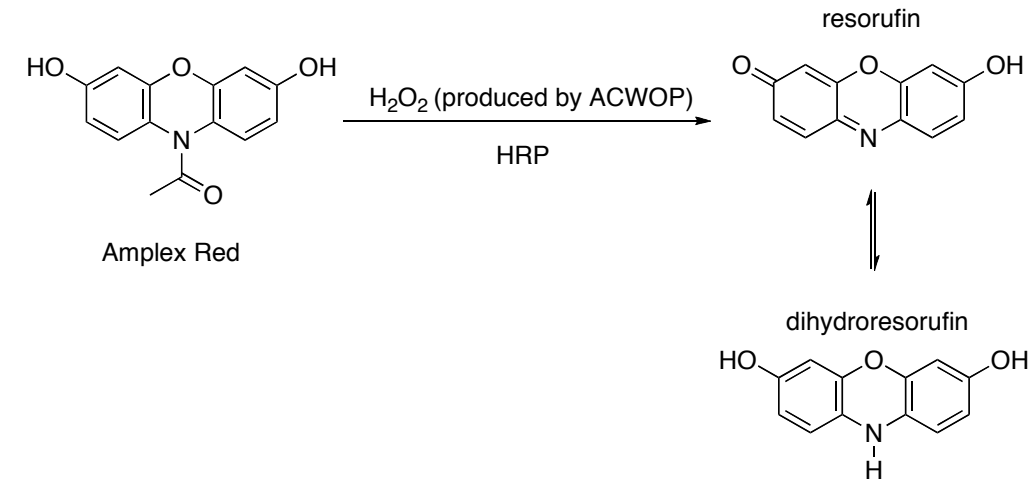

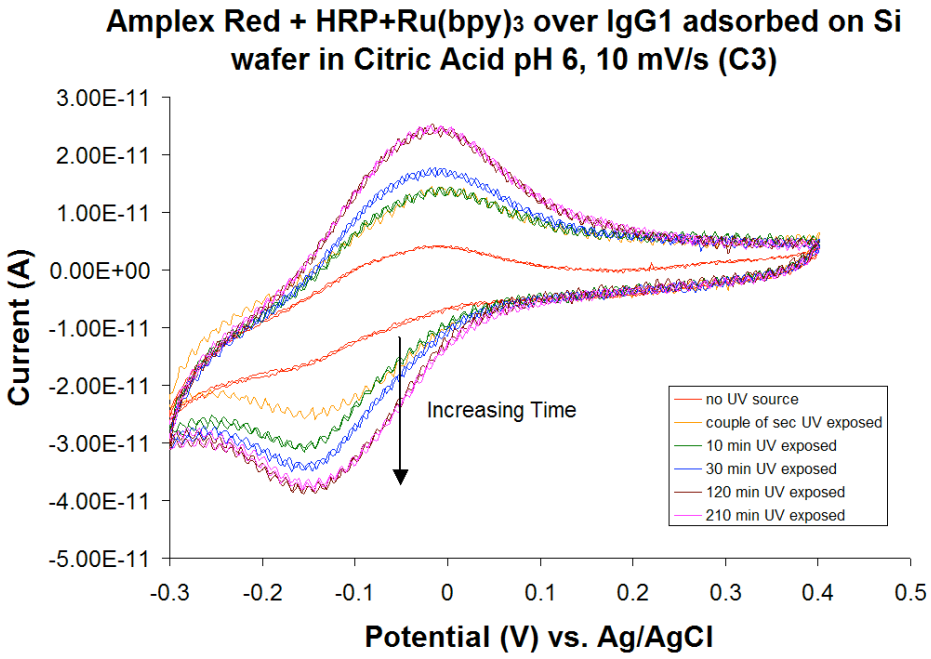

Figure 6.2. Cyclic voltammogram of resorufin formed by the irreversible oxidation of Amplex Red by H_2O_2 in 0.01 M citric acid buffer (pH=6). H_2O_2 was generated by the ACWOP reaction of immobilized anti-DNP IgG antibodies. Height of the resorufin reduction peak (-0.15 V) was taken at each irradiation time. (Data provided by Michele Tague , Abruña research group, Cornell University)

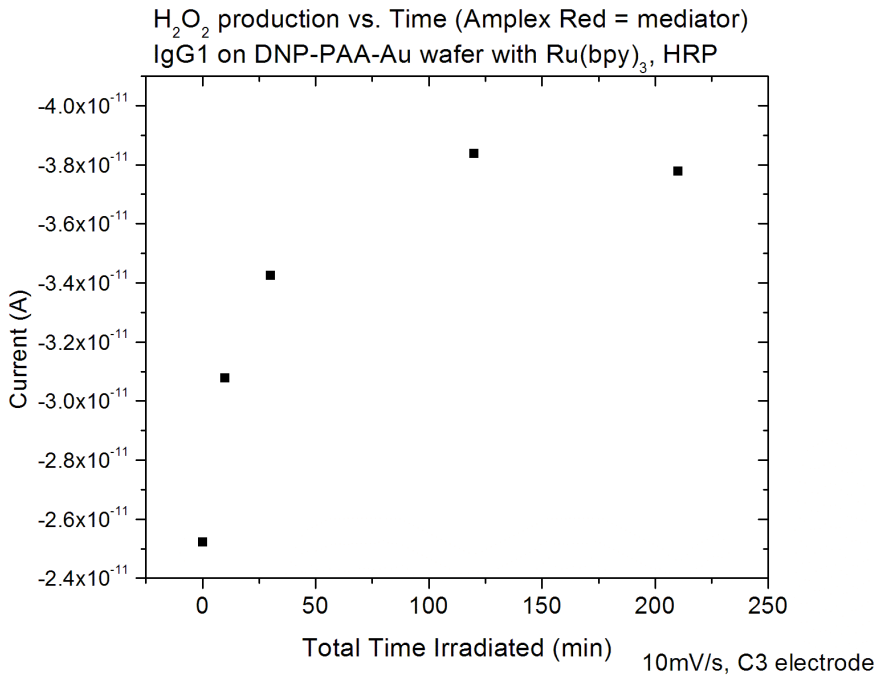

Figure 6.3. Plot of current vs total time of irradiation. The increase in current is attributed to the increase of concentration of H_2O_2. The production of H_2O_2 reached a saturation point after UV exposure for 120 min. (Data provided by Michele Tague, Abruña research group, Cornell University)

Ni-NTA Functionalized Poly(acrylic acid) Brushes (Ni-NTA-PAA).

The development of a biosensor largely relies on the immobilization of bioactive species to the sensor or measurement platforms. Poly(carboxylic acid) brushes are a class of polymer brushes with potential applications in biotechnology, especially in the study of cell-surface interactions and for the immobilization of biomolecules.[27-29] Poly(acrylic acid) brushes grown via ATRP of sodium acrylate were derivatized with Ni-NTA to modify the substrate with his-tagged recombinant proteins associated with Type A influenza diseases. The binding of hexahistidine (His_6) sequence tags to transition metal chelates of NTA has been widely studies for affinity purification of recombinant proteins.[30, 31] Derivatization of PAA brushes with Ni-NTA was performed in three synthetic steps. The scheme for Ni-NTA functionalization of PAA brushes is shown in Scheme 6.1. The carboxylic acid groups were activated with NHS by immersing the PAA brush in a solution of 0.1M NHS and 0.1 M EDC in deionized water for an hour at room temperature. In the second step, the NHS-modified PAA brushes were functionalized with NTA by immersion in a 0.1 M solution of N_α, N_α-bis(carboxymethyl)-L-lysine hydrate for an hour at room temperature. The wafers were rinsed with fresh deionized water and dried under nitrogen. The NTA-Ni^{2+} complex was formed in the final step by immersing the substrates in $NiCl_2$ solution (40 mM) for 2 h at room temperature. The surface composition of the Ni-NTA-PAA brush was characterized using X-ray photoelectron spectroscopy (Figure 6.4). The spectrum shows the expected peaks for C 1s (285.76 eV), O 1s (532.56 eV), N 1s (400. 67 eV), and Ni 2p (857.28 eV). The composition ratio of nickel, nitrogen and oxygen in the Ni-NTA- PAA brush was calculated to be 3.04:6.44:23.39 which is quite close to the theoretical value of 1:2:7. The spectrum shows a higher percentage of carbon on the surface. This is attributed to the deposition of hydrocarbon impurities due to the exposure of the functionalized substrate to air.

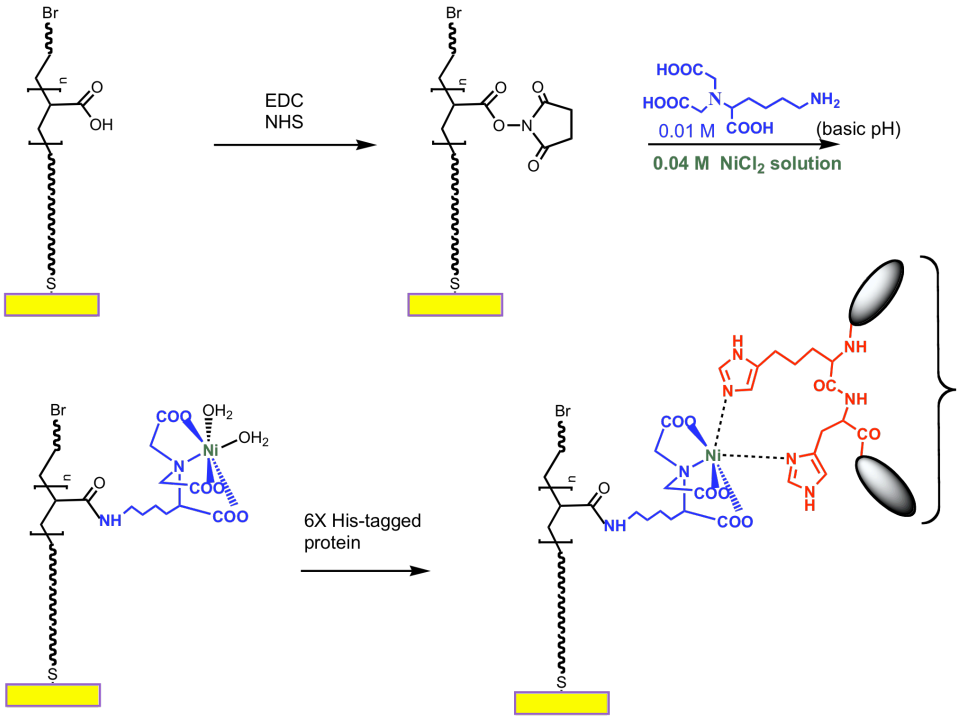

Scheme 6.1. Scheme for the functionalization of PAA brushes with Ni-NTA.

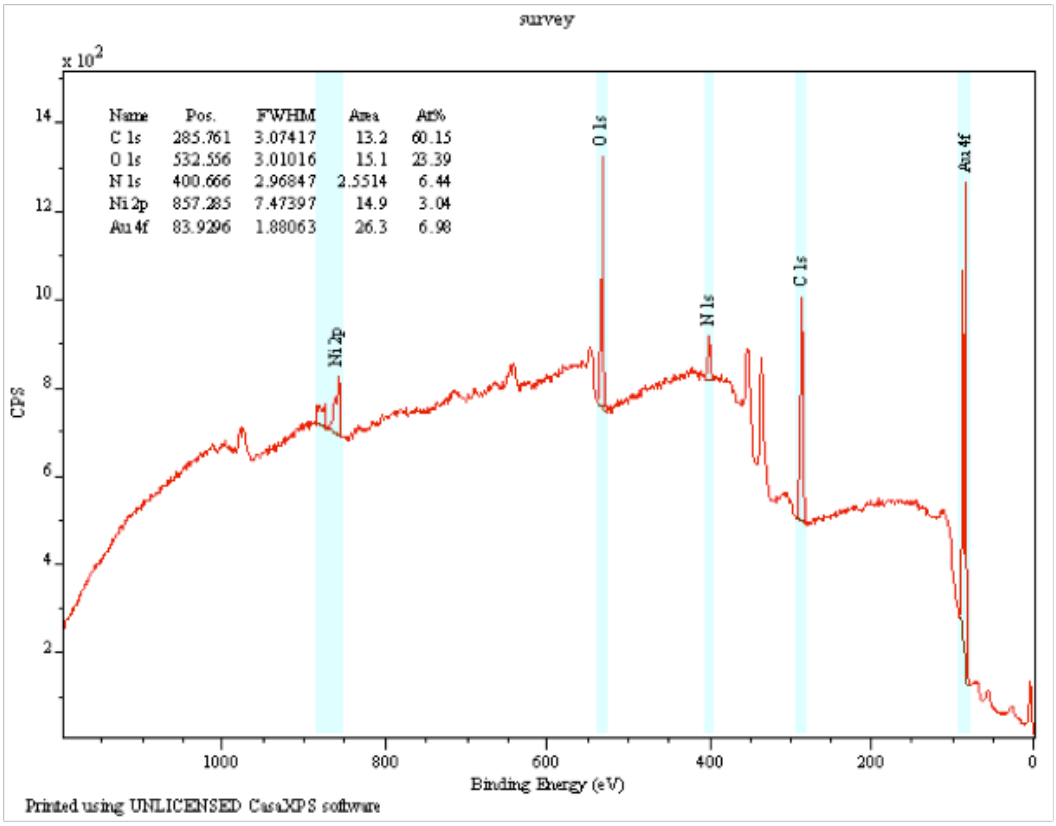

Figure 6.4. XPS spectra of Ni-NTA functionalized PAA brush.

Immobilization of His-tagged GFP on Ni-NTA-PAA Brushes. We evaluated the selectivity of binding of his-tagged GFP to a Ni-NTA-PAA brush by immersing the brush in a dilute solution of his-tagged GFP antibodies in 0.01 M PBS buffer, in the dark at room temperature for 24 h. PAA brushes with no Ni-NTA functionalization were used as control samples. GFP fluoresces green (peak emission at 509 nm) when exposed to blue light (excitation peak at 488 nm).[32] The Ni-NTA-PAA coated gold substrates exhibited green fluorescent images due to the specific attachment of his-tagged GFP to the Ni-NTA groups on the surface. No fluorescence was observed with the PAA brushes indicating that negligible his-tagged GFP was immobilized on the brushes. Fluorescence micrographs for the Ni-NTA-PAA brush and the PAA brush are shown in Figure 6.5 (a) and 6.5 (b), respectively.

Conclusions

In an effort to develop new countermeasures for emerging infectious diseases, a new approach for the detection of low levels of pure antibodies in solution was reported. This approach was tested using a model system for detection of anti-DNP IgG antibodies on DNP-PAA brush covered surfaces. This method takes advantage of the intrinsic catalytic activity of all antibodies, namely the antibody catalyzed water oxidation pathway and combines this process with the amperometric detection of resorufin to detect low levels of antibodies in solution. This detection system may be used for a broad range of antibody detection applications. In order to adapt this detection method for quantitative detection of antibodies specific for hemagglutinin 5 (H5) of the H5N1 avian influenza virus, PAA brushes were functionalized with Ni-NTA. The functionalization was qualitatively evaluated using his-tagged GFP.

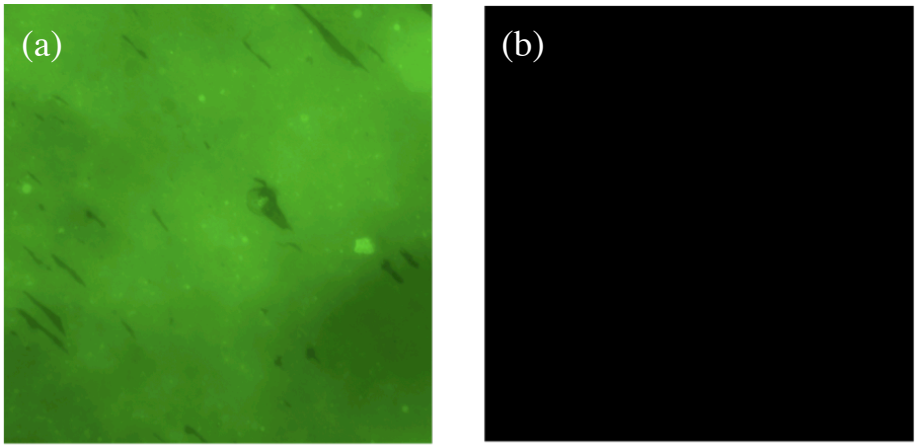

Figure 6.5. Fluorescent images of his-tagged GFP immobilized on a (a) Ni-NTA-PAA brush surface and (b) PAA brush surface. Green fluorescence is observed in (a) due to specific binding of his-tagged GFP to the Ni-NTA groups on the surface. No fluorescence is observed in (b) as his-tagged GFP is not immobilized on surfaces with PAA brushes.

Acknowledgments

This work was made possible by financial support from the Nanobiotechnology Center (NBTC) at Cornell University. The author also thanks Jon Shu (Cornell Center for Materials Research) for the XPS analysis of the brush samples. NBTC and CCMR are also thanked for use of their facilities. The author also thanks Yelena Bisharyan (Clark research group, Dept. of Microbiology and Immunology, Cornell University) for providing his-tagged GFP.

REFERENCES

1. Garvey, J. S.; Cremer, N. E.; Sussdorf, D. H., *Methods in Immunology, 3rd edition*. W. A. Benjamin, Inc.: New York, 1977; p 301.

2. Engrall, E., *Methods of Enzymology* 1980, 70, 419.

3. Wentworth Jr., P.; Jones, L. H.; Wentworth, A. D.; Zhu, X.; Larsen, N. A.; Wilson, I. A.; Xu, X.; Goddard III, W. A.; Janda, K. D.; Eschenmoser, A.; Lerner, R. A., *Science* 2001, 293, 1806.

4. Wentworth, A. D.; Jones, L. H.; Wentworth Jr., P.; Janda, K. D.; Lerner, R. A., *Proc. Natl. Acad. Sci.* 2000, 97, 10930.

5. Nieva, J.; Kerwin, L.; Wentworth, A. D.; Lerner, R. A.; Wentworth Jr., P., *Immunol. Lett.* 2006, 103, 33.

6. Nieva, J.; Wentworth Jr., P., *Trends Biochem. Sci.* 2004, 29, 274.

7. Zhu, X.; Wentworth Jr., P.; Wentworth, A. D.; Eschenmoser, A.; Lerner, R. A.; Wilson, I. A., *Proc. Natl. Acad. Sci.* 2004, 101, 2247.

8. Takeuchi, C.; Wentworth Jr., P., *Catalytic Antibodies* 2005, 336.

9. Nieba, L.; Nieba-Axmann, S. E.; Persson, A.; Hamalainen, M.; Edebratt, F.; Hansson, A.; Lidholm, J.; Magnusson, K.; Karlsson, A. F.; Pluckthun, A., *Anal. Biochem.* 1997, 252, 217.

10. Khan, F.; He, M.; Taussig, M. J., *Anal. Chem.* 2006, 78, 3072.

11. World Health Organization, w. f. a. i. v. http://www.who.int/csr/disease/avian_influenza/en/

12. Smith, D. J.; Lapedes, A. S.; de Jong, J. C.; Bestebroer, T. M.; Rimmelzwaan, G. F.; Osterhaus, A. D. M. E.; Fouchier, R. A. M., *Science* 2004, 305, 371.

13. Diouani, M. F.; Helali, S.; Hafaid, I.; Hassen, W. M.; Sanoussi, M. A.; Ghram, A.; Jaffrezic-Renault, N.; Abdelghani, A., *Materials Science and Engineering C* 2008, 28, 580.

14. Xu, J.; Suarez, D.; Gottfried, S., *Anal. Bioanal. Chem.* 2007, 389, 1193.

15. Liu, S.; Chen, G.; Zhou, Q.; Wei, Y., *Proceedings of SPIE* 2007, 6794, 67943P.

16. Upadhyay, A. K.; Ting, T.; Chen, S., *Talanta* 2009, 79, (1), 38.

17. Camacho, C.; Matias, J. C.; Chico, B.; Cao, R.; Gomez, L.; Simpson, B. K.; Villalonga, R., *Electroanalysis* 2007, 19, (24), 2538.

18. Tong, Z.; Yuan, R.; Chai, Y.; Chen, S.; Xie, Y., *Thin Solid Films* 2007, 515, (20-21), 8054.

19. Seo, K.; Oh, S.; Choi, S.; Oh, S.; Woo, J.; Kim, S., *Key Engineering Materials* 2007, 342-343, 869.

20. Zhu, Q.; Yuan, R.; Chai, Y.; Zhuo, Y.; Zhang, Y.; Li, X.; Wang, N., *Anal. Letters* 2006, 39, (3), 483.

21. Chen, X.; Wang, B.; Dong, S., *Electroanalysis* 2001, 13, (14), 1149.

22. Van Emon, J. P.; Lopez Avila, Y., *Anal. Chem.* 1992, 64, 79A.

23. Wehmeyer, K. R.; Halsall, H. B.; Heineman, W. R.; Volle, C. P.; C., C., *Anal. Chem.* 1986, 58, 135.

24. Tsuji, I.; Egushi, H.; Yasukouchi, K.; Unoki, M.; Taniguchi, I., *Biosens. Bioelectron.* 1990, 5, 87.

25. Blonder, R.; Levi, S.; Tao, G.; Ben-Dov, I.; Willner, I., *J. Am. Chem. Soc.* 1997, 119, 10467.

26. Gajovic-Eichelmann, N.; Bier, F. F., *Electroanalysis* 2005, 17, 1043.

27. Jain, P.; Dai, J.; Baker, G. L.; Bruening, M. L., *Macromolecules* 2008, 41, 8413.

28. Dong, R.; Krishnan, S.; Baird, B. A.; Lindau, M.; Ober, C. K., *Biomacromolecules* 2007, 8, 3082.

29. Dai, J.; Bao, Z.; Sun, L.; Hong, S. U.; Baker, G. L.; Bruening, M. L., *Langmuir* 2006, 22, 4274.

30. Arnold, F. H., *BioTechnology* 1991, 9, 151.

31. Hochuli, E., *Genet. Eng.* 1990, 12, 87.

32. Chalfie, M.; Tu, Y.; Euskirchen, G.; Ward, W.; Prasher, D., *Science* 1994, 263, 802.

CHAPTER 7

SUMMARY AND FUTURE DIRECTIONS

Patterned polymers have found use in a wide variety of applications. This thesis focuses on the high resolution patterning of two different types of polymer films. In one case, the polymer has been spun coated on the solid substrate and is adhered to the surface via physisorption. In the other case, polymer chains are covalently attached to the surface to form a "polymer brush" system.

Environmentally benign $scCO_2$ has been utilized as an "ecologically responsible" solvent for a wide variety of applications. However, nonpolar $scCO_2$ is generally a very poor solvent for polar polymeric photoresists, which limits its use as a processing solvent in high resolution photolithography. Chapter two describes the synthesis of fluorinated $scCO_2$ compatible additives and demonstrates their utility to help dissolve polar polymers in $scCO_2$. This work allowed the development of a commercially available standard TOK photoresist in $scCO_2$. Well-resolved negative tone patterns as small as 100 nm were obtained by e-beam exposure. The various interactions between the QAS additive and the different functionalities on the polymeric photoresist were studies using computational simulations. These studies combining both theory and experimental results provide insight to design better and more efficient dissolution aids for polar polymers in $scCO_2$. The results indicate that there is great potential of using $scCO_2$ as a processing solvent in the presence of such additives.

To make this process of $scCO_2$ development more environmentally friendly, the possibility to design non-fluorinated additives may be considered. Beckman and co-workers have reported that interactions between acetate groups and $scCO_2$ impart

solubility to certain non-fluorinated polymers. This increase in solubility has been attributed to Lewis acid-base type interactions between CO_2 and the oxygen of a carbonyl group. Figure 7.1 shows structures of two compounds that may be used as non-fluorinated additives. These additives are proposed to work due to the favorable interactions of the carbonyl/ester groups with both the polymeric photoresist and $scCO_2$ which may allow the additive to pull the photoresist material into the $scCO_2$ phase. Computational simulations with these non-fluorinated additives will be run by Gregory Toepperwein (de Pablo's research group) at the University of Wisconsin.

Chapter three describes a direct patterning approach to prepare patterned polymer brushes. There are several steps involved in polymer brush patterning using photolithographic schemes or soft lithography techniques. Direct patterning has the advantage of reducing these labor intensive steps. In addition, the use of e-beam lithography gets rid of the diffraction limit of photolithographic processes and allows patterning of brushes down to sub-50 nm features. The direct patterning of PMMA, PHEMA, PNPMA, PIBMA and PTFEMA brushes has been demonstrated. Using this direct patterning approach polymer brush patterns down to 50 nm lines were demonstrated. Computational simulations were used to rationalize the sensitivity of the brushes under e-beam exposure on the basis of the stability of radicals formed on polymer degradation.

Chapter four combines the concept of direct patterning of polymer brushes with the environmentally benign development process in $scCO_2$. Low surface energy polymer thin films comprising of PTFEMA brushes were directly patterned in a single step using e-beam lithography. The patterned brushes were successfully developed in $scCO_2$. Using this environmentally benign processing solvent, patterned polymer brushes down to 100 nm features were obtained.

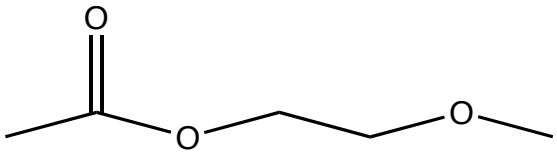

additive - I

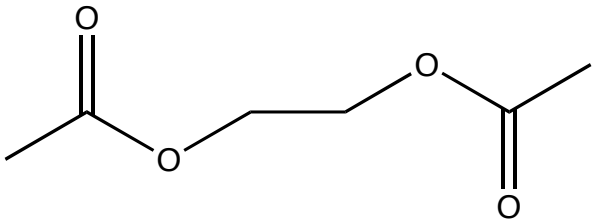

additive - II

Figure 7.1. Structures of some non-fluorinated additives as dissolution aids for polar polymers.

The idea of direct patterning of brushes can be exploited to create interesting nanostructures. Diblock copolymer brushes such as PMMA-b-PS, with a negative tone upper layer and positive tone bottom layer can be directly patterned to form nanochannels. Polystyrene is known to crosslink on e-beam exposure while PMMA undergoes degradation to small fragments. Thus nanochannels of the desired size may be obtained by direct exposure of these diblock brushes under e-beam. Another interesting study would be to evaluate the microstructures formed by diblock copolymer brushes when placed in confined geometries. Direct patterning of diblock or triblock copolymer brushes can provide lateral freedom to the polymer chains on the same length scale as the brush itself. In a suitable processing solvent, the brushes might relax and form new microstructures. Triblock brushes have the added advantage that they can help reduce conformational restrictions caused by brush stretching. The surface topography and pattern shape (phases and microstructures) can be examined by scanning force microscopy (SFM), grazing incidence small angle X-ray scattering (GISAXS) and near edge X-ray adsorption fine structure (NEXAFS) studies. This study can help understand how pattern size influences the polymer brush organization. Using this approach features as small as 10 nm may be achieved.

Mixed polymer brushes are gaining a lot of interest. This single step patterning approach can be used to create mixed polymer brush surfaces.

Polymer brushes have been used extensively to create biologically and electronically compatible surfaces for the development of biosensors. Polymer brushes can be used to provide surfaces that resist and minimize non-specific adsorption. These surfaces can be functionalized with specific haptenic groups via chemical modifications. Chapter five focuses on the synthesis and use of a newly modified ATRP thiol initiator to prevent the non-specific adsorption of pure antibodies on polymer brush surfaces derivatized with haptenic groups. A conventional ATRP thiol

initiator was modified with oligo(ethylene) glycol via a new synthetic route. Electrochemistry of an osmium complex redox mediator indicates that our new initiator mitigates non-specific adsorption of pure biomolecules on the surface. The adsorption of insulin and non-specific IgG antibodies on gold QCM surfaces was quantified. Polymer brush surfaces grown from the new oligo(ethylene glycol) containing intiator showed reduced adsorption of biomoelcules on the surface.

Chapter six describes the development of an antibody detection system based on their intrinsic catalytic activity. Our initial development of substrates for antibody detection was based on our model system of 2,4-dinitrophenyl (DNP) antigen and anti-DNP atibodies. Poly(acrylic acid) brushes were successfully grown using a "Forest Canopy" approach via ATRP and functionalized with DNP. Qualitative analysis of the antibody binding capacity of these brushes was carried out with fluorescent (Alexa488 labeled) anti-DNP IgE antibody. The number of DNP groups and the binding of anti-DNP IgG antibody onto these DNP groups was quantified by cyclic voltammetry. A microelectrode was used to measure the response of the redox mediator, resorufin for the determination of H_2O_2 generated by antibodies via ACWOP

Alternately, we used the nickel chelator, nickel-nitrilotriacetic acid (Ni-NTA), which binds to the multiple histidines in tagged H5 proteins and forms a stable complex. The surface composition of Ni-NTA functionalized brushes was characterized by XPS. Antibody binding on these Ni-NTA functionalized brushes was evaluated with a fluorescent label such as his-tagged Green Fluorescent Protein (GFP) and microscopic visualization.

We may increase the density of immobilized antibodies by exposing the haptens with different configurations of the polymer brushes. Future work involves quantifying and comparing the antibody binding on two different types of polymer brushes that are different in structure. The "English Garden" approach effectively

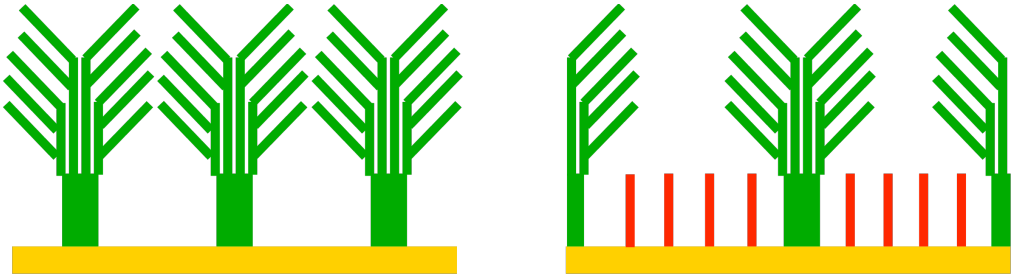

Figure 7.2. Structures of a polymer brush grown using the “Forest Canopy” and the “English Garden” approach.

increases the surface area by providing ample space between the dense brushes (Figure 7.2). This will make the haptenic groups close to the surface accessible to the antibodies. This higher binding may offer advantages over the conventional "Forest Canopy" approach. Future work also involves quantification of the Ni-NTA functionalization and the binding of his-tagged H5 proteins on these surfaces using QCM methods.

Finally, these functionalized polymer brushes will be used with a microelectrode array system as the detector module, fabricated by patterning gold interdigitated electrodes on the surface of a glass wafer to amplify the electrochemical signal. Dr. Nicolas Da Mota (Abruña research group, Cornell) simulated the amplifying ability of such an interdigitated electrochemical sensor. These results indicate that in a conventional microchannel 20 μm high and 500 μm wide, an interdigitated array of 1000 electrode pairs allows ready detection and quantification of the resorufin redox couple in the range of 10 nM using the conventional electrochemical equipment. This initial amplification will be coupled with a highly sensitive potentiostat to result in an overall amplification of 6-9 orders of magnitude.